Surface Enhanced Raman Spectroscopy as a Tool for Waterborne Pathogen Testing

Krista Rule Wigginton

Dissertation submitted to the faculty of the Virginia Polytechnic Institute and State University in partial fulfillment of the requirements for the degree of

Doctor of Philosophy
In
Civil and Environmental Engineering

Committee
Peter J. Vikesland
Patricia M. Dove
John C. Little
Nancy G. Love
James M. Tanko

October 2, 2008
Blacksburg, VA

Keywords: Surface Enhanced Raman Spectroscopy, *Cryptosporidium parvum*, *Giardia lamblia*, waterborne pathogens, virus, immunoassay

Surface Enhanced Raman Spectroscopy as a Tool for Waterborne Pathogen Testing

Krista Rule Wigginton

ABSTRACT

The development of a waterborne pathogen detection method that is rapid, multiplex, sensitive, and specific, would be of great assistance for water treatment facilities and would help protect water consumers from harmful pathogens. Here we have utilized surface enhanced Raman spectroscopy (SERS) in a sensitive multiplex pathogen detection method. Two strategies are proposed herein, one that utilizes SERS antibody labels and one that measures the intrinsic SERS signal of organisms. For the SERS label strategy, gold nanoparticles are conjugated with antibodies specific to *Cryptosporidium parvum* and *Giardia lamblia* and with organic dye molecules. The dye molecules, rhodamine B isothiocyanate (RBITC) and malachite green isothiocyanate (MGITC) were surface enhanced by the gold nanoparticles resulting in unique fingerprint SERS spectra. The SERS label method was successful in detecting *G. lamblia* and C. *parvum* simultaneously. The method was subsequently coupled with a filtration step to both concentrate and capture cysts on a flat surface for detection. Raman mapping across the filter membrane detected ~95% of the spiked cysts in the optimized system.

In the second type of strategy, intrinsic virus SERS signals were detected with silver nanoparticles for enhancement. Principal component analysis performed on the spectra data set resulted in the successful differentiation of MS2 and PhiX174 species and also for the differentiation of viable virus samples and inactivated virus samples.

Acknowledgements

I would like to start by acknowledging my academic advisor, Peter Vikesland. For the last six years Pete has been my mentor, my critical audience, my motivational speaker, my information source, and my friend. I believe that choosing Peter as my advisor is the best professional move I have made thus far. Thanks Pete!

A number of research collaborators have played important roles along the way. To Heather Rectanus, your diligent gold nanoparticle synthesis skills were crucial in getting the project off to a strong start. Becky Halvorson, Christina Anderson, Xiaojun Chang and the rest of the Vikesland research group were also great helps in the laboratory. I would like to acknowledge Dr. Bob Bodnar and Charles Farley for their assistance with the VT Raman work and to Dr. Genevieve Massonet for assistance with the EPFL Raman work. A very big thanks goes to Jody Smiley and Julie Petruska for their six years of technical assistance. I'd like to also thank Dr. Tamar Kohn and her research group at EPFL for welcoming me into their lab this last summer.

To the many friends I've made at VT over the years, I will remember fondly our dinner parties, Gillies ladies' lunches, fried turkeys, tailgates, Sweaterfests, Halloweens, evenings at the Cellar, political lab discussions, Saturday morning runs, German nights, etc.

Finally, I would like to acknowledge my family. My parents John and Maggie Rule are responsible for my interest and success in math and science. They have always been supportive of my academic aspirations, even when I was in 23rd grade! To my sister Becky Rule, who is always good for a talk on the phone about the trials and

tribulations of being an environmental engineering graduate student. And a very special thanks to my new husband, Nicholas Wigginton, whose patience and support during stressful times are very much appreciated.

Attributions

Dr. Peter Vikesland (Department of Civil and Environmental Engineering, Virginia Tech) is the research advisor and committee chair. Dr. Vikesland provided general scientific guidance and assisted in writing chapters 3, 4, and 5. Additionally, Dr. Vikesland provided much of the financial support for the work presented in this dissertation through research grants.

Dr. Tamar Kohn (Environmental Science and Technology Institute, Ecole Polytechnique Fédérale de Lausanne) hosted me in her laboratory at EPFL where she provided scientific and technical assistance with the virus experimental work. Dr. Kohn also assisted in writing chapter 5.

Table of Contents

Table of Figures

Table of Tables

1) Executive Summary

Despite major advances in water treatment and increasingly stringent pathogen regulations throughout the last century, outbreaks of waterborne disease still regularly occur in the U.S. and other highly-developed countries. Between 1991 and 2002, an estimated 207 outbreaks of waterborne disease were reported in the U.S., resulting in 434,947 cases and 73 reported deaths.[1] Outbreaks of disease are costly and in the U. S. alone, it is estimated that $20 billion per year may be lost in productivity due to illnesses caused by waterborne pathogens.[2] The causative agents for these outbreaks range from viruses, consisting simply of either RNA or DNA enclosed in a protein capsid, to bacteria such as Escherichia coli (O157:H7), to highly complex organisms such as the protozoa *Giardia lamblia* and *Cryptosporidium parvum*.

Clearly the detection of pathogenic contaminants is of critical concern to the water treatment community. Because the organisms causing common waterborne illnesses encompass a wide range of biologies and sizes, the methods used to monitor these pathogens vary considerably. Unfortunately, most existing methods for waterborne pathogen monitoring, particularly those for virus and protozoan detection, are plagued by consistently poor recoveries, require personnel with high levels of analytical skill, and include excessively long periods between sample collection and pathogen identification. Faster, less complex, and more reliable pathogen detection methods would greatly assist drinking water treatment utilities and policy makers and would help protect the average drinking water consumer.

The work in this dissertation demonstrates the utility of surface enhanced Raman spectroscopy (SERS) for the identification and enumeration of drinking water pathogens. SERS is amenable for use within rapid detection devices due to its high specificity, its ability to obtain spectra in the presence of water, its potential for automation, and its ability to distinguish between viable and non-viable cells. Two strategies are proposed herein, one that utilizes SERS antibody labels and one that measures the intrinsic SERS signal of organisms. For the SERS label strategy, gold nanoparticles are conjugated with antibodies specific to *Cryptosporidium parvum* and *Giardia lamblia* and with organic dye molecules. The method was subsequently coupled with a filtration step to both concentrate and capture the cysts on a flat surface for Raman mapping detection. In the second type of strategy, the intrinsic virus SERS spectra were characterized with principal component analysis to discriminate the spectra of different virus species and viability states.

Surface-Enhanced Resonance Raman Spectroscopy for the Rapid Detection of *Cryptosporidium parvum* and *Giardia lamblia* (Chapter 3)

This chapter describes the development of a SERS-based methodology for multiplex pathogen detection. Specifically, *Cryptosporidium parvum* oocysts and *Giardia lamblia* cysts were labeled with immuogold Raman labels. The immunogold labels were prepared by conjugating gold nanoparticles with commercial antibodies and dye molecules. After incubation with the immunogold labels, *C. parvum* oocysts and *G. lamblia* could easily be measured and differentiated by Raman spectroscopy. The immunogold signal intensities were optimized by testing several sizes of gold nanoparticles, four different commercially available dye molecules, and two Raman

excitation wavelengths. Raman maps were collected across fixed and labeled *Cryptosporidium* oocysts and *Giardia* cysts and the maps were used to determine which *C. parvum* and *G. lamblia* antibodies exhibited the best specificities and organism coverages. The research presented here demonstrates the feasibility of utilizing SERS labeling for sensitive multi-pathogen monitoring strategies. To our knowledge, this is the first time living organisms have been labeled with immunogold and detected using XY Raman mapping.

Gold-coated polycarbonate membrane filter for drinking water pathogen concentration prior to SERS-based detection (Chapter 4)

This chapter describes a pathogen concentration step that is compatible with the SERS-based detection technique presented in Chapter 3. Specifically, *G. lamblia* cysts were collected from water samples on a filter surface, labeled with immunogold SERS labels, and quantified via Raman spectroscopy. Anodisc® membrane filters, silver membrane filters, and electroless gold-coated polycarbonate track etched (PCTE) membrane filters were investigated for their compatibility with the SERS based detection strategy. The largest pore size available with the Anodisc\ membranes was too small for the proposed method because they led to the physical retention of the immunogold. When silver membranes were employed, cysts were difficult to distinguish from nonspecifically bound labels and cyst recovery from distilled water samples was only ≈12.3%. With gold-coated PCTE membranes, however, cysts were readily detectable and cyst recovery was ≈95%. This Raman based method simplifies *Giardia* detection and has the potential to be extended to the simultaneous detection of numerous pathogenic organisms. To our knowledge, this is the first report coupling the use of membrane filters

for the concentration and detection of organisms from water samples with a SERS based detection strategy.

Investigation of Bacteriophage Viability via Surface-Enhanced Raman Spectroscopy and Principal Component Analysis (Chapter 5)

The purpose of this study was to examine the instrinsic (i.e., non-labeled) signals of ssRNA bacteriophage MS2 and ssDNA bacteriophage PhiX174 by silver nanoparticle enabled SERS. Principal component analysis (PCA) was used to simplify and classify the SERS spectral data. In PCA, new variables are formed (principle components) that are linear combinations of the original variables and are orthogonal to one another. A principal component ordination plot of PC1 and PC2 for viable MS2 and PhiX174 particles led to well-defined clusters of the two species. Test sample spectra were correctly clustered when their PC score values were added to the ordination plot. In addition to differentiating between these viruses, SERS/PCA is also able to classify viable and non-viable (e.g., heat-inactivated, hydroxyl-radical inactivated) viruses (results not shown). These results suggest that a SERS technique could lead to a novel method for the rapid identification of viruses and the evaluation of their viability. The PCA loading data was then used in conjunction with the raw Raman spectra to identify the viral components responsible for the differences in the SERS spectra. Changes in the SERS bands for tryptophan, tyrosine, and α-helix were observed for the heat-treated experiments. For hydroxyl-treated MS2, changes in SERS bands for proline and tyrosine were observed.

Conclusions and Future Work

Here we have demonstrated that SERS has the potential to be a valuable tool in pathogen detection methods. The current state of the art in pathogen detection does not allow for the detection of more than one or two species simultaneously, whereas the methods presented here could be extended to detect for a number of species simultanoeosly. Additionally, both SERS detection techniques presented here rely on the recognition of specific fingerprint spectra and so pathogen identification could be easily automated. A signal-based recognition would be a major advantage over the current pathogen detection techniques as it does not require organism identification by a microscopist or microbiologist. A SERS-based method would therefore be less vulnerable to human-based errors, would take less time to perform, and would ultimately cost less.

Future work will need to address how the immunogold labeling used in Chapter 3 and Chapter 4 is affected by extraneous debris and other water quality parameters in real water samples. Additionally, because bacteriophage viruses were used in the Chapter 5 SERS virus viability study, future work should verify that similar results are obtainable with human viruses.

WORKS CITED

1. Craun, M. F., Craun, G. F., Calderon, R. L., Beach, M. J., Waterborne outbreaks in the United States. *Journal of Water and Health* **2006,** 04, (2), 19-30.
2. Straub, T. M., Chandler, D. P., Towards a unified system for detecting waterborne pathogens. *Journal of Microbiological Methods* **2003,** 53, (2), 185-197.

2) Literature Review

Krista Rule Wigginton and Peter J. Vikesland

Human illness was first tied to poor quality drinking water in the mid-nineteenth century when Robert Snow linked the ongoing cholera outbreak in London to water obtained from the Broad Street pump.[1] Snow, upon inspection of a water sample from the pump, recorded the presence of "white flocculent particles" in the water.[2] He suggested that the water was polluted with fecal matter and was thus facilitating the spread of cholera in London. His epidemiological study helped to discredit the previously accepted "miasma" theory of cholera infection, which had blamed "bad air" for the spread of the disease during the cholera pandemics of the eighteenth and nineteenth centuries. Although *Vibrio cholerae*, the causative agent, was not identified in drinking water until thirty years later,[3] the work by Robert Snow provided the first scientific evidence of the importance of clean drinking water.

Despite major advances in water treatment and increasingly stringent pathogen regulations, outbreaks of waterborne disease still regularly occur in the U.S. and other highly-developed countries. Between 1991 and 2002, an estimated 207 outbreaks of waterborne disease were reported in the U.S., resulting in 434,947 cases and 73 reported deaths.[4] These statistics represent only those cases that were reported to the CDC and EPA and are thus only a fraction of the total number of outbreaks and cases.[5] Many outbreaks are linked to treatment deficiencies such as wastewater contamination or

inadequate disinfection, but for many others, contributing factors are never identified.[6] Outbreaks of disease are costly and in the U.S. alone, it is estimated that $20 billion per year of economic productivity may be lost due to illnesses caused by waterborne pathogens.[7] A comprehensive study of the major reported waterborne outbreaks over the last three decades in the U.S., Canada, Australia, New Zealand, and several European nations showed that the agents responsible for the outbreaks included (outbreak numbers in parentheses): *Cryptosporidium* (20), *Campylobacter* (14), *Giardia* (13), Norwalk virus (12), pathogenic *E. coli* (7), rotavirus (2), *Shigella* (2), hepatitis (1), *Salmonella* (1), *Toxoplasma* (1), and unidentified etiologic agents (5).[6]

2.1 Current pathogen regulations and pathogen detection methods

At present, there are six groups of microorganisms regulated by the Safe Drinking Water Act (Table 2.1) including *Cryptosporidium parvum*, *Giardia lamblia*, viruses, *Legionella*, heterotrophic plate counts (HPCs), and coliform bacteria (including Total Coliform (TC), Fecal coliform (FC) and *Escherichia coli*). In contrast to the numerically defined maximum contaminant levels (MCLs) typically employed for waterborne contaminants, the MCLs for *C. parvum*, *G. lamblia*, viruses, and *Legionella* require minimum levels of treatment that are believed to achieve 99-99.99% of pathogen removal (Table 2.1). Although maximum contaminant level goals (MCLGs) for these organisms have been set at zero, the current methods used to detect these pathogens are time consuming, require high levels of analytical skill, and are quite expensive. Given these limitations it is currently felt that the treatment technology requirement provides an adequate level of safety.

In addition to those currently regulated, additional pathogens are listed on the contaminant candidate list (CCL) and include *Adenovirus, Aeromonas hydrophila, Calcivirus, Coxsackievirus, Echovirus, Helicobacter pylori, Microsporidia, and Mycobacterium avium intracellulare*.[8] As is the case with the currently regulated pathogens, the promulgation of regulations and numerically defined MCLs for the CCL pathogens has been hindered by the lack of straightforward detection methods. Because the pathogens covered by the SDWA and currently on the CCL encompass a wide range of biologies and sizes (Table 2.2), the methods used to monitor for the presence of these pathogens vary considerably.

To comply with current regulations, all public drinking waters in the U.S. are routinely monitored for total coliform (TC), with the required frequency of the tests dependent on the size of the treatment system. The majority of the coliform bacteria detected by TC tests are not pathogenic, but instead serve as indicators of fecal contamination. For this reason, waters that test positive for TC are subsequently tested for either fecal coliform (FC) or *E. coli,* each of which is a subset of the total coliform working group. A number of culture-based methods have been accepted by EPA for the detection and quantification of TC, FC, and *E. coli* in water samples, and these methods are generally rapid and straightforward.[9-11] Unfortunately, the presence of pathogens such as *C. parvum*, *G. lamblia* and viruses, does not necessarily correspond to the presence of coliform bacteria,[12-14] and therefore, the absence of coliform does not guarantee pathogen-free water.

To address the risk of *C. parvum* and *G. lamblia* presence in coliform-free water, EPA promulgated the Long Term 2 Enhanced Surface Water Treatment Rule

(LT2ESWTR). This led to extensive *C. parvum* and *G. lamblia* monitoring in surface water sources and groundwater sources under the direct influence of surface waters. EPA methods 1622/1623 are typically used for the detection of *C. parvum* and *G. lamblia* in water samples.[15, 16] The general protocol for methods 1622 and 1623 is the same; however, method 1622 tests only for *Cryptosporidium* oocysts, while method 1623 tests for both *Cryptosporidium* oocysts and *Giardia* cysts. The methods are immunologically based with the pathogens captured and concentrated by immunomagnet separation and detected via fluorescent antibody staining. Unfortunately, these methods are time consuming, require high levels of expertise, and give inconsistent results. Reported recoveries of spiked oocysts vary from 15-85% in environmental samples and 14-46% in reagent/tap waters.[17-20] In addition, the recoveries depend on the chemistry of the sample[21, 22] and the type of analysis kit employed.[23]

Testing waters for enteric viruses requires specialized techniques that vary from species to species. Virus concentrations are typically very low in surface and finished drinking waters and therefore large sample volumes, sometimes in excess of 1000 L for drinking water, must be filtered to assure adequate viral detection limits. For many viruses, a continuous cell culture is inoculated with a virus sample and after infecting the cell lines, the viruses replicate.[24] Upon replication, viruses such as enteroviruses, reoviruses, and adenoviruses cause cytopathogenic effects that are observable in the host cells. Some viruses, such as rotavirus, do not cause observable cytopathogenic effects and so must be detected by other means such as immunologic detection or nucleic acid probes. Additionally, noravirus and hepatitis A do not currently have permissive cell lines and so must be detected with genetic methods like PCR.[24] Unfortunately, not all

viruses infect the same type of cells and thus a number of different cell lines are required to detect different enteric viruses. Virus detection methods can be slow, with host cell infection taking from one to twenty-one days. As noted previously, due to the complexity and time required by current virus detection methods, viruses in drinking waters are regulated based on drinking water treatment requirements, and thus regular virus monitoring in source and finished drinking water is uncommon.

Faster, less complex, and more reliable pathogen detection methods would greatly assist drinking water treatment utilities and policy makers and would help protect the average drinking water consumer. Bioterrorist threats, rapid global population growth, and increased stresses on our freshwater resources due to global climate change only exacerbate the need for improved drinking water pathogen monitoring. To address these concerns, there have been a number of recent reports of improved methods for detection of bacteria, protozoa, and viral pathogens which have included immunological,[25-27] molecular (PCR),[28-32] and culture techniques.[33] There are expectations that future methods will be capable of detecting numerous species/classes of organisms simultaneously, will discern viable from non-viable organisms, and will be incorporated into a real-time, in-line monitoring system.

One promising area for the future of drinking water monitoring stems from the recent development of nano-enabled detection strategies. In recent years, a vast amount of research has focused on nanoscience and nanotechnology due to the unique physical and chemical characteristics of nanosized materials. In the U.S. alone, an estimated 5.9 billion dollars of federal funding was granted for nano-related research in the five years between 2003-2007.[34] With this unprecedented surge in research effort comes the

anticipation of novel product development, such as new drug delivery methods, medical diagnostic tools, ultrasensitive sensing, etc… Numerous reports of nano-enabled biosensors have been recently published, however, very few have focused specifically on the detection of whole cells, in general, and waterborne pathogens, in particular. We therefore believe that there are significant opportunities for nano-enabled biosensor research in the environmental monitoring field. Specifically, research should focus on expanding the nano-enabled biomolecule detection techniques to detect for whole cells and microorganisms in environmental samples.

2.2 Nanomaterial-enabled biosensors

To detect the low concentrations of pathogens typically found in treated and untreated drinking waters, a biosensor must have both sufficient specificity and sensitivity to pick the proverbial needle out of a haystack. Ideally a biosensor will also have a broad dynamic range. Potentially infectious doses of organisms may be as low as one organism per liter for protozoan and viral pathogens, but much higher for many bacterial agents.[24] Specificity is incorporated through the use of recognition elements that recognize antigenic or other surface epitopes on the exterior of a pathogen. Sensitivity is achieved via signal transduction modalities that explicitly detect the interaction between the pathogen and the recognition element. In a nanomaterial-enabled biosensor, the recognition element is typically bound to the surface of the nanomaterial and the interaction of this conjugate with a pathogen is then monitored via a signal transduction mechanism. A variety of different nanomaterials are currently being used in biosensor applications and the nanomaterial employed has ramifications for both the type of recognition element employed as well as the signal transduction method to use. Potential

recognition elements include antibodies,[35, 36] aptamers,[37] carbohydrates,[38, 39] antimicrobial peptides,[40] and pharmaceuticals,[40] among others. Signal transduction methods range from optical (e.g. surface plasmon resonance (SPR),[41,42] surface enhanced Raman spectroscopy (SERS),[43] fluorescence[44]), to electrochemical,[45] and piezoelectric.[46]

Regardless of what combination of nanomaterial/recognition element/signal transduction is employed, a fully optimized biosensor should be able to: 1) discriminate between closely related pathogenic and nonpathogenic organisms; 2) detect small quantities of a target within a complicated background matrix; 3) maintain binding during repeated wash steps; and 4) exhibit a high degree of stability over time. To ultimately design a sensor that achieves these goals requires sufficient understanding of the methods by which biosensors are produced and the conditions under which they can be employed. This latter point is especially important, because although a large number of 'proof-of-concept' experiments have been done with a variety of biosensors under laboratory conditions, relatively little work has been done to test these biosensors under real-world conditions.

This literature review focuses on the use of antibodies as recognition elements and SERS for signal transduction as these are the techniques discussed in the subsequent chapters. An extended version of this review is currently in preparation for publication and discusses additional nano-enabled signal transduction techniques and compatible recognition elements.

2.3 Antibodies as biosensor recognition elements

The recognition elements employed in whole cell pathogen biosensors are usually biomolecules that have an affinity for epitopes on the pathogen surface. A variety of

recognition elements have been employed in biosensors including antibodies,[26, 27] nucleic acid based aptamers,[37, 47] and cell targeting carbohydrates.[39, 48] At this time, antibody based techniques continue to be faster and more robust than the competing recognition elements and have been used extensively to select for bacteria, virus, toxins, and spores, alike.[49, 50] Highly selective and highly sensitive antibodies are readily available for many pathogenic organisms and there are a number of well-established methods for conjugating antibodies to nanomaterials.[51, 52] For these reasons, immunological detection with antibodies continues to be the most widely used tool for the selective capture and labeling of microorganisms.

Antibodies are immune system glycoproteins, or immunoglobulins, produced by B-lymphocytes and plasma cells to attack foreign substances.[53] The "Y"-shaped structure of antibody monomers consists of four polypeptides including two identical light chains and two identical heavy chains (Figure 2.1). At the two tips of the "Y", the heavy and light chains form a polypeptide sequence that is considered the variable region.[53] A subsection of the variable region is the hypervariable region (HV) that is highly specific to a structure on the organism or material being attacked. This antigenic determinant, or epitope, on the organism or substance can be as small as one unique protruding structure such as an amino acid residue.[53] The variable region of the antibody, or paratope, binds to the antigenic determinant through hydrogen bonding and is further stabilized by van der Waals forces, hydrophobic interactions, and electrostatic forces.[53] Additionally, the three-dimensional structure of the antibody HV region is highly compatible with the antigenic determinant structure.[53] The area of contact can be as small as 1-2 amino acid residues on both the antibody and antigen for small antigenic molecules or protruding peptides. For

larger interactions, 15-20 antibody residues can be in contact with the same number of residues on the antigen equaling an area of 50-100 nm^2.[53]

The remainder of an immunoglobulin molecule is considered the constant region (Figure 2.1), and this region determines how the substance or organism under attack will be destroyed. The constant region, along with the antibody size, dictates which class an antibody belongs to. Mammalian species produce five classes of antibodies including IgM, IgG, IgA, IgD, and IgE.[53] The antibody classes are subdivided into subclasses based on minor differences in the amino acid sequence of the heavy chains (i.e. IgG1, IgG2, IgG3, etc.).[53] Table 2.3 lists the characteristics of mammalian antibody classes.

The affinity, or K_d, of an antibody to an antigen is a thermodynamic property determined by the ratio of the rate of antibody-antigen complex formation relative to the rate of its dissociation.[53] Affinity is a measure of the strength of binding between a single epitope and paratope and does not take into account the valency of the antibody or of the antigen substance. Avidity, on the other hand, is the "functional affinity" of an antibody and includes the valency of the antibody and antigen.[53] For example, IgG antibodies have a valency of two whereas IgM antibodies have a valency of ten. IgM antibodies therefore have higher avidities than IgG antibodies when the two types have similar affinities.

Antibodies are available in a variety of forms including affinity purified polyclonal antibodies, antiserum, and monoclonal antibodies. Polyclonal antibodies (pAbs) are acquired from the serum of animals that have been immunized with the antigen of interest and are then purified to a specified level.[53] pAbs simultaneously contain a number of different antibodies that bind to a number of epitopes on the antigen. Advantages of employing pAbs in immunoassays include a greater number of antibodies

attaching to the antigenic surface, their higher resistance to pH or salt concentration changes, and the fact that they are considerably less expensive than monoclonal antibodies. However, their non-homogenous nature means that the use of polyclonal antibodies can result in increased levels of nonspecific binding (i.e., binding of the antibody to non-antigenic materials via van der Waals interactions).[49, 54]

Monoclonal antibodies are an identical, well-defined population of antibodies that bind to a single epitope. They are produced from continuous cell lines (hybridomas) that are formed by the fusion of cancerous myeloma cells and antibody secreting B-cells.[53] Monoclonal antibodies can be very specific and are selected from the hybridoma parent cell mix based on their affinity. They are less likely to cross react with debris and tend to be homogenous reagents with better-defined specificities.[54] They can be too specific, however, in which case they may not detect variants within the species that lack a particular epitope.[54]

Antibodies are often used for concentration and purification of pathogens in immunomagnetic separation (IMS) based methods. In this technique, magnetic beads are conjugated with antibodies specific to the organism of interest. When immunomagnets are mixed with preconcentrated water sample, they bind with their respective organisms. The bead-organism complex is then separated from extraneous debris with a magnetic field. The IMS particle is released from the organism via pH adjustment thus leaving the organism of interest purified and concentrated. Immunomagnetic separation has been applied for protozoan,[55, 56] viral,[57] bacterial[58, 59] and fungal[60] detection. However research has shown that recoveries vary from one kit to the next,[21, 23] with varying sample turbidity[21, 61] and with sample pH.[22]

Antibodies are also used for pathogen detection by tagging the organisms with an optically detectable label. In fluorescent antibody staining, for example, antibodies are tagged with fluorescent molecules. After the antibodies are incubated with a sample, the tagged microorganism can be detected by fluorescence microscopy. A number of additional antibody based detection techniques have been employed for biomolecule or microorganism detection such as surface enhanced Raman spectroscopy antibody tagging,[51, 62-64] enzyme immunoassays,[36, 65] surface plasmon resonance immunoassays,[52, 66] and many others.

Unfortunately, there are a number of disadvantages involved with the use of antibodies for pathogen recognition including their potential for nonspecific binding, the need for physiological pH and temperature during immunoassay procedures, varied antibody performance from batch to batch, their sensitivity to chemicals such as oxidants in drinking waters, the inability to distinguish viable from non-viable organisms, the high cost of monoclonal antibody production, as well as their limited shelf life and temperature sensitivity.[67]

Despite the long list of drawbacks associated with the use of antibodies, they continue to be the best available option for the selective capture and tagging of a broad range of microorganisms. As a result, many of the recently proposed nano-enabled biomolecule detection techniques employ antibodies for selective biomolecule capture and tagging.

2.4 SERS/SERRS for signal transduction in biosensors

The surface enhanced Raman (SER) effect was first reported in 1974 when pyridine was placed on a roughened silver electrode and a Raman signal enhancement of

10^6 was observed.[68] At the time, this effect was not fully understood and it was not until 1977 that the reasons for the enhancement were fully elucidated.[69, 70] Soon thereafter, scientists saw similar Raman enhancements with other noble metal roughened electrodes as well as noble metal nanoparticles. Today we know that the SER effect is the combined result of electromagnetic and chemical enhancements.[71] The electromagnetic enhancement, which is typically much stronger than chemical enhancement, is the result of the collective oscillation of surface electrons on nanostructured materials. This localized surface plasmon resonance (LSPR) occurs when a noble metal (e.g., gold, silver, copper) is illuminated by incident light. If the excitation source resonates with a plasmon, the metal particle produces electromagnetic radiation that enhances the local field of a molecule in the vicinity (<10-20 nm) of the plasmonic structure. This enhancement can significantly increase the intensity of the Raman scattered light. In addition to SER, a resonance enhancement (SERR) with colored analytes can lead to additional enhancement.[72]

Single molecule SERS/SERRS detection has been reported, suggesting that the sensitivity is comparable to or exceeds the detection limits of fluorescence spectroscopy.[73, 74] In addition to the extremely low detection limits, SERS/SERRS bands are 10-100 times narrower than fluorescence bands and are therefore less likely to overlap in multiplex detection. The cost of Raman instruments and the instrument system footprints have significantly decreased in recent years. SERS as an analytical tool therefore holds great promise for drinking water detection strategies, especially for the detection of pathogens present in low concentrations.

Gold and silver based SERS substrates typically have average enhancement factors between 10^5-10^6, but localized enhancements in the vicinity of 'hot-spots', or locations where the localized surface plasmons from two nanoscale features interact, can be around 10^{15}.[73, 75] Quantitative SERS is more reproducible at the lower enhancement level since the signal is typically more stable and thus more reliable.[76, 77] The lower enhancement regime is sometimes referred to as the low sensitivity regime, while the upper is the high enhancement regime. SERS has been utilized in recent reports for the detection and analysis of biological molecules,[35, 62, 78, 79] in general, and microorganisms in particular.[64, 80, 81] In these techniques, the intrinsic SERS signal of a biomolecule can be measured directly or the molecule can be tagged with a SERS label.

For direct measurement of the intrinsic SERS signal, the bioanalyte is typically placed on a SERS active solid substrate, which often consists of nano-sized gold or silver structures. A number of SERS substrates have been proposed[78, 82-84] and multiple SERS substrates are available commercially (Klarite SERS substrates, Mesophotonics, Southhampton, U.K. and SERS Vials, Real Time Analyzers, Middletown, CT). The Raman measurement is then collected directly from the substrate surface and the bioanalyte can be identified based on its Raman spectrum. Characteristic spectra have been collected with SERS for bacteria,[85-89] virus,[82] and other microorganisms.[81] For example, Shanmukh et al.[90] developed a silver nanorod substrate capable of 10^8 enhancement and used this to detect species and strains of human respiratory viruses down to 100 Plaque Forming Units (PFU)/mL.[82]

Although the detection limit reported by Shanmukh for virus detection is higher than those reported with PCR detection and plaque forming assay detection by at least an

order of magnitude,[91-93] this type of intrinsic SERS method provides valuable information about the analyte species, structure (cytrochrome studies) and physiological/viability state.[81, 94, 95] Our lab, for example, used the intrinsic SERS method to differentiate two different virus species as well as viable and inactivated virus (Chapter 5). Comparatively, genomic methods and antibody tagging methods do not provide physiological/viability state information and plaque culture assays cannot be used to detect more than one species simultaneously. Direct analyte measurements also avoid issues associated with tagging such as non-specific binding and poor molecule-molecule affinities. A drawback of this type of method includes the complex spectra of most microorganisms due to a variety of biomolecule components, which make reproducibility a problem.

In the tagging strategy, a Raman label binds specifically to the bioanalyte and Raman spectroscopy is then used to measure the signal of the tag. Both antibody-antigen interactions[51, 63] and DNA hybridization strategies[96, 97] have been used to bind Raman tags. The tags typically consist of gold or silver nanoparticles conjugated with antibodies or DNA oligomers along with Raman active organic label molecules. When the Raman active labels absorb light of the same wavelength as the incident Raman laser, resonance enhancement can improve detection limits. As there are numerous labels with unique Raman fingerprints that can be incorporated into tags specific for different analytes, hundreds of possible tag combinations are possible. This type of tagging system, therefore, can easily be expanded for multianalyte detection.

A number of proof-of-concept reports have used Raman tags to probe for antigens[35, 51, 62, 63, 98] and oligomers,[96, 97, 99] with many of these examples demonstrating multiplex detection. Few reports, however, have used this type of technique for whole

cells or organisms. Driskell et al. used the tagging method in a sandwich assay to detect feline calcivirus and was able to reach a detection limit of 1×10^6 PFU/mL.[100] Additionally, our lab has developed a SERS tagging method to detect *Cryptosporidium parvum* and *Giardia lamblia* simultaneously (Chapter 3). As mentioned above, SERS/SERRS can be incorporated into a quantitative technique and many studies using tags have created calibration tables based on SERS/SERRS peak intensities.[36, 62-64] A major drawback of the SERS tagging detection method includes the lack of information on the structures and physiological states of the analytes. Additionally, as with other methods utilizing antibodies and oligomers, nonspecific binding of the tags can lead to erroneous positive signals.

Interestingly, Naja et al. combined both the intrinsic organism strategy with the tagging strategy.[101] Here, anti-*E. coli* immunosilver tags were prepared *without* organic dye labels. *E. coli* cells were incubated with the immunosilver tags and subsequently measured for their intrinsic SERS signals. *E. coli* signal was observable as a result of SERS enhancement from the immunogold tag and they were subsequently able to discriminate between *E. coli* and *R. rhodochrous* cells. This type of strategy has an advantage over the other intrinsic SERS methods as it selectively creates a SERS signal only on the organisms tagged with the immunogold. And because it detects the intrinsic signal of the organism and not label molecules, non-specific binding of the antibodies does not lead to false-positive signals.

2.5 Conclusions

As discussed in this review, there has been a tremendous amount of recent work focused on biomolecule SERS detection. These reports have demonstrated the

exceptional sensitivity, specificity, and rapidity of SERS measurements. We believe that both the intrinsic signal SERS technique and the SERS labeling technique have the potential to be incorporated into widely employed pathogen detection methods with major advantages over the current methods. Future work is needed that couples compatible microorganism pre-concentration steps and microorganism capture steps with the SERS detection techniques.

TABLES AND FIGURES

Table 2.1 Microorganism pollutants enforced by the Safe Drinking Water Act

Pollutant	MCLG	MCL or Treatment Requirement
Cryptosporidium parvum	Zero	99% Removal/inactivation
Giardia lamblia	Zero	99.9% Removal
Viruses	Zero	99.99% Removal
Legionella	Zero	No limit- belief that sufficient *G. lamblia* and virus removal will assure control
HPC	n/a	< 500 bacterial colonies / mL
Total coliform (TC) Fecal coliform (FC) *E. coli*	Zero	< 5% positive samples per month. Positive TC samples must be tested for FC or *E. coli*. Two consecutive TC results along with one positive E. coli or fecal coliform is MCL violation.

Table 2.2 Waterborne pathogen types and characteristics

Organism	**Diameters (μm)**	**Shape**	**Environmentally relevant stage**	**Waterborne pathogenic species and groups**
Viruses	0.01-0.1	Variable	Virion	norovirus (Norwalk) rotavirus hepatitis A hepatitis E, Enteroviruses (coxsackie A and B, echovirus) astrovirus
Bacteria	0.1-10	Rod, spherical, spiral, comma	Spores or dormant cells	*Cholera vibrae* *Campylobacter* *Salmonella* *Shigella* *E. coli* *Toxoplasma*
Protozoa	1-100	Variable	Cysts and oocysts	*Cryptosporidium parvum* *Giardia lamblia* *Entamoeba histolytica* *Balantidium coli* *Sarcocystis* *Toxoplasma gondi* *Cyclospora, Microsporidia*

Table 2.3. Characteristics of antibody classes

Class	Molecular weight (Da)	Class Information
IgG	150,000	Dominant antibody in blood Long term protection from disease as secondary response
IgM	950,000	Primary response to infection Pentamer held together by disulfide bonds
IgA	150,000 – 500,000	Secondary response to infection Protects respiratory and gastrointestinal systems from infection
IgE	190,000	Present in blood extremely low concentrations Triggers allergic response
IgD	180,000	Minor blood component

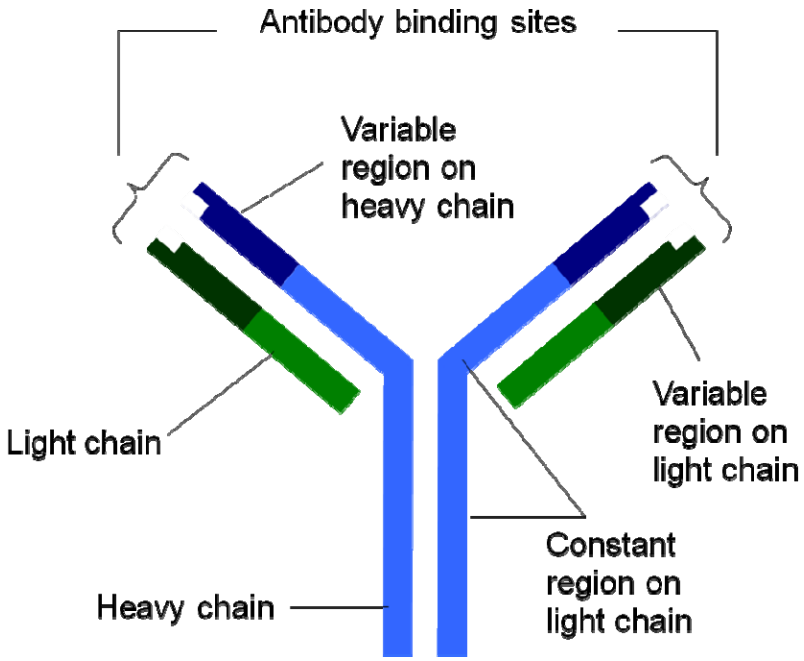

Figure 2.1 Generic antibody structure and basic components

WORKS CITED

1. Snow, J. *On the Mode of Communication of Cholera*; London, 1855.
2. Buck, C., Llopis, A., Najera, E., Terris, M., The Challenge of Epidemiology: Issues and Selected Readings. In Harvard University Press: Washington, D.C., 1988.
3. Wachsmuth, K., Blake, P. A., *Vibrio Cholerae and Cholera: Molecular to Global Perspectives*. ASM Press: Herndon, VA, 1994.
4. Craun, M. F., Craun, G. F., Calderon, R. L., Beach, M. J., Waterborne outbreaks in the United States. *Journal of Water and Health* **2006,** 04, (2), 19-30.
5. Schuster, C. J., Ellis, A. G., Robertson, W. J., Charron, D. E., Aramini, J. J., Marshall, B. J., Medeiros, D. T., Infectious disease outbreaks related to drinking water in Canada, 1974-2001. *Canadian Journal of Public Health-Revue Canadienne De Sante Publique* **2005,** 96, (4), 254-258.
6. Hrudey, S. E., Hrudey, E. J., Published case studies of waterborne disease outbreaks - Evidence of a recurrent threat. *Water Environment Research* **2007,** 79, (3), 233-245.
7. Straub, T. M., Chandler, D. P., Towards a unified system for detecting waterborne pathogens. *Journal of Microbiological Methods* **2003,** 53, (2), 185-197.
8. USEPA, Drinking Water Contaminant Candidate List 2. National Register: 2005; Vol. 70, pp 9071-9077.
9. USEPA, Method 1103.1: *Escherichia coli* (*E. coli*) in Water by Membrane Filtration Using membrane- Thermotolerant *Escherichia coli* Agar (mTEC), 2002.
10. USEPA, Method 1604: Total Coliforms and *Escherichia coli* in Water by Membrane Filtration Using a Simultaneous Detection Technique (MI Medium), 2002.
11. USEPA, Method 1603: *Escherichia coli (E. coli) in Water by Membrane Filtration Using Modified membrane-Thermotolerant Escherichia coli Agar (Modified mTEC)*, 2002.
12. Ottoson, J., Hansen, A., Westrell, T., Johansen, K., Norder, H., Stenstrom, T. A., Removal of noro- and enteroviruses, *Giardia* cysts, *Cryptosporidium* oocysts, and fecal indicators at four secondary wastewater treatment plants in Sweden. *Water Environment Research* **2006,** 78, (8), 828-834.
13. Harwood, V. J., Levine, A. D., Scott, T. M., Chivukula, V., Lukasik, J., Farrah, S. R., Rose, J. B., Validity of the indicator organism paradigm for pathogen reduction in reclaimed water and public health protection. *Applied and Environmental Microbiology* **2005,** 71, (6), 3163-3170.
14. Payment, P., Plante, R., Cejka, P., Removal of indicator bacteria, human enteric viruses, *Giardia* cysts, and *Cryptosporidium* oocysts at a large wastewater primary treatment facility. *Canadian Journal of Microbiology* **2001,** 47, (3), 188-193.
15. EPA, Method 1622: *Cryptosporidium* in water by Filtration/IMS/FA, 2005.
16. EPA, Method 1623: *Cryptosporidium* and *Giardia* in Water by Filtration/IMS/FA, 2005.
17. Simmons, O. D., Sobsey, M. D., Heaney, C. D., Schaefer, F. W., Francy, D. S., Concentration and detection of *Cryptosporidium* oocysts in surface water samples by

method 1622 using ultrafiltration and capsule filtration. *Applied and Environmental Microbiology* **2001,** 67, (3), 1123-1127.
18. LeChevallier, M. W., Di Giovanni, G. D., Clancy, J. L., Bukhari, Z., Bukhari, S., Rosen, J. S., Sobrinho, J., Frey, M. M., Comparison of method 1623 and cell culture-PCR for detection of *Cryptosporidium* spp. in source waters. *Applied and Environmental Microbiology* **2003,** 69, (2), 971-979.
19. Feng, Y. Y., Ong, S. L., Hu, J. Y., Song, L. F., Tan, X. L., Ng, W. J., Effect of particles on the recovery of *Cryptosporidium* oocysts from source water samples of various turbidities. *Applied and Environmental Microbiology* **2003,** 69, (4), 1898-1903.
20. Hu, J. Y., Feng, Y. Y., Ong, S. L., Ng, W. J., Song, L. F., Tan, X. L., Chu, X. N., Improvement of recoveries for the determination of protozoa *Cryptosporidium* and *Giardia* in water using method 1623. *Journal of Microbiological Methods* **2004,** 58, (3), 321-325.
21. Bukhari, Z., McCuin, R. M., Fricker, C. R., Clancy, J. L., Immunomagnetic separation of *Cryptosporidium parvum* from source water samples of various turbidities. *Applied and Environmental Microbiology* **1998,** 64, (11), 4495-4499.
22. Kuhn, R. C., Rock, C. M., Oshima, K. H., Effects of pH and magnetic material on immunomagnetic separation of *Cryptosporidium* oocysts from concentrated water samples. *Applied and Environmental Microbiology* **2002,** 68, (4), 2066-2070.
23. Rochelle, P. A., De Leon, R., Johnson, A., Stewart, M. H., Wolfe, R. L., Evaluation of immunomagnetic separation for recovery of infectious *Cryptosporidium parvum* oocysts from environmental samples. *Applied and Environmental Microbiology* **1999,** 65, (2), 841-845.
24. Percival, S. L. A., *Microbiology of waterborne diseases*. Elsevier Academic Press: Amsterdam, 2004.
25. Morozov, V. N., Groves, S., Turell, M. J., Baileyt, C., Three minutes-long electrophoretically assisted zeptornolar microfluidic immunoassay with magnetic-beads detection. *Journal of the American Chemical Society* **2007,** 129, (42), 12628.
26. Abdel-Hamid, I., Ivnitski, D., Atanasov, P., Wilkins, E., Highly sensitive flow-injection immunoassay system for rapid detection of bacteria. *Analytica Chimica Acta* **1999,** 399, (1-2), 99-108.
27. Campbell, G. A., Mutharasan, R., Near real-time detection of *Cryptosporidium parvum* oocyst by IgM-functionalized piezoelectric-excited millimeter-sized cantilever biosensor. *Biosensors & Bioelectronics* **2008,** 23, (7), 1039-1045.
28. Fontaine, M., Guillot, E., An immunomagnetic separation-real-time PCR method for quantification of *Cryptosporidium parvum* in water samples. *Journal of Microbiological Methods* **2003,** 54, (1), 29-36.
29. Kniel, K. E., Higgins, J. A., Trout, J. M., Fayer, R., Jenkins, M. C., Characterization and potential use of a *Cryptosporidium parvum* virus (CPV) antigen for detecting *C. parvum* oocysts. *Journal of Microbiological Methods* **2004,** 58, (2), 189-195.
30. Ochiai, Y., Takada, C., Hosaka, M., Detection and discrimination of *Cryptosporidium parvum* and *C. hominis* in water samples by immunomagnetic separation-PCR. *Applied and Environmental Microbiology* **2005,** 71, (2), 898-903.
31. Rodriguez-Lazaro, D., D'Agostino, M., Herrewegh, A., Pla, M., Cook, N., Ikonomopoulos, J., Real-time PCR-based methods for detection of *Mycobacterium avium*

Subsp paratuberculosis in water and milk. *International Journal of Food Microbiology* **2005,** 101, (1), 93-104.
32. Wolf, S., Williamson, W. M., Hewitt, J., Rivera-Aban, M., Lin, S., Ball, A., Scholes, P., Greening, G. E., Sensitive multiplex real-time reverse transcription-PCR assay for the detection of human and animal noroviruses in clinical and environmental samples. *Applied and Environmental Microbiology* **2007,** 73, (17), 5464-5470.
33. Rochelle, P. A., Ferguson, D. M., Handojo, T. J., DeLeon, R., Stewart, M. H., Wolfe, R. L., An assay combining cell culture with reverse transcriptase PCR to detect and determine the infectivity of waterborne *Cryptosporidium parvum*. *Applied and Environmental Microbiology* **1997,** 63, (5), 2029-2037.
34. NNI National Nanotechnology Initiative. http://www.nano.gov/html/about/funding.html.
35. Cui, Y., Ren, B., Yao, J. L., Gu, R. A., Tian, Z. Q., Synthesis of AgcoreAushell bimetallic nanoparticles for immunoassay based on surface-enhanced Raman spectroscopy. *Journal of Physical Chemistry B* **2006,** 110, (9), 4002-4006.
36. Dou, X., Takama, T., Yamaguchi, Y., Yamamoto, H., Ozaki, Y., Enzyme immunoassay utilizing surface-enhanced Raman scattering of the enzyme reaction product. *Analytical Chemistry* **1997,** 69, (8), 1492-1495.
37. Tombelli, S., Minunni, A., Mascini, A., Analytical applications of aptamers. *Biosensors & Bioelectronics* **2005,** 20, (12), 2424-2434.
38. De la Fuente, J. M., Penades, S., Glyconanoparticles: Types, synthesis and applications in glycoscience, biomedicine and material science. *Biochimica Et Biophysica Acta-General Subjects* **2006,** 1760, (4), 636-651.
39. Shen, Z. H., Huang, M. C., Xiao, C. D., Zhang, Y., Zeng, X. Q., Wang, P. G., Nonlabeled quartz crystal microbalance biosensor for bacterial detection using carbohydrate and lectin recognitions. *Analytical Chemistry* **2007,** 79, (6), 2312-2319.
40. Ngundi, M. M., Kulagina, N. V., Anderson, G. P., Taitt, C. R., Nonantibody-based recognition: alternative molecules for detection of pathogens. *Expert Review of Proteomics* **2006,** 3, (5), 511-524.
41. Haes, A. J., Van Duyne, R. P., A nanoscale optical biosensor: Sensitivity and selectivity of an approach based on the localized surface plasmon resonance spectroscopy of triangular silver nanoparticles. *Journal of the American Chemical Society* **2002,** 124, (35), 10596-10604.
42. Bokken, G., Corbee, R. J., van Knapen, F., Bergwerff, A. A., Immunochemical detection of Salmonella group B, D and E using an optical surface plasmon resonance biosensor. *FEMS Microbiology Letters* **2003,** 222, (1), 75-82.
43. Xu, S. P., Ji, X. H., Xu, W. Q., Zhao, B., Dou, X. M., Bai, Y. B., Ozaki, Y., Surface-enhanced Raman scattering studies on immunoassay. *Journal of Biomedical Optics* **2005,** 10, (3).
44. Tully, E., Hearty, S., Leonard, P., O'Kennedy, R., The development of rapid fluorescence-based immunoassays, using quantum dot-labelled antibodies for the detection of *Listeria monocytogenes* cell surface proteins. *International Journal of Biological Macromolecules* **2006,** 39, (1-3), 127-134.

45. Brewster, J. D., Mazenko, R. S., Filtration capture and immunoelectrochemical detection for rapid assay of *Escherichia coli O157:H7*. *Journal of Immunological Methods* **1998,** 211, (1-2), 1-8.
46. Campbell, G. A., Mutharasan, R., A method of measuring *Escherichia coli O157:H7* at 1 cell/mL in 1 liter sample using antibody functionalized piezoelectric-excited millimeter-sized cantilever sensor. *Environmental Science & Technology* **2007,** 41, (5), 1668-1674.
47. Homann, M., Goringer, H. U., Combinatorial selection of high affinity RNA ligands to live African trypanosomes. *Nucleic Acids Research* **1999,** 27, (9), 2006-2014.
48. El-Boubbou, K., Gruden, C., Huang, X., Magnetic glyco-nanoparticles: A unique tool for rapid pathogen detection, decontamination, and strain differentiation. *Journal of the American Chemical Society* **2007,** 129, (44), 13392-+.
49. Iqbal, S. S., Mayo, M. W., Bruno, J. G., Bronk, B. V., Batt, C. A., Chambers, J. P., A review of molecular recognition technologies for detection of biological threat agents. *Biosensors & Bioelectronics* **2000,** 15, (11-12), 549-578.
50. Leonard, P., Hearty, S., Brennan, J., Dunne, L., Quinn, J., Chakraborty, T., O'Kennedy, R., Advances in biosensors for detection of pathogens in food and water. *Enzyme and Microbial Technology* **2003,** 32, (1), 3-13.
51. Ni, J., Lipert, R. J., Dawson, G. B., Porter, M. D., Immunoassay readout method using extrinsic Raman labels adsorbed on immunogold colloids. *Analytical Chemistry* **1999,** 71, (21), 4903-4908.
52. Kalele, S. A., Kundu, A. A., Gosavi, S. W., Deobagkar, D. N., Deobagkar, D. D., Kulkarni, S. K., Rapid detection of *Escherichia coli* by using anti body-conjugated silver nanoshells. *Small* **2006,** 2, (3), 335-338.
53. Elgert, K. D., *Immunology: Unterstanding the Immune System*. Wiley-Liss: New York, 1996.
54. Desphande, S. S., *Enzyme Immunoassays: From Concept to Product Development*. Chapman & Hall: New York, 1996.
55. Sturbaum, G. D., Klonicki, P. T., Marshall, M. M., Jost, B. H., Clay, B. L., Sterling, C. R., Immunomagnetic Separation (IMS)-Fluorescent Antibody Detection and IMS-PCR Detection of Seeded *Cryptosporidium parvum* Oocysts in Natural Waters and Their Limitations. *Applied and Environmental Microbiology* **2002,** 68, (6), 2991-2996.
56. USEPA, Method 1623: *Cryptosporidium* and *Giardia* in Water by Filtration/IMS/FA. In United States Environmental Protection Agency: 2005; p 76.
57. Park, Y., Cho, Y. H., Jee, Y., Ko, G., Immunomagnetic separation combined with real-time reverse transcriptase PCR assays for detection of norovirus in contaminated food. *Applied and Environmental Microbiology* **2008,** 74, (13), 4226-4230.
58. Pyle, B. H., Broadaway, S. C., McFeters, G. A., Sensitive detection of Escherichia coli O157 : H7 in food and water by immunomagnetic separation and solid-phase laser cytometry. *Applied and Environmental Microbiology* **1999,** 65, (5), 1966-1972.
59. Liu, G. M., Han, Y. L., Li, X., Song, S. Y., Applicability of a rapid method based on immunomagnetic capture-fluorescent PCR assay for Camphylobacter jejuni. *Food Control* **2006,** 17, (7), 527-532.

60. Hoffman, R. M., Wolk, D. M., Spencer, S. K., Borchardt, M. A., Development of a method for the detection of waterborne microsporidia. *Journal of Microbiological Methods* **2007,** 70, (2), 312-318.
61. Campbell, A., Smith, H., Immunomagnetic separation of Cryptosporidium oocysts from water samples: Round robin comparison of techniques. *Water Science and Technology* **1997,** 35, (11-12), 397-401.
62. Grubisha, D. S., Lipert, R. J., Park, H. Y., Driskell, J., Porter, M. D., Femtomolar detection of prostate-specific antigen: An immunoassay based on surface-enhanced Raman scattering and immunogold labels. *Analytical Chemistry* **2003,** 75, (21), 5936-5943.
63. Xu, S. P., Ji, X. H., Xu, W. Q., Li, X. L., Wang, L. Y., Bai, Y. B., Zhao, B., Ozaki, Y., Immunoassay using probe-labelling immunogold nanoparticles with silver staining enhancement via surface-enhanced Raman scattering. *Analyst* **2004,** 129, (1), 63-68.
64. Driskell, J. D., Kwarta, K. M., Lipert, R. J., Porter, M. D., Neill, J. D., Ridpath, J. F., Low-level detection of viral pathogens by a surface-enhanced Raman scattering based immunoassay. *Analytical Chemistry* **2005,** 77, (19), 6147-6154.
65. Abdel-Hamid, I., Ivnitski, D., Atanasov, P., Wilkins, E., Flow-through immunofiltration assay system for rapid detection of E-coli O157 : H7. *Biosensors & Bioelectronics* **1999,** 14, (3), 309-316.
66. Endo, T., Kerman, K., Nagatani, N., Hiepa, H. M., Kim, D. K., Yonezawa, Y., Nakano, K., Tamiya, E., Multiple label-free detection of antigen-antibody reaction using localized surface plasmon resonance-based core-shell structured nanoparticle layer nanochip. *Analytical Chemistry* **2006,** 78, (18), 6465-6475.
67. Jayasena, S. D., Aptamers: An emerging class of molecules that rival antibodies in diagnostics. *Clinical Chemistry* **1999,** 45, (9), 1628-1650.
68. Fleischmann, M., Hendra, P., McQuillan, A., Raman Spectra of Pyridine Adsorbed at a Silver Electrode. *Chemical Physics Letters* **1974,** 26, (2), 163-166.
69. Albrecht, M. G., Albrecht, M. Grant; J. Alan Creighton (1977). Anomalously Intense Raman Spectra of Pyridine at a Silver Electrode. *Journal of the American Chemical Society* **1977,** 99, (15), 5215-5219.
70. Jeanmaire, D. L., Duyne, R. P. V., Surface raman spectroelectrochemistry Part I. Heterocyclic, aromatic, and aliphatic amines adsorbed on the anodized silver electrode. *Journal of Electroanalytical Chemistry* **1977,** 84, (1), 1-20.
71. Moskovits, M., Surface-enhanced Raman spectroscopy: a brief retrospective. *Journal of Raman Spectroscopy* **2005,** 36, (6-7), 485-496.
72. Stacy, A. M., Vanduyne, R. P., Surface enhanced Raman and resonance Raman-spectroscopy in a non-aqueous electrochemical environment- Tris(2,2'-Bipyridine)Ruthenium(II) adsorbed on silver from acetonitrile *Chemical Physics Letters* **1983,** 102, (4), 365-370.
73. Nie, S. M., Emery, S. R., Probing single molecules and single nanoparticles by surface-enhanced Raman scattering. *Science* **1997,** 275, (5303), 1102-1106.
74. Kneipp, K., Wang, Y., Kneipp, H., Perelman, L. T., Itzkan, I., Dasari, R., Feld, M. S., Single molecule detection using surface-enhanced Raman scattering (SERS). *Physical Review Letters* **1997,** 78, (9), 1667-1670.

75. Kneipp, K., Kneipp, H., Manoharan, R., Hanlon, E. B., Itzkan, I., Dasari, R. R., Feld, M. S., Extremely large enhancement factors in surface-enhanced Raman scattering for molecules on colloidal gold clusters. *Applied Spectroscopy* **1998,** 52, (12), 1493-1497.
76. Chourpa, I., Lei, F. H., Dubois, P., Manfait, M., Sockalingum, G. D., Intracellular applications of analytical SERS spectroscopy and multispectral imaging. *Chemical Society Reviews* **2008,** 37, (5), 993-1000.
77. Bell, S. E. J., Sirimuthu, N. M. S., Quantitative surface-enhanced Raman spectroscopy. *Chemical Society Reviews* **2008,** 37, (5), 1012-1024.
78. Allain, L. R., Vo-Dinh, T., Surface-enhanced Raman scattering detection of the breast cancer susceptibility gene BRCA1 using a silver-coated microarray platform. *Analytica Chimica Acta* **2002,** 469, (1), 149-154.
79. Faulds, K., Smith, W. E., Graham, D., DNA detection by surface enhanced resonance Raman scattering (SERRS). *Analyst* **2005,** 130, (8), 1125-1131.
80. Goeller, L. J., Riley, M. R., Discrimination of bacteria and bacteriophages by Raman spectroscopy and surface-enhanced Raman spectroscopy. *Applied Spectroscopy* **2007,** 61, (7), 679-685.
81. Grow, A. E., Wood, L. L., Claycomb, J. L., Thompson, P. A., New biochip technology for label-free detection of pathogens and their toxins. *Journal of Microbiological Methods* **2003,** 53, (2), 221-233.
82. Shanmukh, S., Jones, L., Driskell, J., Zhao, Y. P., Dluhy, R., Tripp, R. A., Rapid and sensitive detection of respiratory virus molecular signatures using a silver nanorod array SERS substrate. *Nano Letters* **2006,** 6, (11), 2630-2636.
83. Schwartzberg, A. M., Grant, C. D., Wolcott, A., Talley, C. E., Huser, T. R., Bogomolni, R., Zhang, J. Z., Unique gold nanoparticle aggregates as a highly active surface-enhanced Raman scattering substrate. *Journal of Physical Chemistry B* **2004,** 108, (50), 19191-19197.
84. Banholzer, M. J., Millstone, J. E., Qin, L. D., Mirkin, C. A., Rationally designed nanostructures for surface-enhanced Raman spectroscopy. *Chemical Society Reviews* **2008,** 37, (5), 885-897.
85. Sengupta, A., Laucks, M. L., Dildine, N., Drapala, E., Davis, E. J., Bioaerosol characterization by surface-enhanced Raman spectroscopy (SERS). *Journal of Aerosol Science* **2005,** 36, (5-6), 651-664.
86. Zeiri, L., Bronk, B. V., Shabtai, Y., Czege, J., Efrima, S., Silver metal induced surface enhanced Raman of bacteria. *Colloids and Surfaces a-Physicochemical and Engineering Aspects* **2002,** 208, (1-3), 357-362.
87. Zeiri, L., Bronk, B. V., Shabtai, Y., Eichler, J., Efrima, S., Surface-enhanced Raman spectroscopy as a tool for probing specific biochemical components in bacteria. *Applied Spectroscopy* **2004,** 58, (1), 33-40.
88. Zeiri, L., Efrima, S., Surface-enhanced Raman spectroscopy of bacteria: the effect of excitation wavelength and chemical modification of the colloidal milieu. *Journal of Raman Spectroscopy* **2005,** 36, (6-7), 667-675.
89. Escoriza, M. F., VanBriesen, J. M., Stewart, S., Maier, J., Treado, P. J., Raman spectroscopy and chemical imaging for quantification of filtered waterborne bacteria. *Journal of Microbiological Methods* **2006,** 66, (1), 63-72.

90. Chaney, S. B., Shanmukh, S., Dluhy, R. A., Zhao, Y. P., Aligned silver nanorod arrays produce high sensitivity surface-enhanced Raman spectroscopy substrates. *Applied Physics Letters* **2005,** 87, (3).
91. Casas, N., Sunen, E., Detection of enteroviruses, hepatitis A virus and rotaviruses in sewage by means of an immunomagnetic capture reverse transcription-PCR assay. *Microbiological Research* **2002,** 157, (3), 169-175.
92. Vivier, J. C., Ehlers, M. M., Grabow, W. O. K., Detection of enteroviruses in treated drinking water. *Water Research* **2004,** 38, (11), 2699-2705.
93. Hwang, Y. C., Leong, O. M., Chen, W., Yates, M. V., Comparison of a reporter assay and immunomagnetic separation real-time reverse transcription-PCR for the detection of enteroviruses in seeded environmental water samples. *Applied and Environmental Microbiology* **2007,** 73, (7), 2338-2340.
94. Escoriza, M. F., Vanbriesen, J. M., Stewart, S., Maier, J., Studying bacterial metabolic states using Raman spectroscopy. *Applied Spectroscopy* **2006,** 60, (9), 971-976.
95. Escoriza, M. F., VanBriesen, J. M., Stewart, S., Maier, J., Raman spectroscopic discrimination of cell response to chemical and physical inactivation. *Applied Spectroscopy* **2007,** 61, (8), 812-823.
96. Park, T., Lee, S., Seong, G. H., Choo, J., Lee, E. K., Kim, Y. S., Ji, W. H., Hwang, S. Y., Gweon, D. G., Highly sensitive signal detection of duplex dye-labelled DNA oligonucleotides in a PDMS microfluidic chip: confocal surface-enhanced Raman spectroscopic study. *Lab on a Chip* **2005,** 5, (4), 437-442.
97. Cao, Y. W. C., Jin, R. C., Mirkin, C. A., Nanoparticles with Raman spectroscopic fingerprints for DNA and RNA detection. *Science* **2002,** 297, (5586), 1536-1540.
98. Su, X., Zhang, J., Sun, L., Koo, T. W., Chan, S., Sundararajan, N., Yamakawa, M., Berlin, A. A., Composite organic-inorganic nanoparticles (COINs) with chemically encoded optical signatures. *Nano Letters* **2005,** 5, (1), 49-54.
99. Jin, R. C., Cao, Y. C., Thaxton, C. S., Mirkin, C. A., Glass-bead-based parallel detection of DNA using composite Raman labels. *Small* **2006,** 2, (3), 375-380.
100. Driskell, J. D., Lipert, R. J., Porter, M. D., Labeled gold nanoparticles immobilized at smooth metallic substrates: Systematic investigation of surface plasmon resonance and surface-enhanced Raman scattering. *Journal of Physical Chemistry B* **2006,** 110, (35), 17444-17451.
101. Naja, G., Bouvrette, P., Hrapovic, S., Luong, J. H. T., Raman-based detection of bacteria using silver nanoparticles conjugated with antibodies. *Analyst* **2007,** 132, (7), 679-686.

3) Surface-Enhanced Resonance Raman Spectroscopy for the Rapid Detection of *Cryptosporidium parvum* and *Giardia lamblia*

Krista L. Rule and Peter J. Vikesland*

Department of Civil and Environmental Engineering, Virginia Polytechnic Institute and State University, 418 Durham Hall, Blacksburg, VA 24060-0246

ABSTRACT

A rapid surface enhanced resonance Raman spectroscopy (SERRS) method has been developed for the detection of two waterborne pathogens, *Cryptosporidium parvum* and *Giardia lambia*. Raman labels were prepared by conjugating gold nanoparticles with commercial antibodies and dye molecules. After incubation with the immunogold labels, *C. parvum* oocysts and *G. lamblia* could easily be measured and differentiated by Raman spectroscopy. The immungold signal intensities were optimized by testing several sizes of gold nanoparticles, four different commercially available dye molecules, and two Raman excitation wavelengths. Raman maps were collected across fixed and labeled *Cryptosporidium* oocysts and *Giardia* cysts and the maps were used to determine which *C. parvum* and *G. lamblia* antibodies exhibited the best specificities and organism coverages. Ultimately, 40 nm gold nanoparticles were conjugated with Rhodamine B

isothiocyanate and Malachite Green isothiocyanate for the *C. parvum* and *G. lamblia* immunogold syntheses, respectively. *C. parvum* monoclonal IgM antibodies and *G. lamblia* monoclonal IgG1 antibodies resulted in the best immunogold coverage. The research presented here demonstrates the feasibility of utilizing SERRS labeling for sensitive multi-pathogen monitoring strategies.

3.1 INTRODUCTION

Despite major advances in water treatment, periodic outbreaks of waterborne disease continue to plague both developing and developed countries. In addition, human population growth and climate change are expected to lead to increases in the number of species and concentrations of waterborne pathogens in surface and ground waters. To minimize the chances for outbreaks to occur, drinking water utilities monitor their finished drinking waters for pathogens that survive the treatment process. Pathogen monitoring programs protect the public against both naturally occurring pathogens and potential bioterrorist threats to drinking water supplies.

In the U.S., finished drinking waters are commonly monitored for total coliform, *Cryptosporidium parvum*, and *Giardia lamblia*.[1] Coliform bacteria are a subset of gram-negative bacteria that have historically been used as fecal surrogates in water monitoring. *C. parvum* and *G. lamblia* are protozoan pathogens that can cause gastrointestinal illnesses that are potentially deadly for immunocompromised individuals. During water treatment, *C. parvum* and *G. lamblia* are removed by flocculation/sedimentation and filtration, but are not readily inactivated by commonly employed drinking water disinfectants.[2-4] EPA methods 1622 and 1623, the methods used in the U.S. for *C. parvum* and *G. lamblia* monitoring, are consistently plagued by poor recoveries.

Furthermore, these methods include a number of steps that require high levels of analytical and biological expertise and are thus not readily done onsite. There has been a push for innovative approaches to pathogen detection in drinking water to overcome the shortcomings of these pathogen-monitoring strategies. Proposed techniques include PCR,[5-8] antibody-antigen based detection,[9] and cell culture.[10] Ideally, future methods will be capable of real time, multiplex detection and will have extremely low detection limits.

Raman scattering techniques have elicited significant attention for biomolecule detection as they provide several advantages over other spectroscopic techniques.[11-13] Unlike IR and NMR, Raman signals are not affected by the presence of water and Raman bands are much narrower than fluorescence bands. Raman active molecules exhibit characteristic "fingerprint" spectra that can be used to definitively identify a molecule. Additionally, Raman responses are less susceptible to photobleaching than fluorescence responses, thus allowing longer signal collection times and improved signal averaging. Normal Raman signals are too weak to be of use in ultrasensitive detection methods, but surface enhanced Raman spectroscopy (SERS) results in Raman signal enhancement factors as high as 10^{14}.[14] SERS is the result of chemical and electromagnetic interactions between the surface plasmons in a noble metal (gold or silver most commonly) and a surface associated chemical.[15] A resonance enhancement (SERRS) in addition to SERS enhancement can be observed when the target molecule has an electronic transition close to or coincident with the Raman excitation laser wavelength. SERS/SERRS have been used to study bacteria,[16] for medical diagnostics,[17] and for multiplex DNA and protein detection strategies.[18, 19] Despite a recent surge in SERS/SERRS-based biochemical

detection, significantly less attention has been given to whole cell or microorganism detection.

Here we report on SERRS immunogold labeling for the detection of *C. parvum* and *G. lamblia*. The immunogold conjugates used in our study consist of gold nanoparticles conjugated with antibodies specific to *C. parvum* or *G. lamblia* and SERRS active reporter molecules. This type of label has been used for SERS detection in a number of biomolecule detection studies.[20-25] Unlike previous reports that have dealt with relatively small biomolecules such as proteins, viruses, and nucleic acids; we report here on the detection of protozoan pathogens in their infective, environmental form. With diameters between 3 and 13 μm, these organisms are large enough to be identified with an optical microscope when they have been fixed to glass microscope slides. We were therefore able to collect Raman maps across the surfaces of *C. parvum* cysts and *G. lamblia* oocysts, probing the interaction between the SERS active immunogold and the organisms' surfaces. The Raman results elucidated the specificities and affinities of the immunogold conjugates to their respective analytes and allowed optimization of the immunogold synthesis procedure (i.e., antibody type, reporter dye identity, nanoparticle size). Our results suggest this type of detection strategy can be readily multiplexed to simultaneously detect numerous waterborne pathogens. To our knowledge this is the first time living organisms have been labeled with immunogold and detected using XY Raman mapping.

3.2 MATERIALS AND METHODS

3.2.1 Reagents and buffer solutions

$HAuCl_4 \cdot 3H_2O$, trisodium citrate dihydrate (+99%), rhodamine B isothiocyanate (RBITC), fluorescein isothiocyanate (FITC), bovine serum albumin (BSA), and Tween 80 were purchased from Sigma-Aldrich (St. Louis, MO) and were used without further purification. Malachite green isothiocycante (MGITC) and X-rhodamine isothiocyanate (XRITC) were acquired from Invitrogen Corp. (Grand Island, NY). Mouse monoclonal IgG1 antibodies against *G. lamblia* and mouse polyclonal IgG fraction antibodies against *G. lamblia* were obtained from Meridian Life Sciences (Cincinnati, OH). Mouse monoclonal IgM antibodies against *C. parvum* were obtained from Millipore Antibodies (Temecula, CA) and mouse polyclonal IgG fraction antibodies against *C. parvum* were purchased from Abcam Inc., (Cambridge, MA). Ultrapure water (>18 $M\Omega cm^{-1}$) was used in all aqueous solutions. The following buffer solutions were used in the experiments: phosphate buffered saline (PBS, 10 mM KH_2PO_4/Na_2HPO_4, 150 mM NaCl, 3 mM KCl, pH 7.4), borate buffer (BB, 2 mM, pH 9).

C. parvum oocysts and *G. lamblia* cysts were purchased from Waterborne, Inc. (New Orleans, LA). (Oo)cysts were washed twice by centrifugation and stored in a reagent water/0.1% Tween 80 solution at 4 °C. Washed cyst and oocyst stocks were enumerated with a hemacytometer prior to use. Oocyst solutions were used within three months of purchase and cysts were used within one month of purchase.

3.2.2 Instrumentation

Raman spectra were obtained with a JY Horiba LabRAM HR 800 spectrometer, with 600 grooves/mm gratings and a slit width of 150 μm. The instrument is equipped

with an Olympus BX-41 petrographic microscope and an Ancor electronically cooled CCD detector. Excitation was provided by a 632.8 nm He-Ne laser. A long working distance 40× objective (N.A. = 0.75) was used to focus the laser beam. Sample slides were mounted on a motorized microscope stage (Marzhauser EK-32) and an automated video camera fitted to the microscope was used to capture the optical image of the map area. For mapping experiments, Raman spectra from 1000 to 1800 cm^{-1} were collected at each map position with 1 s acquisition. This spectral range was large enough to include several characteristic reporter molecule peaks and was small enough to prevent the 600 lines/mm grating from moving during collection. Transmission electron micrographs were collected with a JEOL 100 CX-II transmission electron microscope (TEM). UV-VIS-NIR absorption spectra were obtained with a Varian Cary 5000 spectrophotometer.

3.2.3. Gold nanoparticle and immunogold conjugate syntheses

Gold nanoparticle seeds with diameters of 13 nm were prepared by the method of Frens.[26] Gold nanoparticles with average diameters between 20 and 80 nm were prepared by a seeding method in order to obtain nanoparticle solutions with improved diameter homogeneities. Contaminants on glassware surfaces and particulates in the reagent solutions can act as nucleation sites for particle growth and can thus lead to nanoparticle solutions with large diameter dispersivities.[27] For this reason, all glassware was bathed in aqua regia (75% HCl, 25% HNO_3) and rinsed copiously with ultrapure water prior to use and all reagent solutions were filtered through polycarbonate membrane filters with 0.2 μm pores prior to their use in nanoparticle synthesis. Immediately following nanoparticle synthesis, UV-Vis absorption spectra were collected to measure the intrinsic surface plasmon peak whose position and width give information about the nanoparticle size and

homogeneity, respectively.[28] If the surface plasmon peaks indicated the prepared nanoparticles were of the expected size and homogeneity, TEM images were collected and were used in conjunction with NIH ImageJ software to accurately quantify average nanoparticle diameters and particle homogeneity. Solutions that were found to have diameter dispersivities greater than 20% were discarded. Nanoparticle solutions were stored in amber glass bottles at 4 °C and under these conditions the solutions were stable for several months.

Synthesis of the optimized *C. parvum* and *G. lamblia* immunogold conjugates was conducted by spiking 0.3 mL aliquots of 40 nm gold nanoparticles with 1.2 μL of methanolic RBITC and MGITC stock solutions (5 μM), respectively. The gold nanoparticles were allowed to react with the dye molecules overnight. The conjugates were centrifuged at 2000 rpm for 10 minutes at which point the clear centrate containing unbound dye molecules was discarded and the loose sediment was resuspended in borate buffer. To the RBITC nanoparticle conjugates, 3 μL of *C. parvum* IgM antibody concentrate was added and to the MGITC nanoparticle conjugates, 40 μL of *G. lamblia* IgG1 antibody concentrate was added. After reacting for 30 minutes, 30 μL of 10% BSA in borate buffer was added to each of the immunogold solutions to prevent immunogold loss during the following centrifugation steps. After reacting for another 90 minutes, the immunogold conjugates were centrifuged for 10 minutes at 2000 RPM. The centrate was discarded and the loose sediment was resuspended in borate buffer. After a final centrifugation, the immunogold conjugates were resuspended in PBS buffer containing 0.1% Tween 80. The immunogold conjugates were filtered through polycarbonate membrane filters with 0.4 μm pores and stored at 4 ˚C prior to use.

3.3 RESULTS AND DISCUSSION

3.3.1 Gold nanoparticle production and labeling

Small, organic molecules such as thiophenol, mercaptobenzoic acid, and napthalenethiol[22, 24, 29] are commonly used as reporter molecules in SERS immunogold as they can be readily conjugated to gold substrates. Resonance enhancement of the Raman signal, however, is not achieved with these molecules when visible excitation is employed. Resonance Raman can lead to an additional enhancement of the Raman signal and is desirable for low-level analyte detection. To address this, Doering and Nie labeled gold nanoparticles with dye molecules containing isothiocyanate groups.[30] In addition to binding strongly with gold through their isothiocyanate functional groups, these molecules have strong electronic transitions in the visible range. They are therefore capable of surface enhanced resonance Raman spectroscopy (SERRS) when visible excitation lasers are employed. We considered four dye molecules with isothiocyanate functional groups for our *C. parvum* and *G. lamblia* immunogold conjugates: Fluorescein Isothiocyanate (FITC), Rhodamine B Isothiocyanate (RBITC), Malachite Green Isothiocyanate (MGITC), and X-Rhodamine Isothiocyanate (X-RITC). When added to the gold nanoparticle solutions, FITC Raman signals were much weaker than the signals of the other three molecules at the same dye concentration (Figure 3.1). FITC has an absorption maximum at 488 nm, while the other three molecules have maxima closer to the laser excitation wavelength of 633 nm (Figure 3.1), and thus resonance Raman plays less of a role in the FITC signal enhancement. RBITC and X-RITC exhibit very similar SERRS spectra, and so the two dyes would be difficult to distinguish from one another in a multiplex Raman assay. MGITC and RBITC, however, have very different SERS

spectra and thus allow for simultaneous SERS detection of MGITC and RBITC conjugated immunogold. We employed MGITC and RBITC in the *G. lamblia* and the *C. parvum* immunogold conjugates, respectively. The MGITC and RBITC nanogold conjugates were prepared by spiking aliquots of nanogold with methanolic dye stocks, allowing the solution to react for several hours, and then collecting the conjugates with centrifugation. Too much coverage by the dye molecule on the nanoparticles can lead to a destabilized immunogold solution. As stable conjugate solutions are important for immuno-recognition events, the appropriate dye concentrations for stable immunogold conjugates were established through dye stabilization assays;[22] See the Supporting Information for additional details.

Gold nanoparticles of 13 nm diameter prepared by citrate-reduction of $HAuCl_4$ were initially used in this study because this size nanoparticle can be readily synthesized. Use of the 13 nm particles, however, lead to poor SERRS enhancements of the RBITC and MGITC dye signals (Supporting Information Figure 3.S1). The SERS signals from immunogold prepared with the 13 nm particles could not be detected on the surface of oocysts and cysts incubated with their respective immunogold labels. Previous research has demonstrated that gold nanoparticles of ≈63 nm diameter are optimal for SERRS enhancement with 647-nm laser excitation.[31] We therefore prepared gold nanoparticles with average diameters between 20 and 80 nm by seed-mediated growth[27] and compared the resulting SERS enhancements of RBITC solutions when excited with the 633 nm laser. Similar to previous reports, the Raman RBITC signals increased as the average diameter of the gold nanoparticles increased up to about 60 nm (Supporting Information 3.S2). TEM images of the solutions with particle diameters greater than 50 nm, however,

showed irregularly shaped particles and often also contained un-nucleated seed-sized particles. Furthermore, SERS enhancements of the >50 nm solutions were difficult to reproduce despite consecutive batches having similar average diameters. On the other hand, nanoparticle solutions prepared with average diameters below 50 nm were more spherical in shape and SERS enhancements were highly reproducible (Supporting Information Figure 3.S3). Although they exhibited lower enhancements than the 60 nm particles, they exhibited signals 100× greater than the 13 nm particles (Supporting Information Figure 3.S1). Nanoparticle solutions with average diameters of 38-42 nm could be repeatedly synthesized with standard deviations less than 5 nm and were employed in all subsequent immunogold conjugate syntheses.

Gold nanoparticles with average diameters of 20, 40, 60, and 80 nm were also purchased from a common supplier (Ted Pella, Redding, CA). SERRS RBITC signals collected in the presence of these commercial nanoparticles were consistently lower than those collected with the nanoparticles prepared in our laboratory for each of the diameters. TEM analysis of both the commercial and the synthesized nanoparticles indicated that although the solutions had particles with similar average diameters and dispersivities, the nanoparticles prepared in-house tended to be more faceted and ovoid in shape relative to the purchased nanoparticles (Figure 3.2). Ellipsoidal gold nanoparticles and gold nanoparticles with sharp structural features have been shown to be better SERS enhancers than spherical gold nanoparticles in previous work.[32] It is also possible that the differences in SERS enhancements were due differences in the commercial nanoparticles' surface chemistries or aggregation states. Unfortunately, the manufacturer does not

disclose the employed nanoparticle synthesis method although they do report that the nanoparticles are citrate stablized.

3.3.2 Immunogold optimization

Protozoa were fixed by placing 20 μL drops containing 1000 oocysts and/or 1000 cysts into the wells of glass microscope slides. The slides were incubated with a 5% BSA solution to discourage nonspecific binding of the immunogold. After rinsing away unbound BSA, 50 μL of immunogold was added to the wells and the slides were placed in a humidity chamber for 30 minutes. Slides were rinsed in PBS buffer with 0.1% Tween 80, dried, and then 50 μL of immunogold-SERS label solution was pippetted onto the protozoa spots. The slides were incubated with immunogold in the humidity chamber for two hours and then dried after rinsing with PBS/0.1% Tween 80. A drop of 60% glycerol/40% PBS mounting media was placed over the wells and a coverslip was sealed in place with adhesive. Finished slides were stored at 4 °C until analysis. Prior to the collection of Raman spectra, brightfield microscopy was used to locate organisms on the slide and to focus the Raman laser on an organism. *C. parvum* oocysts are spherical with average diameters of 3-5 μm and *G. lamblia* are ovoid with long axis diameters of approximately 11-14 μm and short axis diameters of approximately 8-10 μm. Both organisms were clearly identifiable on the prepared slides.

Immunogold labels were prepared for *C. parvum* and *G. lamblia* with both polyclonal and monoclonal antibodies. For *C. parvum*, an IgM antibody immunogold and a polyclonal IgG fraction antibody immunogold were prepared. For *G. lamblia*, an IgG1 antibody immunogold and a polyclonal IgG fraction immunogold were prepared. Past papers describing the synthesis of immunogold for SERS detection have

recommended antibody concentrations that are 150% of the concentration needed to coat the particle surface, as determined by flocculation tests,[33, 34] to maximize particle stability.[21, 22] We therefore performed flocculation tests for each of our commercial antibodies to determine the amount required to coat the nanoparticle surfaces. The commercial *C. parvum* and *G. lamblia* polyclonal IgG antibodies saturated the 40 nm particle-dye molecule conjugates when the antibody concentrations were >8 μg/mL and thus 12 μg/mL was used in subsequent polyclonal immunogold syntheses. *C. parvum* IgM monoclonal antibodies saturated the surface of the 40 nm gold nanoparticles when >6 μL of the monoclonal IgM solution (the exact ascites IgM concentration was not provided by the supplier) was added to 1 mL of nanoparticle solution and so 9 μL of the antibody concentrate was used per mL of nanoparticles in subsequent syntheses. Interestingly, the addition of the *G. lamblia* and *C. parvum* IgG1 monoclonal antibodies led to destabilized nanoparticle solutions at all tested antibody concentrations and thus it was impossible to find an appropriate IgG1 concentration with flocculation tests. We did, however, find that adding BSA to the nanoparticle-antibody conjugates after they had reacted for 20 minutes resulted in a stabilized immunogold solution. In subsequent IgG1 antibody immunogold syntheses, we used the concentration of antibodies determined to be adequate in the polyclonal IgG flocculation assays (12 μg/mL) and included this BSA stabilization step.

The monoclonal immunogold and the polyclonal immunogold solutions were incubated with their respective organisms and their binding characteristics were compared. Raman measurements were collected at three points across the surface of the oocysts and six points along the cyst surfaces and the collected peak intensities were

averaged for each type of immunogold. Raman signals collected on *Giardia* cysts incubated with monoclonal *Giardia* IgG1 immunogold resulted in positive label signals on 20 out of 20 cysts, while cysts incubated with polyclonal *Giardia* immunogold resulted in positive signals on 18 of 20 cysts. On average, the immunogold SERS signals were an order of magnitude higher for the monoclonal *Giardia* IgG1 immunogold labeled cysts than they were for the polyclonal *Giardia* immunogold labeled cysts. For *C. parvum* immunogold, 20 out of 20 oocysts resulted in positive signals when incubated with the *C. parvum* IgM monoclonal antibody immunogold and 18 out of 20 oocysts had positive signals when incubated with *C. parvum* polyclonal antibody immunogold. The average signal intensities were approximately 20% higher on the oocysts incubated with monoclonal *C. parvum* IgM antibody immunogold. Maps collected across oocysts and cysts incubated with the two polyclonal immunogolds showed inconsistent coverage of the labels, while maps collected across oocysts and cysts incubated with the monoclonal immunogolds show full coverage of the immunogold signals. Specification sheets provided by the antibody vendors indicated that the monoclonal antibodies were specific to surface antigens on the oocysts and cysts. The polyclonal IgG antibodies to *C. parvum* and *G. lambia* were probably less successful in SERS detection because they consist of a mixture of antibodies specific to different oocyst and cyst antigens. Based on these results, it was determined that the monoclonal antibodies were better suited for SERS immunogold labeling. Subsequently, immunogold was prepared only with monoclonal antibodies.

The selectivity and sensitivity of the monoclonal immunogold solutions to their respective organisms were determined by examining twenty oocysts and twenty cysts for

the characteristic MGITC and RBITC signals after incubation with both anti-*Giardia* and anti-*C. parvum* monoclonal immunogold solutions. Raman measurements were collected at three points across the surface of an oocyst and six points along the surface of a cyst. A RBITC signal was considered a true positive if it was co-located with *C. parvum* and a MGITC signal was considered a true positive if it was co-located with *G. lamblia*. Signals were considered false positives if they were obtained on the incorrect organism. *Cryptosporidium* immunogold showed a specificity of 85% and a sensitivity of 100%. The specificity of the *Giardia* immunogold was 100% and the sensitivity was 100%.

As illustrated in Figure 3.3A and 3.3B, a map of the intensity of the characteristic Raman RBITC peak at 1647 cm^{-1} shows the location of the *Cryptosporidium parvum* oocysts. A map of the characteristic RBITC peak at 1360 cm^{-1} gives similar results (Figure 3.3C). The area on the Raman map exhibiting an RBITC signal has a diameter of approximately 12 μm which is approximately twice the size of the oocyst. The 40× objective has a nominal spot size of ~ 4 μm and thus the RBITC signal is detected over a larger area than the actual area of the organism. Similarly, the characteristic MGITC peaks at 1618 cm^{-1} and 1175 cm^{-1} were observed across the surface of the *G. lamblia* surface (Figures 3.3E and 3.3F). As expected based on the specificity determinations, there were no MGITC signals observed across the surface of the *C. parvum* oocysts and only rarely was an RBITC signal observed at any point on the surface of the *Giardia* cysts. This result indicates that the respective antibodies of the two protozoa do not cross-react. It also suggests that the RBITC and MGITC dyes in the immunogold conjugates do not swap between one type of immunogold and another during incubation.

Raman maps of the intensities of the RBITC 1647 cm^{-1} peak (Figure 3.3B) and the MGITC 1618 cm^{-1} peak (Figure 3.3E) correctly differentiate between oocysts and cysts. This type of simplistic characteristic-peak identification, however, may lead to the misidentification of organisms. For example, upon close inspection of the map in Figure 3.3C, one can see that there is a slight detection of the RBITC 1360 cm^{-1} peak over the area of the Giardia cyst. Similarly in Figure 3.3F, it appears that the MGITC 1175 cm^{-1} peak is detected over the surface of the *C. parvum* oocyst. This occurs due to an interfering peak in the MGITC SERRS spectrum at 1365 cm^{-1} that is detected in the 1360 cm^{-1} map (Figure 3.3F) and an interfering peak in the RBITC SERRS spectrum at 1200 cm^{-1} that is detected in the 1175 cm^{-1} map (Figure 3.3C). This type of interference demonstrates the need to use entire spectra to correctly identify immunogold labels in multiplex detection rather than only one or two characteristic peaks. This requirement will become increasingly important as additional organism-immunogold pairs are added to the technique and when real drinking water samples are analyzed.

Small SERRS maps were collected across the surfaces of oocysts and cysts with 1 μm increment steps to better characterize immunogold label distribution (Figure 3.4). In Figure 3.4A, the MGITC 1618 cm^{-1} signal is sporadic with localized hot spots on the cyst surface. The RBITC 1647 cm^{-1} signal in Figure 3.4B, on the other hand, is consistent across the surface of the oocyst. Average RBITC intensities on the oocyst surfaces were ~1.5-2 times larger than the intensities of the MGITC signals on the *Giardia* cysts. Raman measurements of MGITC and RBITC dyes in 40 nm nanoparticle solutions showed similar differences in signal intensities (Figure 3.1). When anti-*Giardia* immunogold was prepared with RBITC instead of MGITC and incubated with *Giardia*,

the RBITC Raman signals were consistently measured across the *Giardia* cysts and were as high as those observed when *C. parvum* oocysts were incubated with RBITC anti-*C. parvum* immunogold. Therefore, it was determined that the sporadic coverage and weaker MGITC signals across the *Giardia* cysts were due mostly to the weaker MGITC signal instead of being the result of differences in the binding affinities of the two types of antibodies to their respective organisms.

A major problem with the current EPA pathogen detection methods is the length of time it takes laboratories to perform the analyses. Thus, the proposed SERS based method would be a major improvement to these methods if it is capable of providing rapid results. Accordingly, a Raman-mapping method to detect reporter immunogold bound to pathogens will require the careful selection of appropriate step sizes. Larger steps allow greater areas to be scanned in less time, but can skip over organisms, whereas small step sizes clearly outline organisms but require longer collection times. For *C. parvum* oocyst detection with a 40× objective, a step size of 7 μm was capable of detecting most oocysts (Supporting Information Figure 3.S4), but a step size of 10 μm 'missed' many oocysts. The 43×43 Raman map shown in Figure 3.S4 with 7 μm steps scans an area of about 0.3 mm^2. With 1 s acquisition times, a map this size took approximately 1 hour to collect. It may be necessary in future methods to quickly scan large areas with large steps (7 μm), and then zoom in on the map areas that have demonstrated positive hits. If the zoomed-in map with small steps produces a map of the label corresponding to the size and shape of the organism, a positive result would be recorded.

We have reported here on work towards the development of a SERRS based detection technique for *C. parvum* and *G. lamblia*. This work is especially promising as there are numerous Raman active molecules available that are capable of being incorporated into immunogold labels that can detect a number of waterborne pathogens simultaneously. Because it depends on spectral recognition instead of fluorescence microscopy, this type of detection can be incorporated into a fully automated monitoring strategy. Our lab is currently working on the synthesis of a filter capable of collecting and concentrating waterborne pathogens that will be coupled with SERRS based detection.

ACKNOWLEDGMENTS

This work was supported by a National Science Foundation Graduate Student Fellowship, a Waste Policy Institute Fellowship, and an AdvanceVT doctoral fellowship to K.L.R. and through a research grant from the National Science Foundation (BES-0606995). We thank Charles Farley and Steve McCartney for their help with the Raman and TEM instrumentation.

FIGURES

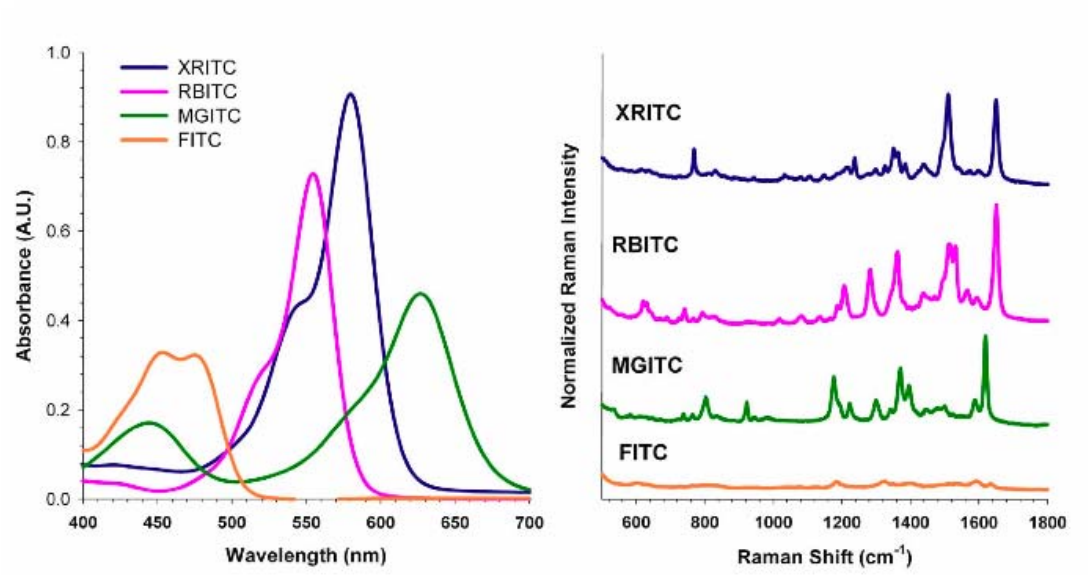

Figure 3.1 Absorption and SERRS spectra of fluorescent dyes. Left: Absorption bands of XRITC, RBITC, MGITC, and FITC. Right: SERRS spectra of XRITC (20 nM), RBITC (20 nM), MGITC (50 nM), and FITC (50 nM) in the presence of 40 nm gold nanoparticles.

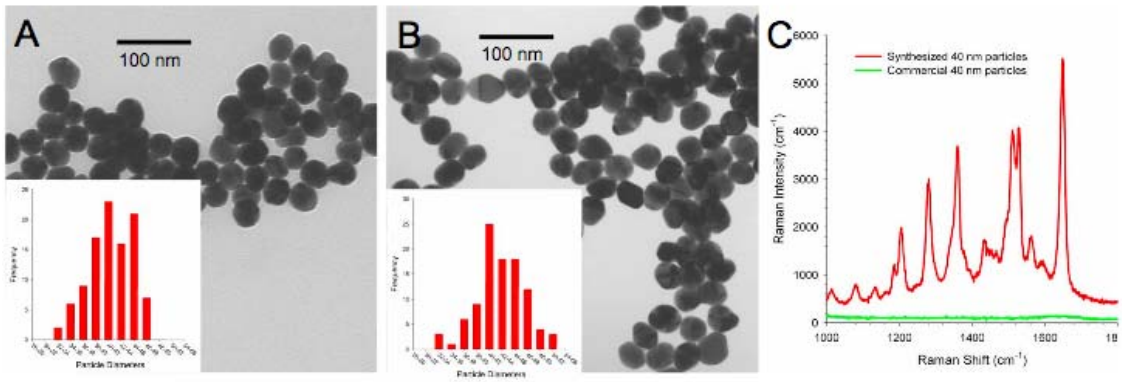

Figure 3.2 SERS enhancement of commercial gold nanoparticles versus that for synthesized nanoparticles. A) TEM image of commercial 40 nm particles. Average diameters: Major axis = 41.3 nm (S.D. = 3.4) Minor axis = 37.8 nm (S.D. = 3.6). Inset: histogram of major axis diameters as determined by NIH ImageJ software. (B) TEM image of synthesized nanoparticles. Average diameters: Major axis = 43.0 nm (S.D. = 3.9) Minor axis = 35.0 nm (S.D. = 3.6). Insert: histogram of major axis diameters as determined by NIH ImageJ software. C) Raman spectra of RBITC (20 nM) in commercial and synthesized nanoparticle solutions. Acquisition parameters: 10x objective, 10 s acquisition time.

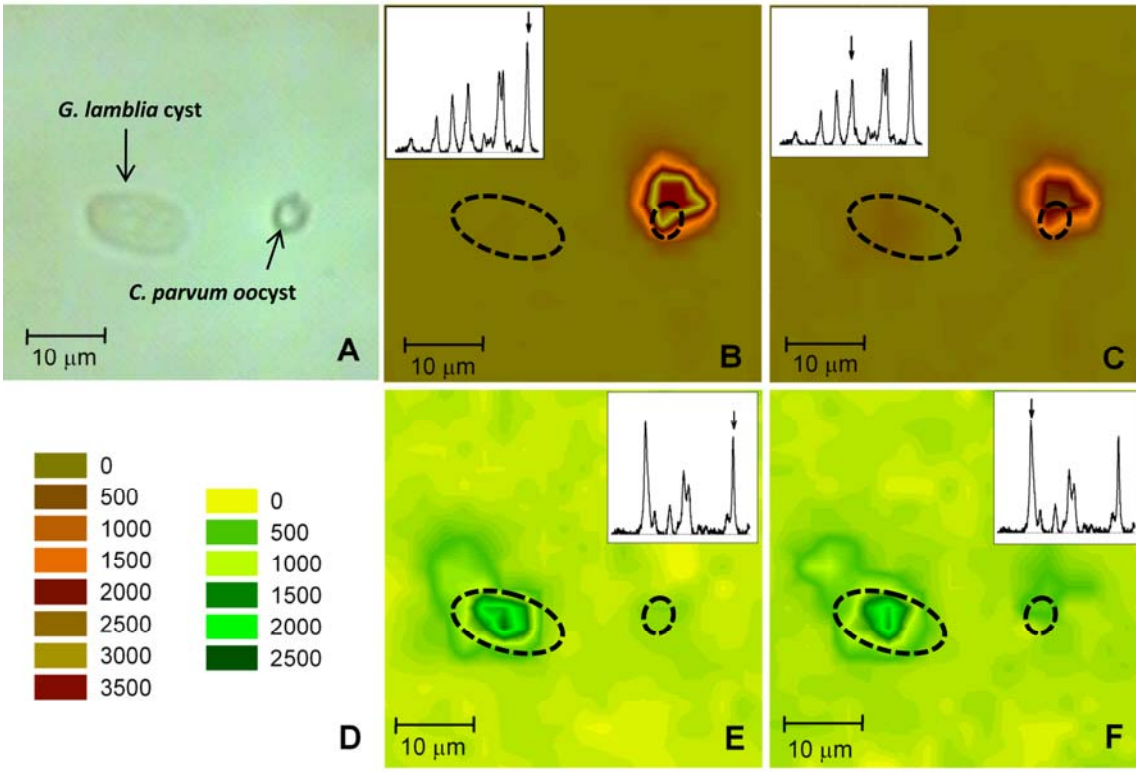

Figure 3.3 Raman X-Y maps of *G. lamblia* cyst and *C. parvum* oocyst. Dashed lines represent outlines of organism location. Raman mapping settings: 20×20 measurements (400 total), 2 μm steps, 1s acquisition time. A) Optical microscope image of cyst and oocyst. B) Raman map of 1645 cm^{-1} RBITC peak. Inset: RBITC SERRS spectrum with arrow identifying 1645 cm^{-1} peak. C) Raman map of 1360 cm^{-1} RBITC peak. Inset: RBITC SERRS spectrum with arrow identifying 1360 cm^{-1} peak. D) Legend of peak intensities in Raman maps. E) Raman map of 1618 cm^{-1} MGITC peak. Inset: MGITC SERRS spectrum with arrow identifying 1618 cm^{-1} peak. F) Raman map of 1175 cm^{-1} MGITC peak. Inset: MGITC SERRS spectrum with arrow identifying 1175 cm^{-1} peak.

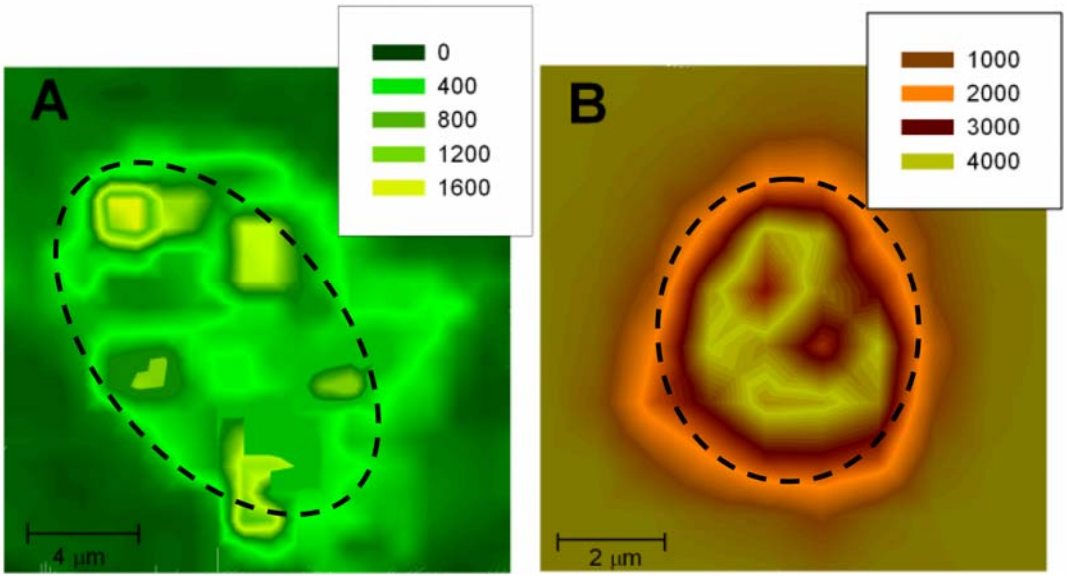

Figure 3.4 Raman X-Y maps of *C. parvum* oocyst (A) and *G. lamblia* cyst (B). Dashed line represents outline of organism as determined with optical microscopy. A) Intensity of 1645 cm^{-1} RBITC peak across surface of *C. parvum* oocyst. Mapping settings: 10×10 map with 1 µm steps, 1 s acquisition times. B) Intensity of 1618 cm^{-1} MGITC peak on surface of *Giardia* cyst. Mapping settings: 20×20 map with 1 µm steps, 1 s acquisition times.

WORKS CITED

1. USTD, Bacterial Standard for Drinking Water. In *Public Health Report*, Washington, D.C, 1914; Vol. 29, pp 2959-2966.
2. Korich, D. G., Mead, J. R., Madore, M. S., Sinclair, N. A., Sterling, C. R., Effects of Ozone, Chlorine Dioxide, Chlorine, and Monochloramine on *Cryptosporidium parvum* Oocyst Viability. *Applied and Environmental Microbiology* **1990,** 56, (5), 1423-1428.
3. Venczel, L. V., Arrowood, M., Hurd, M., Sobsey, M. D., Inactivation of *Cryptosporidium parvum* Oocysts and *Clostridium perfringens* Spores by a Mixed-Oxidant Disinfectant and by Free Chlorine. *Applied and Environmental Microbiology* **1997,** 63, (4), 1598-1601.
4. Betancourt, W. Q., Rose, J. B., Drinking water treatment processes for removal of Cryptosporidium and Giardia. *Veterinary Parasitology* **2004,** 126, (1-2), 219-234.
5. Deng, M. Q., Cliver, D. O., Mariam, T. W., Immunomagnetic Capture PCR to Detect Viable *Cryptosporidium parvum* Oocysts from Environmental Samples. *Applied and Environmental Microbiology* **1997,** 63, (8), 3134-3138.
6. Fontaine, M., Guillot, E., An immunomagnetic separation- real-time PCR method for quantification of *Cryptosporidium parvum* in water samples. *Journal of Microbiological Methods* **2003,** 54, 29-36.
7. Xiao, L., Singh, A., Limor, J., Graczyk, T. K., Gradus, S., Lal, A., Molecular Characterization of Cryptosporidium Oocysts in Samples of Raw Surface Water and Wastewater. *Applied and Environmental Microbiology* **2001,** 67, (3), 1097-1101.
8. Di Giovanni, G. D., Hashemi, F. H., Shaw, N. J., Abrams, F. A., LeChevallier, M. W., Abbaszadegan, M., Detection of Infectious Cryptosporidium parvum Oocysts in Surface and Filter Backwash Water Samples by Immunomagnetic Separation and Integrated Cell Cultrue-PCR. *Applied and Environmental Microbiology* **1999,** 65, (8), 3427-3432.
9. Kalele, S. A., Kundu, A. A., Gosavi, S. W., Deobagkar, D. N., Deobagkar, D. D., Kulkarni, S. K., Rapid detection of Escherichia coli by using anti body-conjugated silver nanoshells. *Small* **2006,** 2, (3), 335-338.
10. LeChevallier, M. W., Giovanni, G. D. D., Clancy, J. L., Bukhari, Z., Bukhari, S., Rosen, J. S., Sobrinho, J., Frey, M. M., Comparison of Method 1623 and Cell Culture-PCR for Detection of *Cryptosporidium* spp. in Source Waters. *Applied and Environmental Microbiology* **2003,** 69, (2), 971-979.
11. Vo-Dinh, T., Stokes, D. L., Griffin, G. D., Volkan, M., Kim, U. J., Simon, M. I., Surface-enhanced Raman scattering (SERS) method and instrumentation for genomics and biomedical analysis. *Journal of Raman Spectroscopy* **1999,** 30, (9), 785-793.
12. Kneipp, K., Kneipp, H., Itzkan, I., Dasari, R. R., Feld, M. S., Ultrasensitive chemical analysis by Raman spectroscopy. *Chemical Reviews* **1999,** 99, (10), 2957-+.
13. Gessner, R., Rosch, P., Petry, R., Schmitt, M., Strehle, M. A., Kiefer, W., Popp, J., The application of a SERS fiber probe for the investigation of sensitive biological samples. *Analyst* **2004,** 129, (12), 1193-1199.
14. Kneipp, K., Wang, Y., Kneipp, H., Perelman, L. T., Itzkan, I., Dasari, R., Feld, M. S., Single molecule detection using surface-enhanced Raman scattering (SERS). *Physical Review Letters* **1997,** 78, (9), 1667-1670.

15. Haynes, C. L., McFarland, A. D., Van Duyne, R. P., Surface-enhanced Raman spectroscopy. *Analytical Chemistry* **2005,** 77, (17), 338A-346A.
16. Premasiri, W. R., Moir, D. T., Klempner, M. S., Krieger, N., Jones, G., Ziegler, L. D., Characterization of the Surface Enhanced Raman Scattering (SERS) of bacteria. *Journal of Physical Chemistry B* **2005,** 109, (1), 312-320.
17. Allain, L. R., Vo-Dinh, T., Surface-enhanced Raman scattering detection of the breast cancer susceptibility gene BRCA1 using a silver-coated microarray platform. *Analytica Chimica Acta* **2002,** 469, (1), 149-154.
18. Cao, Y. W. C., Jin, R. C., Mirkin, C. A., Nanoparticles with Raman spectroscopic fingerprints for DNA and RNA detection. *Science* **2002,** 297, (5586), 1536-1540.
19. Jin, R. C., Cao, Y. C., Thaxton, C. S., Mirkin, C. A., Glass-bead-based parallel detection of DNA using composite Raman labels. *Small* **2006,** 2, (3), 375-380.
20. Driskell, J. D., Kwarta, K. M., Lipert, R. J., Porter, M. D., Neill, J. D., Ridpath, J. F., Low-level detection of viral pathogens by a surface-enhanced Raman scattering based immunoassay. *Analytical Chemistry* **2005,** 77, (19), 6147-6154.
21. Cui, Y., Ren, B., Yao, J. L., Gu, R. A., Tian, Z. Q., Synthesis of AgcoreAushell bimetallic nanoparticles for immunoassay based on surface-enhanced Raman spectroscopy. *Journal of Physical Chemistry B* **2006,** 110, (9), 4002-4006.
22. Xu, S. P., Ji, X. H., Xu, W. Q., Li, X. L., Wang, L. Y., Bai, Y. B., Zhao, B., Ozaki, Y., Immunoassay using probe-labelling immunogold nanoparticles with silver staining enhancement via surface-enhanced Raman scattering. *Analyst* **2004,** 129, (1), 63-68.
23. Grubisha, D. S., Lipert, R. J., Park, H. Y., Driskell, J., Porter, M. D., Femtomolar detection of prostate-specific antigen: An immunoassay based on surface-enhanced Raman scattering and immunogold labels. *Analytical Chemistry* **2003,** 75, (21), 5936-5943.
24. Ni, J., Lipert, R. J., Dawson, G. B., Porter, M. D., Immunoassay Readout Method Using Extrinsic Raman Labels Adsorbed on Immunogold Colloids. *Analytical Chemistry* **1999,** 71, 4903-4908.
25. Su, X., Zhang, J., Sun, L., Koo, T. W., Chan, S., Sundararajan, N., Yamakawa, M., Berlin, A. A., Composite organic-inorganic nanoparticles (COINs) with chemically encoded optical signatures. *Nano Letters* **2005,** 5, (1), 49-54.
26. Frens, G., Controlled Nucleation for the Regulation of the Particle Size in Monodisperse Gold Suspensions. *Nature Physical Science* **1973,** 241, 20-22.
27. Brown, K. R., Walter, D. G., Natan, M. J., Seeding of colloidal Au nanoparticle solutions. 2. Improved control of particle size and shape. *Chemistry of Materials* **2000,** 12, (2), 306-313.
28. Keating, C. D., Musick, M. D., Keefe, M. H., Natan, M. J., Kinetics and Thermodynamics of Au Colloid Monolayer Self-Assembly. *Journal of Chemical Education* **1999,** 76, (7), 949-955.
29. Mulvaney, S. P., Musick, M. D., Keating, C., Natan, M. J., Glass-Coated, Analyte-Tagged Nanoparticles: A New Tagging System Based on Detection with Surface-Enhanced Raman Scattering. *Langmuir* **2003,** 19, 4784-4790.

30. Doering, W. E., Nie, S., Spectroscopic Tags Using Dye-Embedded Nanoparticles and Surface-Enhanced Raman Scattering. *Analytical Chemistry* **2003,** 75, (22), 6171-6176.
31. Krug, J. T., Wang, G. D., Emory, S. R., Nie, S. M., Efficient Raman enhancement and intermittent light emission observed in single gold nanocrystals. *Journal of the American Chemical Society* **1999,** 121, (39), 9208-9214.
32. Orendorff, C. J., Gole, A., Sau, T. K., Murphy, C. J., Surface-enhanced Raman spectroscopy of self-assembled monolayers: Sandwich architecture and nanoparticle shape dependence. *Analytical Chemistry* **2005,** 77, (10), 3261-3266.
33. Hayat, M. A., *Colloidal Gold*. Academic Press, Inc.: San Diego, CA, 1989; Vol. 1-3.
34. Ni, J., Lipert, R. J., Dawson, G. B., Porter, M. D., Immunoassay readout method using extrinsic Raman labels adsorbed on immunogold colloids. *Analytical Chemistry* **1999,** 71, (21), 4903-4908.

SUPPORTING INFORMATION

Three batches of nanoparticles with average diameters ≈40 nm were synthesized and the resulting RBITC SERS signals of the solutions are presented in Figure 3.S3. Based on these results, it was concluded that gold nanoparticle solutions with 40 nm diameters could be repeatedly synthesized with similar enhancing abilities. Dye coverage of the nanoparticle surfaces was determined by exposing aliquots of the gold nanoparticle solutions to increasing dye concentrations. Specifically, 1.5 mL aliquots of 40 nm nanoparticles were allowed to react with either RBITC or MGITC for four hours. They were then collected by centrifugation and reuspended in water at which point their surface plasmon band was measured. A decrease in intensity or shift to the longer wavelengths of the band indicates that sufficient citrate molecules on the gold nanoparticle surface have been displaced to cause nanoparticle destabilization (Figure 3.S5). Based on these assays, approximately 80 nM RBITC and 80 nM MGITC would lead to nanoparticle destabilization in the 40 nm particle solutions. In order to leave adequate space on the nanoparticle surface for antibody binding in subsequent steps, only 25% of this RBITC or MGITC concentration (20 nM) was employed in the immunogold syntheses.

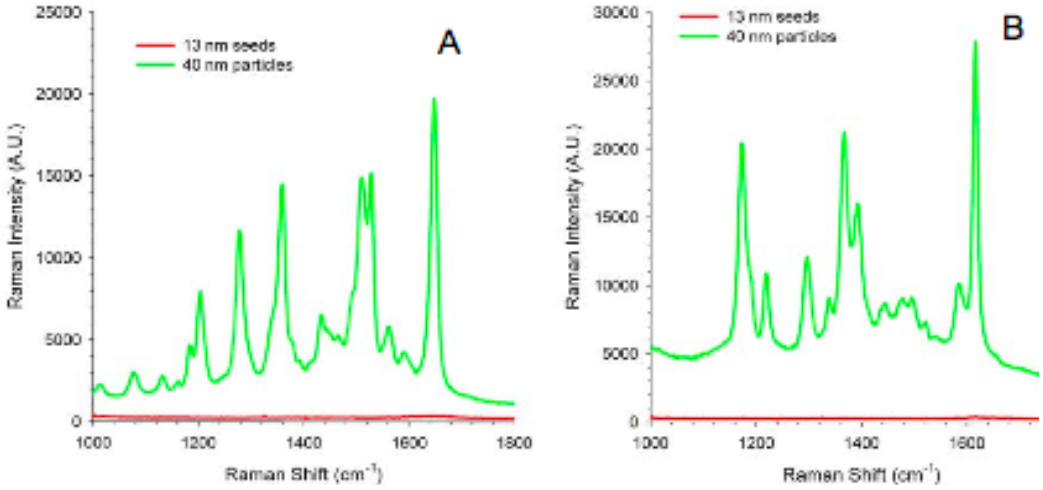

Figure 3.S1 SERS enhancements resulting from synthesized 13 nm gold particle solutions and synthesized 40 nm gold particle solutions. A) 20 nM RBITC SERS signal spectra. B) 50 nM MGITC SERS spectra. Acquisition parameters: 10x objective, 30 s acquisition times.

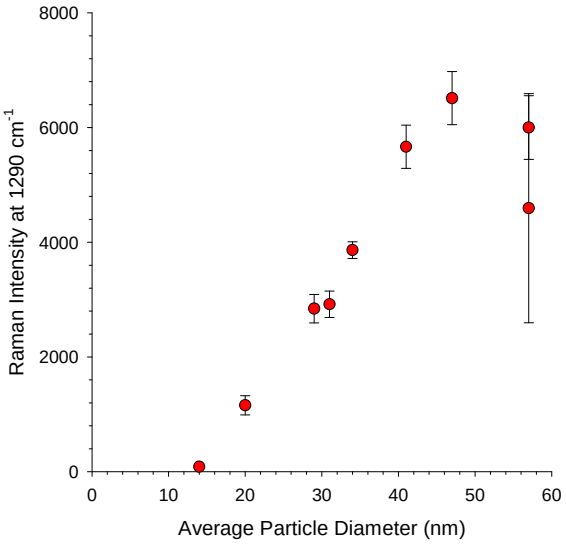

Figure 3.S2 SERRS peak intensity of RBITC at 1290 cm^{-1} as a function of average gold nanoparticle diameter. Conditions: [Au] = 0.25 mM, [RBITC] = 50 nM. Raman spectra measured four hours after NP solutions spiked with RBITC. Acquisition parameters: 632.8 nm excitation, 10x objective, 10 s acquisition time

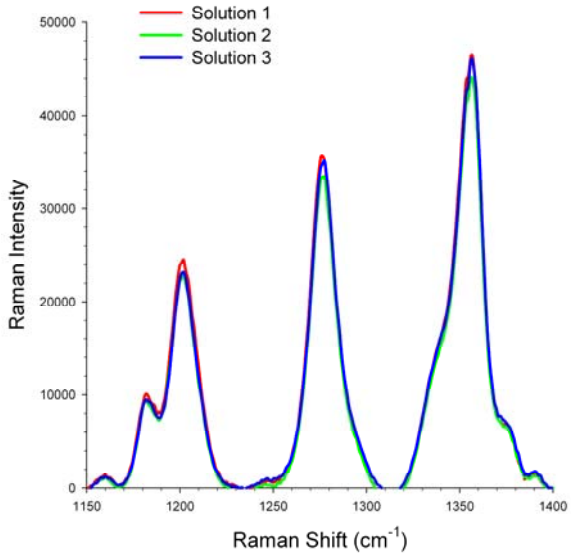

Figure 3.S3 Reproducibility of RBITC SERS peaks from three synthesized 40 nm gold nanoparticle solutions. [RBITC] = 100 nM. Average solution particle diameters and standard deviations: Solution 1, major axis = 38.8 nm (4.0 nm), minor axis = 34.9 nm (3.5 nm). Solution 2, major axis = 40.2 nm (4.3 nm), minor axis = 35.2 nm (3.8 nm). Solution 3, major axis = 43.5 nm (3.2 nm), minor axis = 39.8 nm (3.4 nm). Acquisition parameters: 10x objective, 30 s acquisition times.

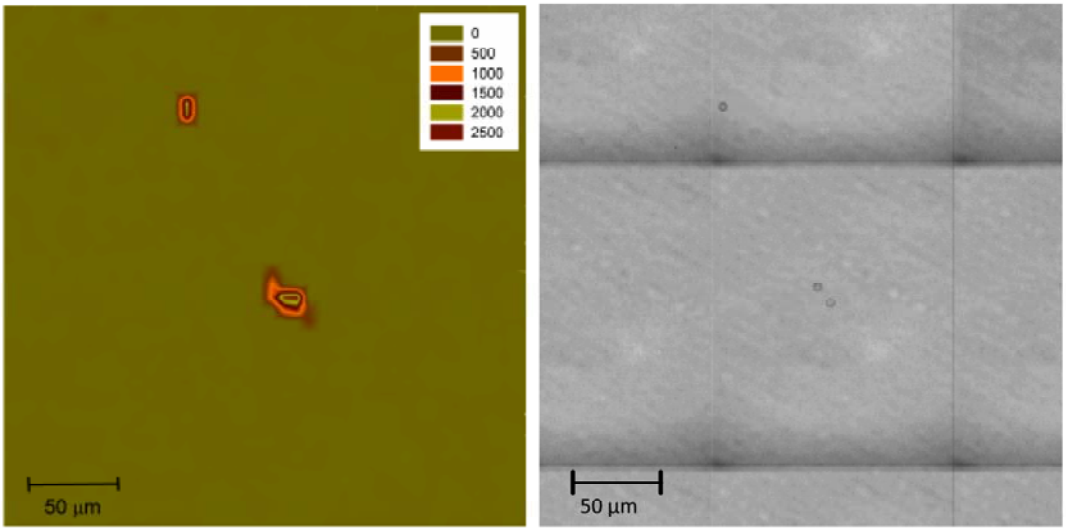

Figure 3.S4 Raman x-y map of three *C. parvum* oocysts. Left: Photograph of 300 µm by 300 µm area with three oocysts. Right: Intensity of 1645 cm-1 RBITC peak across map. Mapping conditions: 43 x 43 spectra (1849 total) with 7 µm steps, 1 s acquisition times, laser focused through 40× objective.

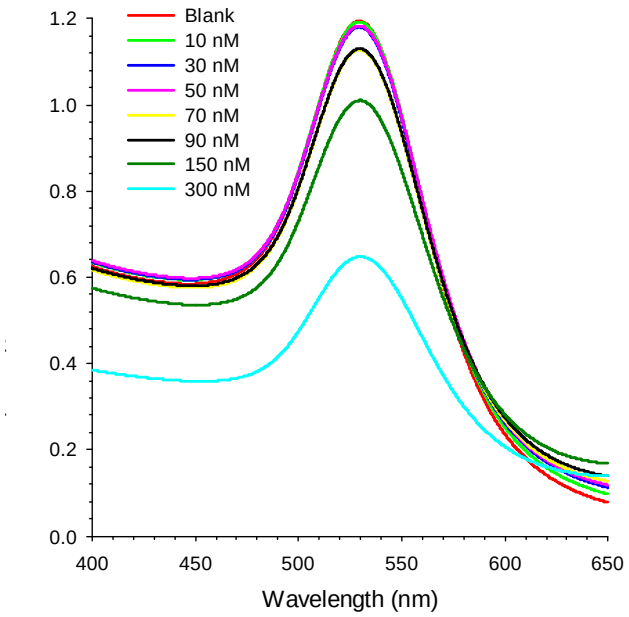

Figure 3.S5 Stability test results from the reaction between 40 nm gold particles and RBITC dye molecules. [Au] = 0.25 mM

4) Gold-coated polycarbonate membrane filter for drinking water pathogen concentration prior to SERS-based detection

Krista Rule Wigginton and Peter J. Vikesland*

Department of Civil and Environmental Engineering, Virginia Polytechnic Institute and State University, 418 Durham Hall, Blacksburg, VA 24060-0246

ABSTRACT

A SERS-based method for the concentration and detection of *Giardia lamblia* cysts in finished drinking water is reported. In this method, samples are concentrated with a membrane filter and then cysts captured on the filter surface are labeled with immunogold SERS labels and quantified via Raman spectroscopy. Anodisc® membrane filters, silver membrane filters, and electroless gold-coated polycarbonate track etched (PCTE) membrane filters were investigated for their compatibility with the SERS based detection strategy. The largest pore size available with the Anodisc® membranes was too small for the proposed method because they led to the physical retention of the immunogold. When silver membranes were employed, cysts were difficult to distinguish from nonspecifically bound labels and cyst recovery from distilled water samples was only ≈12.3%. With gold-coated PCTE membranes, however, cysts were readily detectable and cyst recovery was ≈95%. This Raman based method simplifies *Giardia*

detection and has the potential to be extended to the simultaneous detection of numerous pathogenic organisms. To our knowledge, this is the first report coupling the use of membrane filters for the concentration and detection of organisms from water samples with a SERS based detection strategy.

4.1 INTRODUCTION

Many waterborne illnesses are readily contracted by consumption of low numbers of etiologic agents. For instance, gastrointestinal illness caused by verocytotoxigenic *Escherichia coli* (VTEC) can be contracted by consumption of <100 cells, and giardiasis and cyrptosporidiosis can be contracted after the ingestion of <10 cysts or oocysts, respectively.[1] For this reason, the detection limits of pathogen monitoring methodologies for drinking water must be extremely low. To achieve such limits, the methods currently employed for pathogen detection typically involve a number of complicated steps such as concentration, purification, cell culture, staining/labeling, detection, etc. Most existing detection methods have pathogen specific methodologies and thus simultaneous detection of multiple pathogens (i.e., multiplex detection) is typically not possible.

U.S. EPA method 1623 enables detection of both *C. parvum* oocysts and *G. lamblia* cysts simultaneously.[2] However, the method is extremely complex and as a result, requires highly trained analysts. In many cases, sample turnaround times can be as long as two weeks. In this method, pre-concentration of the large sample volumes involves capsule filtration and centrifugal concentration. Immunomagnetic separation (IMS) is then used to separate the (oo)cysts from extraneous material. Following staining with fluorescent-antibody labels and 4',6-diamidino-2-phenylindole (DAPI), the (oo)cysts are examined using fluorescence and differential interference contrast (DIC) microscopy.

Oo(cysts) are identified and enumerated by microscopists based on their size, shape, and fluorescence characteristics and are confirmed by their DAPI stain characteristics using DIC microscopy. Unfortunately, method 1623 consistently gives inconsistent results. Reported recoveries of the organisms vary from 14-85% for *C. parvum* oocysts[3-6] and 0.5-61% for *G. lamblia* cysts.[7] A recent report demonstrated that the majority of the unrecovered (oo)cysts are lost in the concentration step when the filtered sample is eluted from the filter.[8] A more rapid, simple, and reliable method for the detection of protozoan pathogens would greatly benefit policy makers and water utilities, and would enhance the safety of water for consumers.

Our laboratory recently proposed a new strategy for *C. parvum* and *G. lamblia* detection that utilizes surface enhanced Raman spectroscopy and Raman mapping (Chapter 3). In this method, gold nanoparticles are functionalized with monoclonal antibodies specific against either *C. parvum* or *G. lamblia*. The *C. parvum* specific nanoparticles are then tagged with dye molecules that serve as surface enhanced Raman labels due to their proximity to the gold nanoparticle surface. The chosen dyes, rhodamine B isothiocyanate (RBITC) and malachite green isothiocyanate (MGITC), are subject to resonance Raman enhancement because they are in resonance with the 632.8 nm laser employed in this work. Gold nanoparticles conjugated with antibodies and dye molecules, or immunogold, bind to their respective organisms and are detected via Raman spectroscopy. The "fingerprint" spectra that are obtained when labeled oo(cysts) are probed have high intensities and are easily distinguishable from one another. A SERS based technique has many advantages over fluorescence based methods for a number of reasons, including the narrower bands associated with SERS versus those

obtained with fluorescence spectroscopy. The narrower bands make signal overlap less of an issue with SERS and it is therefore better suited for muliplex detection. Raman signals are also less prone to photobleaching than fluorescence signals and this allows for longer acquisition times.[9] Additionally, SERS labels have very specific fingerprint spectra. A microscopist is therefore not required to identify the (oo)cyst and the label signals can instead be detected via a computer-based method.

In our previous work (Chapter 3), (oo)cysts were fixed directly onto microscope slides, labeled with SERS immunogold conjugates, and then detected via Raman mapping. To expand this detection strategy to pathogen detection in water samples, a concentration step that collects cysts and oocysts on a flat surface such that they can be analyzed via Raman mapping is required. Herein we propose the use of a membrane filter that enables organism isolation from a water sample by physical trapping (Figure 4.1). Previously, Escoriza et al. filtered water samples containing the bacteria *Staphylococcus epidermidis* and *Escherichia coli* and then probed the filter surface for the intrinsic (i.e., non-labeled) Raman signals of the bacteria.[10] To observe the bacterial signal over the background signal of the filter, they used extremely high bacterial cell concentrations (3×10^7 cells/13 mm diameter filter). To acquire their intrinsic signal, they used normal Raman which is inherently much weaker than the SERRS detection we have used for protozoan detection. Additionally, they simply studied random spots on the filter surface for signals and did not employ Raman mapping which can systematically scan the filter surface and relay information about cell distributions.

In the method proposed here, immunogold conjugates are added to the top of the membrane and incubated with captured *G. lamblia* (Figure 4.1). As the immunogold

conjugates are much smaller than the *G. lamblia* cysts, unbound immunogold passes through the filter pores in a wash step without the loss of captured, labeled organisms. If the filter surface is sufficiently flat and the organisms are sitting on top of the filter, Raman mapping should detect the signal of the immunogold bound to the cysts. To our knowledge, this is the first time a filter concentration step has been coupled with Raman mapping for the detection of organisms in water.

4.2 MATERIALS AND METHODS

Polycarbonate track-etched (PCTE) membrane and silver membrane filters with 3.0 μm pores and 13 mm diameter were purchased from Millipore (Bedford, MA) and Sterlitech (Kent, WA), respectively. Anodisc® filter membranes (pore size <200 nm) were purchased from Fisher Scientific. $HAuCl_4 \bullet 3H_2O$, trisodium citrate dihydrate, rhodamine B isothiocyanate (RBITC), $SnCl_2$, trifluoroacetic acid, formaldehyde, $AgNO_3$, Na_2SO_3, bovine serum albumin (BSA), sodium phosphate dihydrate, potassium phosphate monohydrate, sodium tetraborate, Tween-80, nitric acid, and methanol were obtained from Sigma-Aldrich (St. Louis, MO) and were used without further purification. Anti-*Giardia* IgG1 monoclonal antibodies were purchased from Meridian Life Sciences (Saco, ME). Gold plating solution (Oromerse Part B.) was acquired from Technique Inc. (Cranston, RI). *G. lamblia* cysts were obtained from Waterborne Inc. and enumerated prior to use with a hemacytometer.

Polycarbonate track-etched membrane (PCTE) filters were gold plated via an established method.[11] Briefly, 13 mm PCTE membranes were soaked in a solution of 26 mM $SnCl_2$ and 70 mM trifluoroacetic acid prepared in 50:50 water:MeOH for three minutes. After rinsing with three sequential 100 mL methanol washes, the membranes

were soaked in 29 mM $AgNO_3$ for two minutes and then rinsed twice with 100 mL portions of methanol and once with water. The filters were then immersed in solution containing a 40× dilution of the Oromerse B stock solution, 127 mM Na_2SO_3, and 0.625 M formaldehyde at 4 °C for 12 hours. The filters were rinsed with water and stored in 25% HNO_3. Prior to use, filters were washed several times in distilled water and soaked overnight in a solution of 10% BSA. The BSA step was incorporated as it discouraged non-specific binding of the immunogold labels. Anti-*Giardia* immunogold was prepared with 40 nm gold nanoparticles, Rhodamine B isothiocyanate (RBITC) and IgG1 monoclonal antibodies as previously described (Chapter 3). *G. lamblia* cysts were prepared on glass slides for the mapping optimization experiments. The cysts were fixed and labeled with the SERS immunogold as previously described (Chapter 3).

For the filter mapping experiments, 50 mL samples containing 200 cysts/mL in deionized water were gravity filtered through the membrane at a rate of approximately 10 mL/min. Following the filter step, 100 μL of immunogold label was added to the membrane surface. The filtration reservoir was covered with a glass Petri dish to minimize evaporation, and the filter surface was incubated for 30 minutes. Following this period, the unbound SERS immunogold solution was pulled through the membrane filter with 10 mL of PBS/Tween80 rinse solution via light vacuum. Dry membranes were removed from the filtration apparatus, placed in a microscope well, and sealed with a drop of fixing media (60% glycerol, 40% PBS). Blank samples with no cysts were prepared in exactly the same manner as cyst containing samples. Samples were stored at 4 °C until Raman analysis.

Raman spectra were obtained with a JY Horiba LabRAM HR 800 spectrometer, with a 600 grooves/mm grating and a slit width of 150 μm. The instrument is equipped with an Olympus BX-41 petrographic microscope and an Ancor electronically cooled CCD detector. Excitation was provided by a 632.8 nm He-Ne laser. Two objectives were used for Raman measurements in the current study. A 10× objective (N.A. = 0.25) was employed for low resolution mapping experiments and a long working distance 40× objective (N.A. = 0.75) was employed for higher resolution mapping experiments. Sample slides were mounted on a motorized microscope stage (Marzhauser EK-32) and an automated video camera fitted to the microscope was used to capture the optical image of the map area. For mapping experiments, Raman spectra from 1000 to 1800 cm^{-1} were collected at each map position with 1 s acquisition. This spectral range was large enough to include several characteristic reporter molecule peaks and was small enough to prevent the 600 lines/mm grating from moving during collection. Fluorescence microscopy was performed with a Carl Zeiss Axioskop 2 epifluorescence microscope equipped with a Zeiss MRm camera. Dynamic Light Scattering (DLS) particle size distributions were obtained using a Malvern Nano Zeta-sizer with a 633 nm laser source, a detection angle of 173º, and a folded capillary cell.

4.3 RESULTS AND DISCUSSION

4.3.1 Optimization of microscope objective

Experiments were conducted to determine whether the 10× objective or the 40× objective worked best for the acquisition of XY Raman maps. A higher numerical aperture lens generally results in more amplified Raman signals.[12] This general relationship is more complicated for transparent or translucent samples because the lower

magnifying objective illuminates a larger sample volume and thus there are a larger number of Raman scatterers probed simulaneously.[12] To determine the appropriate objective for these experiments, *Giardia* cysts were fixed onto glass slides and labeled with SERS immunogold. The fixed cysts were located with an optical microscope and Raman maps were then collected across the cysts using both objectives.

The 10× and 40× objectives used in these experiments have spot diameters of approximately 3 μm and 1 μm, respectively.[13] As a result, *Giardia* cyst resolution improves with the higher magnification objective (Figure 4.2). Intensities measured with the 40× objective are also approximately threefold higher than those measured with the 10× objective. On the other hand, the lower resolution objective covers a larger area (7.5 μm^2 vs. 0.88 μm^2) with each mapping step and therefore results in a greater number of positive signals per organism. As the purpose of this mapping experiment were to quantify cysts captured on a relatively large filter, the objective that can scan larger areas with fewer steps (larger step sizes) saves analysis time and results in smaller data sets.

Nonspecific binding is a common problem associated with antibody labeling techniques and occurs when antibodies bind to sites other than epitopes on the analyte. Such nonspecific binding can lead to false positives. RBITC signals measured at locations void of cysts, as determined by light microscopy, were the result of nonspecific binding and in general, these signals were much less intense than signals measured over cysts. It should be noted that the anti-*Giardia* IgG1 antibodies employed in the immunogold conjugates enabled complete coverage of the cysts by immunogold and as a result, they turned pink upon immunogold exposure. Accordingly, the signal collected directly over a cyst simultaneously incorporates Raman signals from numerous

immunogold labels. In contrast, measured Raman volumes at sites with nonspecific binding include fewer immunogold label conjugates. As a result, RBITC signals collected over a cyst are consistently stronger than signals observed from nonspecific binding. In mapping experiments of the same samples, the 10× objective measured fewer signals from nonspecific binding in areas void of cysts (Figure 4.2) compared to the 40×. This was likely a result of the generally weaker signals measured with the 10× compared to the 40× objective. Because the 10× objective had the advantage of detecting fewer non-specific binding event signals and because it detected a larger area of adjacent positive signals per cyst, it was selected for the filter detection experiments.

4.3.2 Optimization of step size

Experiments were conducted to determine an appropriate mapping stage step size to be used in the mapping experiments. Step sizes that are too large can skip over organisms on the membrane surface. Step sizes that are too small, however, can lead to excessive acquisition times as well as unnecessary amounts of data. For this reason, a range of step sizes was tested using fixed *Giardia* cysts. As expected, smaller step sizes led to a greater number of positive measurements per cyst. Ultimately, a step size of 5 μm was chosen for the filter mapping experiments. This step size resulted in an average of 9 ± 4 adjacent signals per *Giardia* cyst. RBITC signals detected in areas void of cysts (due to nonspecific binding) generally consisted of 1-4 adjacent signals. Therefore, a step size of 5 μm made it possible to readily distinguish between RBITC signals due to nonspecific binding from the positive RBITC signals that signal the presence of a *Giardia* cyst. When a step size of 5 μm was employed, a map of 400 μm × 400 μm took

approximately 5 hours to collect with the instrument and software employed. Raman instruments with rapid mapping capabilities are now commercially available and as such, the time required for this type of mapping experiment with a rapid scan Raman instrument would be significantly faster.

4.3.3 Optimization of filter type

Membrane filters were employed to concentrate cysts from a water sample, to hold the cysts in place for immunogold labeling, and finally as a substrate for the acquisition of Raman XY maps. Membrane filters were chosen over other filter types as they have little z-depth and thus cysts should be captured close to the membrane surface. The filter material should exhibit little background fluorescence as this could mask the Raman signal from cyst-bound immunogold. Aluminum oxide Anodisc® filters were first considered because inorganic filter substrates typically exhibit less background fluorescence than organic filters. Although they break easily and are expensive relative to other membrane filters, Anodisc® filters exhibit very low fluorescence (Figure 4.3). At the time of publication, however, Anodisc® filters were only readily available with pore sizes up to 200 nm. For a pathogen detection strategy to be successful, the membrane pore size must be small enough to capture the organisms of interest yet large enough for unbound immunogold conjugates to easily pass through the filter. If the pores are too small, immunogold conjugates that are unassociated with cysts will remain trapped on the filter surface and will result in the measurement of false positive RBITC signals. Based on the size of the gold nanoparticles (40 nm) and the average diameter of the IgG antibodies (~13 nm), the *Giardia* immunogold conjugates should be approximately 65-70 nm in physical diameter and DLS measurements of our immunogold conjugates diluted

in nanopure water resulted in an average hydrodynamic radius equal to 85.6 nm. Although the immunogold labels were smaller than the 200 nm pores, they were nonetheless highly retained by the Anodisc® filter in the absence of *Giardia*. For this reason, Anodisc® filters were not considered to be compatible with a SERS based protozoan detection strategy until they are available with pore sizes above 200 nm.

Silver membrane filters also exhibited low background fluorescence (Figure 4.3). These commercially available filters have pore sizes ranging from 0.2 μm to 5 μm, are composed of molecularly bonded silver filter media, and are reportedly reusable after chemical, ignition, or ultrasonic treatment.[14] Silver filters with 3 μm pores were selected for the experiments as this pore size has been used previously for the capture of *Giardia* cysts.[15] This pore size was large enough for unbound SERS immunogold labels to easily pass through the membrane.

Triplicate Raman maps were collected at different positions on the membrane surface and Raman mapping data was then analyzed with the LabSpec® software. Raman maps of one of the blank samples and one of the 200 cysts/mL samples are presented in Figure 4.4. The total number of RBITC signals was enumerated for each map and the total number of captured cysts were calculated based on groups of adjacent RBITC signals. As mentioned previously, cysts mapped with the 10× objective and 5 μm mapping steps result in an average of 9 ± 4 adjacent RBITC signals. Therefore, a group of 5-13 adjacent RBITC signals was enumerated as one cyst. Groups consisting of fewer than 5 adjacent signals were assumed to be due to non-specific immunogold binding. Groups containing greater than 13 signals were often observed in the mapping

experiments. In these cases, the number of adjacent RBITC signals was rounded to the nearest factor of nine to estimate the number of cysts present in a group.

In early experiments, nonspecific immunogold binding to the silver membrane surface was a significant problem and cyst containing samples could not be differentiated from blanks. To ameliorate this problem, the silver membranes were soaked overnight in 5% BSA/PBS buffer prior to use. BSA is often used as a blocking agent in immunoassays since the protein acts to cover surface sites that the immunogold would otherwise be attracted to. This wash step effectively blocked the majority of the nonspecific binding sites and as a result, the number of positive signals measured in the blank sample filters decreased significantly.

As illustrated in Table 4.1 and Figure 4.5, the number of cysts detected on the silver membrane was consistently lower than the number of cysts expected to be present. Specifically, 18 cysts per mm^2 were detected on the silver membranes, while an average of 143 cysts per mm^2 was expected assuming an even distribution of cysts across the membrane filter surface. In comparison, an average of 2 cysts per mm^2 were detected on the blank sample membranes. Also illustrated in Figure 4.5 are the total number of RBITC pixels measured per mm^2 in the cyst sample and the blank. These values include the positive signals that resulted from non-specific binding.

To gain a better understanding of the presence and distribution of the cysts on top of the silver membrane filters, experiments were conducted in which samples were spiked with cysts and then filtered in the same manner with the SERS experiments. Instead of labeling with the SERS immunogold solution, samples were incubated with commercial fluorescent antibodies and the filters were then studied using a fluorescence

microscope. As expected from the SERS experimental results, cysts on the surface of the filter were often present in groups. It was also evident from the fluorescence microscope studies that the cysts were not always sitting directly on top of the filter and instead were often tucked into the filter with only part of the cyst protruding above the membrane surface (Figure 4.6). In some cases, the cysts were completely submerged within the membrane and only a muffled fluorescence signal in the shape of a cyst was visible from within the filter. The silver membrane filters are approximately 50 μm thick with 60% void volume and thus many of the cysts (~10 μm diameter) become lodged in the void volume of the filter. The Raman signal of material buried below the focal plane decreases exponentially with depth.[16, 17] Signals from the cysts buried more than a couple of micrometers within the filter are therefore likely missed during mapping experiments.

Polycarbonate track-etched (PCTE) membrane filters provide a number of advantages over other filter membranes such as their smooth, glasslike surface, low protein binding, a wide range of commercially available absolute pore sizes, and essentially no void volume. PCTE membrane filters have been used extensively for the separation and purification of microorganisms when other types of pathogen detection strategies such as fluorescence microscopy,[15] or electrochemical detection[18] are employed. The results from a number of these studies suggest that PCTE filters result in higher recoveries of *Giardia* cysts and *Cryptosporidium* oocysts from water samples than other filter types.[19, 20] A major problem with the direct employment of PCTE membranes for SERS studies is the high fluorescence background of the PCTE substrates. As illustrated in Figure 4.3, the fluorescence background signal is so high that it effectively conceals the signal of Raman active molecules on the PCTE surface.

A method for the electroless gold plating of PCTE membranes was developed by Menon and Martin.[11] This method enables deposition of a thin layer of gold on the PCTE membrane. Several biosensor applications of the gold-coated PCTE membranes have been reported including methods for the amperometric detection of glucose[21] and H_2O_2,[22] and the fluorescence-based detection of Pb(II).[23] Selective protein separation has been reported by immobilizing antibodies to the sides of the gold-coated PCTE membrane pores.[24] To our knowledge, however, electroless gold-coated PCTE membranes have not been previously utilized for pathogen detection or in any Raman/SERS study. Gold quenches fluorescence[25] and thus the electroless gold coating of PCTE membrane filters (Figure 4.7) led to a major decrease in the fluorescence background exhibited by the PCTE substrate (Figure 4.3). Based on previous reports, approximately 100-150 nm of gold is deposited on the PCTE pore surfaces after a 12-hour deposition time[26] and therefore the 3 μm pores should be reduced to ≈2.75 μm diameter after the electroless gold plating. Figure 4.7 shows a light microscope image of the gold-coated PC membrane filter making it evident that the pores are not blocked by the gold coating.

The cyst filtration experiments conducted with the silver membrane filters were repeated with the gold-coated PCTE filters. Like the silver membrane experiments, it was necessary to soak the gold-coated membrane filters overnight in a 5% BSA/PBS buffer. Otherwise, significant nonspecific binding of the immunogold was observed. Cyst enumeration results are presented in Table 4.2 and Figure 4.5 and representative maps of the 200 cyst/mL sample and the blank sample are presented in Figure 4.4. Cyst recovery is much higher with the gold-coated membrane filters relative to the silver membrane filters. Based on the predicted number of cysts filtered through the 70 mm^2

filter, approximately 143 cysts are expected in 1 mm^2 of filter surface and an average of 139 cysts were detected on the gold-coated membrane filters. Experiments were also performed with aqueous fluorescent antibody labels to study the distribution of cysts on the surface of the membrane with the fluorescence microscope. In contrast to the observations made in the silver membrane filter experiment, all cysts on the gold-coated membrane filters were sitting above the filter plane and no cysts were found tucked within the pores of the filter. We believe this explains the higher cyst recoveries obtained with the gold-coated membranes as cysts sitting on top of the gold coated filter were readily detected by Raman mapping.

4.4 CONCLUSIONS

In conclusion, we have tested three types of membrane filters for their compatibility with a SERS-based detection method for pathogens in drinking water. Anodisc® filters, silver membrane filters, and electroless gold-coated PCTE filters all demonstrated low fluorescence background thus making them compatible with Raman detection. However, the gold-coated membrane filter was determined to be the best for our particular detection strategy. To our knowledge, this is the first time gold-coated PCTE membrane filters have been utilized as SERS detection substrates in general, and as substrates for Raman mapping experiments for pathogen detection, in particular. As Raman spectrometers are continuing to be miniaturized and becoming better at Raman mapping, this type of detection method is becoming more attractive to environmental analytical chemists. Additionally, because there are numerous Raman labels commercially available each of which has its own distinctive "fingerprint" spectra, this method has the potential to be expanded for the detection of multiple pathogens

simultaneously. Future work is needed to examine the feasibility of this type of concentration and detection method in real waters containing materials that may interfere with the antibody label binding as well as the Raman RBITC detection.

TABLES AND FIGURES

Table 4.1. SERS detection of *Giardia* cysts filtered through silver membrane filter

	Scan Area (mm^2)	Detected cysts	Detected cysts/mm^2	Expected cysts/mm^2	% Recovery
Blank A	0.06	0	0	0	*
Blank B	0.22	1	4	0	*
Sample A	0.08	0	0	143	0
Sample B	0.20	4	20	143	14
Sample C	0.34	11	32	143	23

Table 4.2. SERS detection of *Giardia* cysts filtered through gold-coated PCTE filter

	Scan Area (mm^2)	Detected cysts	Detected cysts/mm^2	Expected # cysts/mm^2	% Recovery
Blank A	0.31	1	3	0	*
Blank B	0.11	0	0	0	*
Blank C	0.12	1	8	0	*
Sample A	0.12	19	161	143	113
Sample B	0.22	32	149	143	104
Sample C	0.15	16	108	143	75

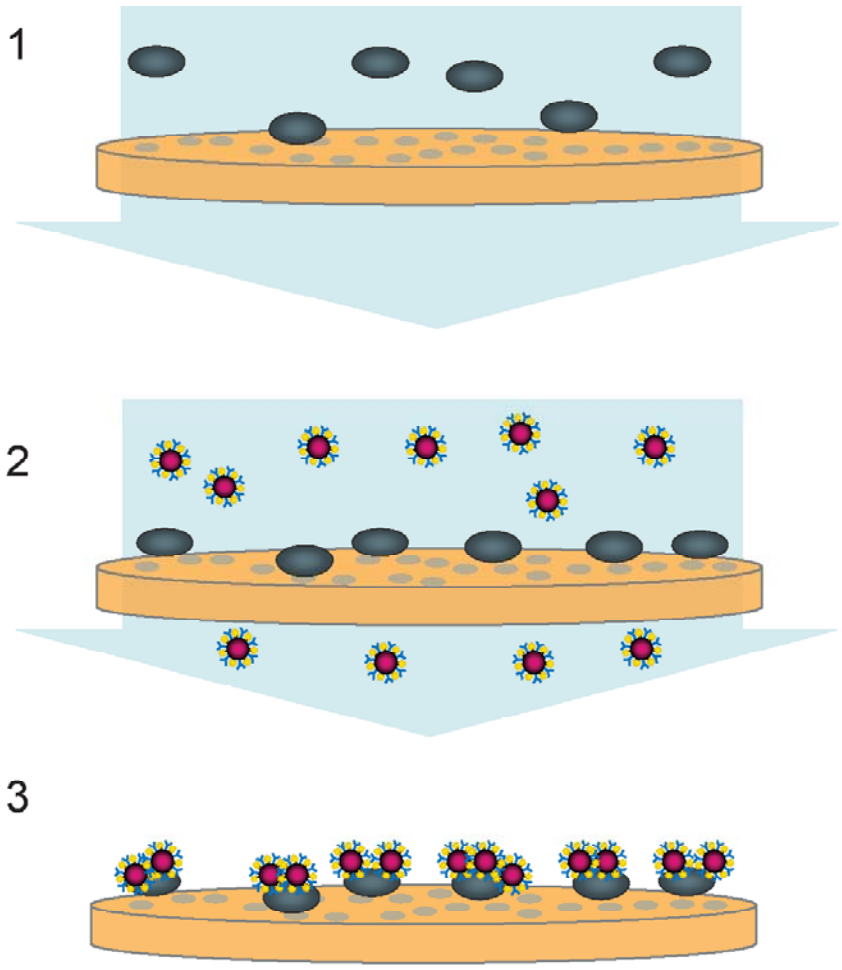

Figure 4.1 Schematic of proposed method for detection of *Giardia lamblia* in drinking waters. 1) Samples containing cysts are filtered through a membrane filter and captured on top of the membrane. 2) Immunogold labels are added to the top of the filter and allowed to incubate for 30 minutes. Unbound immunogold labels are washed through the pores of the filter. 3) Labeled cysts are detectable via Raman mapping.

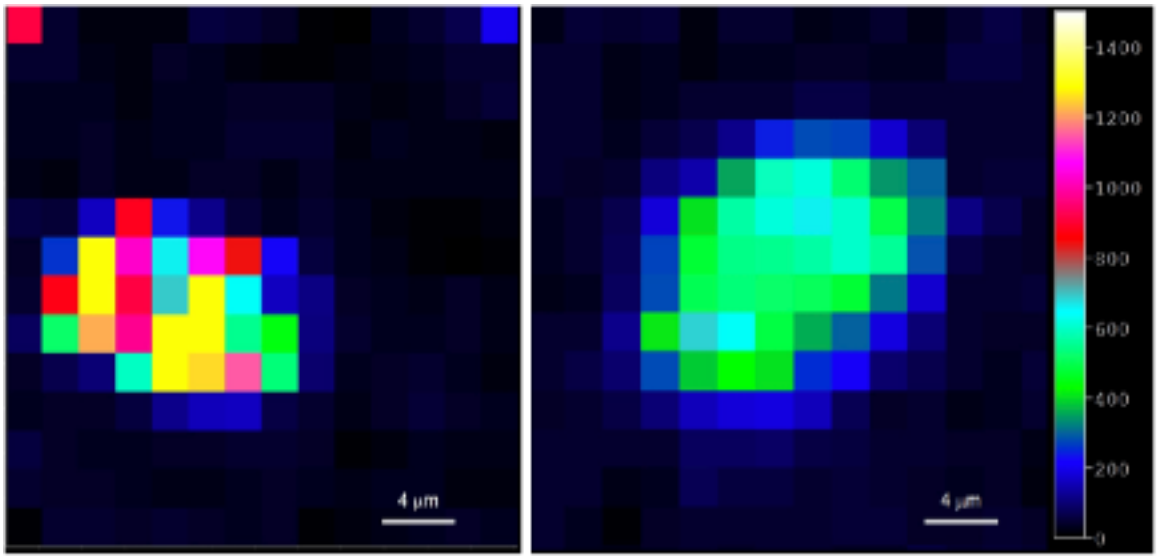

Figure 4.2 Raman maps collected across a *Giardia* cyst surface with a 40× objective (left) and a 10× objective (right) illustrating the RBITC 1645 cm^{-1} peak intensity. Raman mapping acquisition conditions: 633 nm excitation source, 1 s acquisition, 2 µm step size. Colored pixels separate from the cyst are the result of non-specific binding.

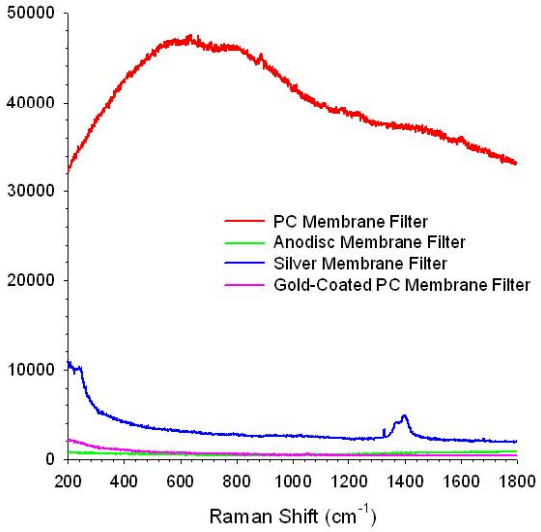

Figure 4.3 Raman spectra of membrane filters. Raman acquisition conditions: 633 nm excitation source, 10 s acquisition, 40× objective.

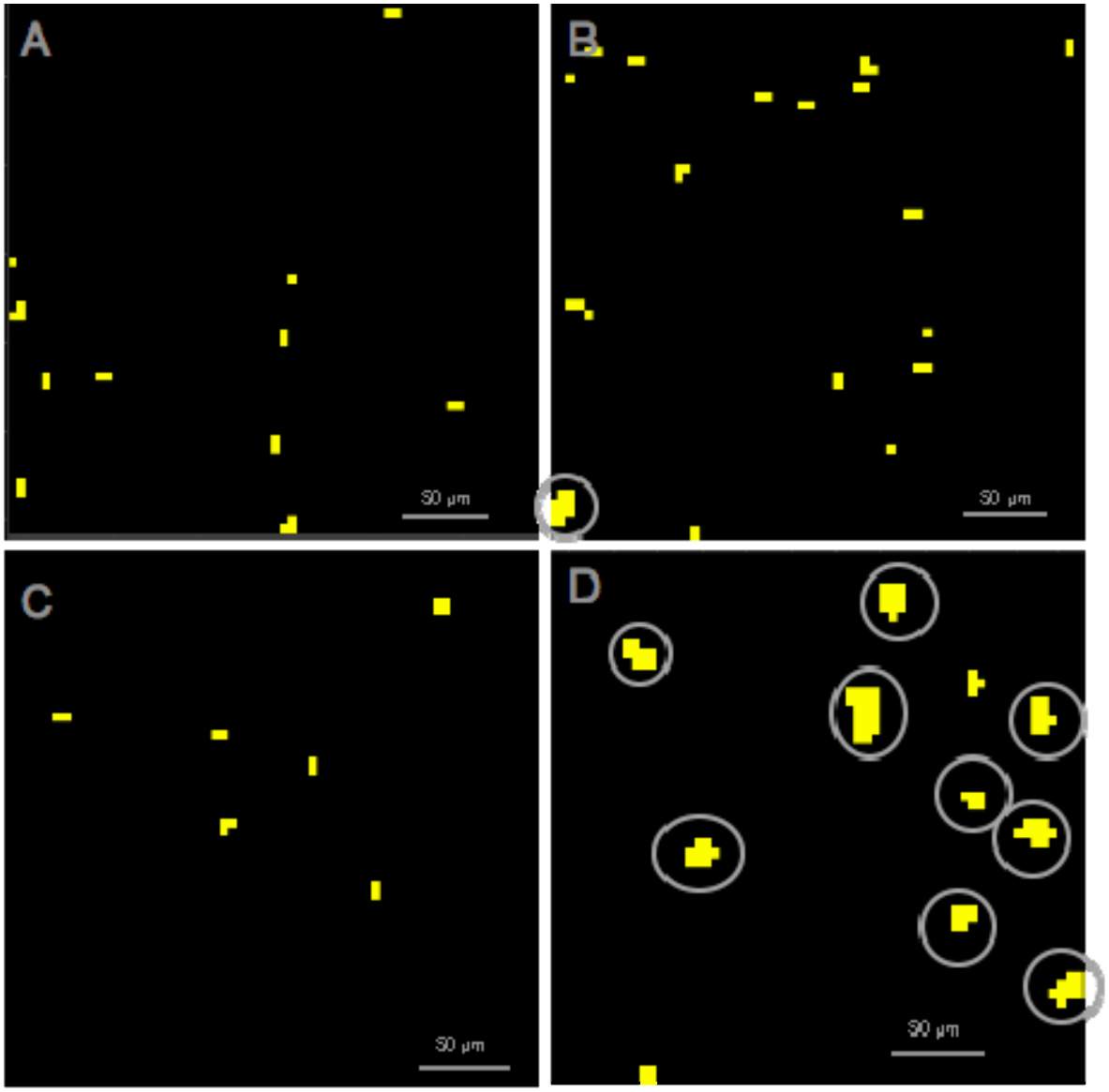

Figure 4.4 Representative Raman maps collected on membrane surfaces. A) 300 µm × 300 µm map of blank sample filtered with silver membrane filter. B) 300 µm × 300 µm map of sample of 100 cysts/mL sample filtered with silver membrane filter. C) 300 µm × 300 µm map of blank sample filtered with gold-coated membrane filter. D) 300 µm × 300 µm map of sample with 100 cysts/mL filtered with gold-coated membrane. Yellow pixels represent RBITC signals. Circles indicate detected cyst locations. Mapping conditions: 10× objective, 5 µm steps, 1 s acquisition times, 633 excitation wavelength.

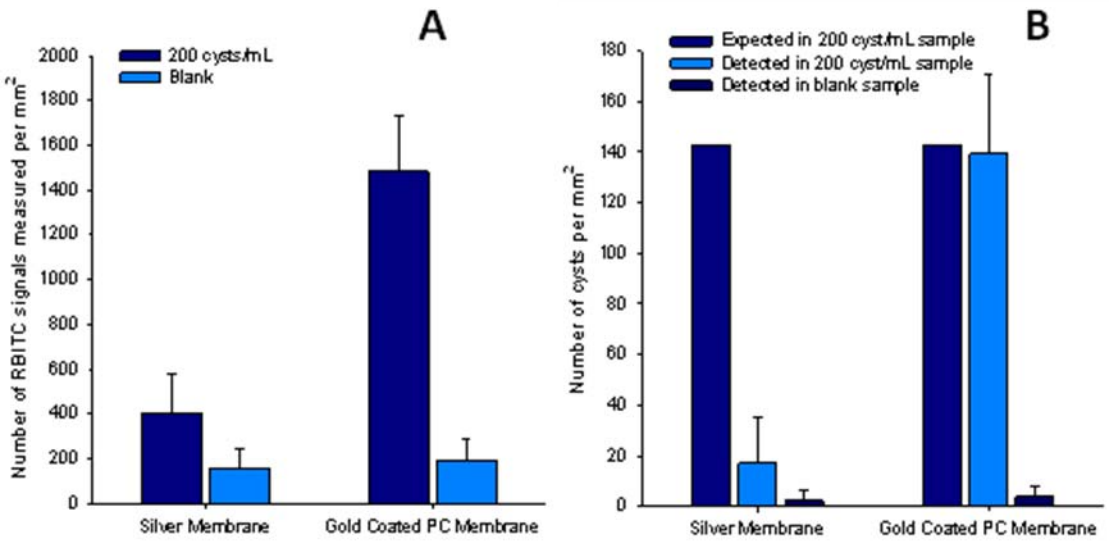

Figure 4.5 A) Total number of RBITC signals detected per mm^2 mapped membrane and B) total number of cysts detected per mm^2 mapped membrane.

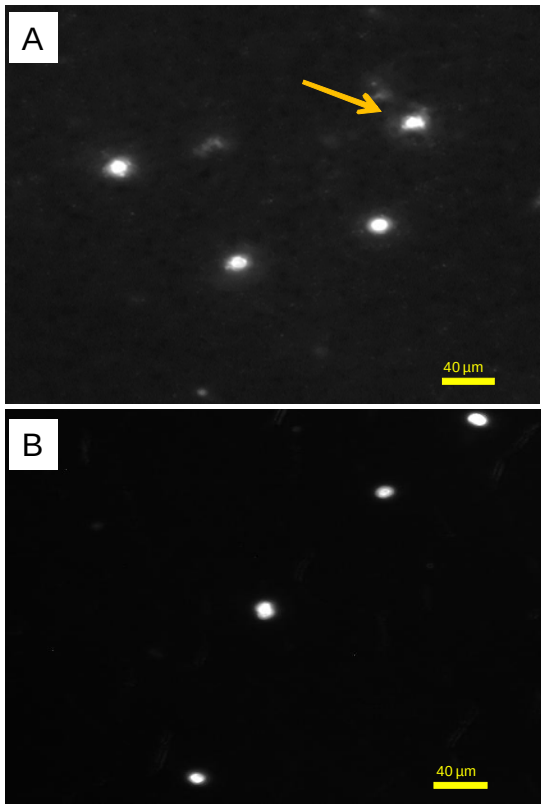

Figure 4.6 Fluorescent antibody labeled cysts trapped on A) a silver membrane filter and B) a gold-coated PCTE membrane filter.

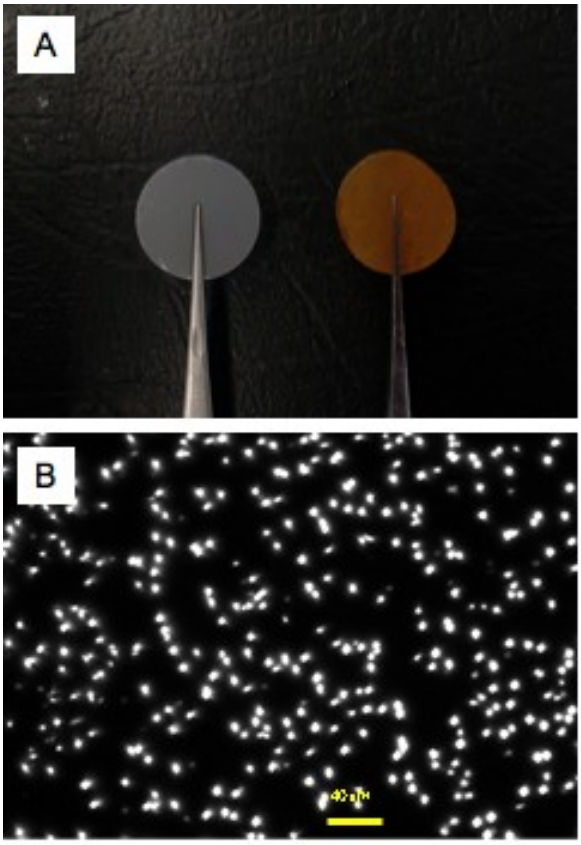

Figure 4.7 A) PCTE membrane filter before (left) and after (right) electroless gold coating. B) Optical light microscopy picture of gold-coated PCTE membrane filter.

WORKS CITED

1. Percival, S. L. A., *Microbiology of waterborne diseases*. Elsevier Academic Press: Amsterdam, 2004.
2. USEPA, Method 1623: *Cryptosporidium* and *Giardia* in Water by Filtration/IMS/FA. In United States Environmental Protection Agency: 2005; p 76.
3. Simmons, O. D., Sobsey, M. D., Heaney, C. D., Schaefer, F. W., Francy, D. S., Concentration and detection of Cryptosporidium oocysts in surface water samples by method 1622 using ultrafiltration and capsule filtration. *Applied and Environmental Microbiology* **2001,** 67, (3), 1123-1127.
4. Feng, Y. Y., Ong, S. L., Hu, J. Y., Song, L. F., Tan, X. L., Ng, W. J., Effect of particles on the recovery of Cryptosporidium oocysts from source water samples of various turbidities. *Applied and Environmental Microbiology* **2003,** 69, (4), 1898-1903.
5. Hu, J. Y., Feng, Y. Y., Ong, S. L., Ng, W. J., Song, L. F., Tan, X. L., Chu, X. N., Improvement of recoveries for the determination of protozoa Cryptosporidium and Giardia in water using method 1623. *Journal of Microbiological Methods* **2004,** 58, (3), 321-325.
6. LeChevallier, M. W., Di Giovanni, G. D., Clancy, J. L., Bukhari, Z., Bukhari, S., Rosen, J. S., Sobrinho, J., Frey, M. M., Comparison of method 1623 and cell culture-PCR for detection of Cryptosporidium spp. in source waters. *Applied and Environmental Microbiology* **2003,** 69, (2), 971-979.
7. DiGiorgio, C. L., Gonzalez, D. A., Huitt, C. C., Cryptosporidium and Giardia recoveries in natural waters by using environmental protection agency method 1623. *Applied and Environmental Microbiology* **2002,** 68, (12), 5952-5955.
8. Kim, K. J., Jung, H. H., Lee, K., Evaluation of cyst loss in standard procedural steps for detecting of Giardia lamblia and Cryptosporidium parvum in water. *Biotechnology and Bioprocess Engineering* **2006,** 11, (4), 368-371.
9. Grubisha, D. S., Lipert, R. J., Park, H. Y., Driskell, J., Porter, M. D., Femtomolar detection of prostate-specific antigen: An immunoassay based on surface-enhanced Raman scattering and immunogold labels. *Analytical Chemistry* **2003,** 75, (21), 5936-5943.
10. Escoriza, M. F., VanBriesen, J. M., Stewart, S., Maier, J., Treado, P. J., Raman spectroscopy and chemical imaging for quantification of filtered waterborne bacteria. *Journal of Microbiological Methods* **2006,** 66, (1), 63-72.
11. Menon, V. P., Martin, C. R., Fabrication and evaluation of nanoelectrod ensembles. *Analytical Chemistry* **1995,** 67, (13), 1920-1928.
12. Wei, A., Kim, B., Sadtler, B., Tripp, S. L., Tunable surface-enhanced Raman scattering from large gold nanoparticle arrays. *Chemphyschem* **2001,** 2, (12), 743-+.
13. Adar, F., In Wigginton, K. R., Ed. HORIBA Jobin Yvon: Edison, NJ, 2008.
14. Corporation, S. Sterlitech Silver Membrane Filter. (October 10),
15. Oda, T., Sakagami, M., Ito, H., Yano, H., Rai, S. K., Kawabata, M., Uga, S., Size selective continuous flow filtration method for detection of Cryptosporidium and Giardia. *Water Research* **2000,** 34, (18), 4477-4481.

16. Everall, N., Depth profiling with confocal Raman microscopy, part II. *Spectroscopy* **2004,** 19, (11), 16-+.
17. Everall, N., Depth profining with confocal Raman microscopy, part I. *Spectroscopy* **2004,** 19, (10), 22-+.
18. Mazenko, R. S., Rieders, F., Brewster, J. D., Filtration capture immunoassay for bacteria: optimization and potential for urinalysis. *Journal of Microbiological Methods* **1999,** 36, (3), 157-165.
19. Hsu, B. M., Huang, C. P., Hsu, Y. F., Jiang, G. Y., Hsu, C. L. L., Evaluation of two concentration methods for detecting Giardia and Cryptosporidium in water. *Water Research* **2001,** 35, (2), 419-424.
20. Nieminski, E. C., Schaefer, F. W., Ongerth, J. E., Comparison of 2 method for detection of Giardia cysts and Cryptosporidium oocysts in water *Applied and Environmental Microbiology* **1995,** 61, (5), 1714-1719.
21. Delvaux, M., Demoustier-Champagne, S., Walcarius, A., Flow injection amperometric detection at enzyme-modified gold nanoelectrodes. *Electroanalysis* **2004,** 16, (3), 190-198.
22. Delvaux, M., Walcarius, A., Demoustier-Champagne, S., Electrocatalytic H2O2 amperometric detection using gold nanotube electrode ensembles. *Analytica Chimica Acta* **2004,** 525, (2), 221-230.
23. Wernette, D. P., Swearingen, C. B., Cropek, D. M., Lu, Y., Sweedler, J. V., Bohn, P. W., Incorporation of a DNAzyme into Au-coated nanocapillary array membranes with an internal standard for Pb(II) sensing. *Analyst* **2006,** 131, (1), 41-47.
24. Huang, S. S., Sheng, C., Yin, Z. F., Shen, J., Li, R. N., Peng, B., Immunoreaction-based separation of antibodies using gold nanotubules membrane. *Journal of Membrane Science* **2007,** 305, (1-2), 257-262.
25. Kneipp, K., Haka, A. S., Kneipp, H., Badizadegan, K., Yoshizawa, N., Boone, C., Shafer-Peltier, K. E., Motz, J. T., Dasari, R. R., Feld, M. S., Surface-enhanced Raman Spectroscopy in single living cells using gold nanoparticles. *Applied Spectroscopy* **2002,** 56, (2), 150-154.
26. Demoustier-Champagne, S., Delvaux, M., Preparation of polymeric and metallic nanostructures using a template-based deposition method. *Materials Science & Engineering C-Biomimetic and Supramolecular Systems* **2001,** 15, (1-2), 269-271.

5) Investigation of Bacteriophage Viability via Surface-Enhanced Raman Spectroscopy and Principal Component Analysis

Krista Rule Wigginton, Tamar Kohn, and Peter J. Vikesland*

Department of Civil and Environmental Engineering, Virginia Polytechnic Institute and State University, 418 Durham Hall, Blacksburg, VA 24060-0246

ABSTRACT

The inactivation of ssRNA bacteriophage MS2 and ssDNA bacteriophage PhiX174 was studied by surface enhanced Raman spectroscopy (SERS). Live virus SERS spectra were compared with SERS spectra for heat-inactivated virus and virus inactivated by hydroxyl radical produced by metal-catalyzed oxidation (H_2O_2 and Cu^{2+}). Principal component analysis (PCA) was used to simplify and classify the SERS spectral data. A principal component ordination plot of viable MS2 and PhiX174 particles led to well-defined clusters of the two species. Heat-treated MS2 and heat-treated PhiX174 were differentiated from viable MS2 and viable PhiX174, respectively, in PC ordination plots, although the PC clusters were not well defined. Test samples were fed into the PCA

models and correctly predicted by their PC scores. The PCA loading data was then used in conjunction with the raw Raman spectra to identify the viral components responsible for the differences in the SERS spectra. Changes in the SERS bands for tryptophan, tyrosine, and α-helix were observed for the heat-treated experiments. For hydroxyl-treated MS2, changes in SERS bands for proline and tyrosine were observed.

5.1 INTRODUCTION

Drinking water is considered a highly probable vehicle for the transmission of human viruses in both developing and industrialized countries.[1] Viruses present particular challenges for wastewater and drinking water treatment for several reasons, including: 1) the high numbers of virus particles excreted from infected individuals (values as high as 10^{13} virus particles per gram of fecal matter),[2] 2) the infectious dose is believed to be as low as a single plaque forming unit (PFU),[3] and 3) their small size (10-100 nm) and resistance to common wastewater and drinking water oxidants[4] make it easier for viral particles to break through traditional multi-barrier treatment processes relative to most pathogenic organisms.

To better understand the potential risk of viral infection via contaminated drinking water, the Information Collection Rule (ICR) promulgated by EPA required nationwide virus monitoring in drinking water sources over an eighteen-month period between July 1997 and December 1998. Utilities tested waters using a total culturable virus method[5] and detected viruses in 13.5% (lowest month) to 37.8% (highest month) of sourcewaters.[6] Despite these alarming values, source and finished drinking waters are not currently monitored for virus contamination. Instead, virus levels are regulated by ill-defined

treatment technologies that should result in 99.99% of virus removal.[7, 8] While fecal indicator organisms such as *E. coli* are regularly measured in source and finished drinking waters, research has indicated that the presence or absence of indicator organisms does not necessarily correspond to the presence or absence of many waterborne viruses.[8, 9]

A number of virus species have been implicated as the etiological agents for human waterborne illness including enteroviruses (e.g., echo-, coxsackie- and polio-virus), hepatitis A virus, adenovirus, and human caliciviruses (e.g., norovirus).[3] Many of these species have been placed on the EPA's contaminant candidate lists (CCL2 and CCL3), however, implementation of virus monitoring and regulation have been hindered by a lack of simple virus detection methods.

At this time, the most common methods for virus detection in water samples are via cell culture infection and genomic or PCR based tests. In the cell culture methods, animal cell lines are exposed to a virus sample and cell infection is determined by measuring cell cytopathic effects.[3] A major advantage of cell culture over the alternative genomic methods is that cell culture only detects viable viruses. PCR, on the other hand, detects all of the DNA/RNA present in a sample, regardless if it was from a viable virus. Unfortunately, cell culture methods are labor intensive and it can take weeks to obtain results. Additionally, some human viruses such as hepatitis A and norovirus do not have permissive cell lines presently available and so these viruses are only detectable in environmental samples via genomic methods.[3]

There is an ongoing effort for the development of rapid microorganism detection strategies for both clinical diagnosis and environmental monitoring. Ideally, future

microorganism detection methods will be multiplex and compatible with automated analysis. Surface enhanced Raman spectroscopy (SERS) has been suggested as a tool for ultrasensitive pathogen detection as it is capable of rapid, multiplex data collection with extremely low sensitivities.[10, 11] Additionally, Raman spectrometers have become much more affordable for the average laboratory and the instrument footprint has decreased to a point where field Raman spectrometers are readily available.

Many proposed SERS methods for biomolecule detection have used immunogold labels that bind to the analyte biomolecule. The SERS immunogold labels consist of dye molecules and antibodies that are conjugated with gold nanoparticles. The dye molecules have characteristic "fingerprint spectra" and are surface enhanced by the gold nanoparticles. This type of SERS strategy has been successfully applied for protein,[12, 13] and virus[14] detection, and has enabled a multiplex protozoan pathogen detection strategy (Chapter 3). Drawbacks of this type of labeled detection method include the lack of information it provides about the physiological state of the organism (dead or alive, viable or nonviable), and the fact that many antibodies are not able to discriminate between similar strains or species. Additionally, non-specific immunogold binding to extraneous material in the sample often leads to false positive signals.

Normal Raman spectroscopy has been used to measure the intrinsic spectra of unlabeled organisms.[15, 16] As this strategy measures the spectrum of the organism itself and not that of a label molecule, it avoids the nonspecific-binding problems associated with antibody labeling. Also, intrinsic measurements reportedly detect the physiological state of the microorganisms.[17-21] Unfortunately, low detection limits are not possible with normal Raman spectroscopy, especially with short acquisition times. SERS, on the other

hand, can collect intense signals with much shorter acquisition times (several seconds rather than 30-60 minutes) and with weaker laser power.[22] Additionally, the gold and silver substrates used for SERS enhancements effectively quench fluorescence, which can be a major background interference when biological samples are measured with normal Raman.[22]

Intrinsic SERS evaluation of microorganisms was first reported by Efrima et al. who impregnated bacterial cells with silver[23] and a number of recent reports have employed SERS for bacteria,[24-30] virus,[31] and other bioanalyte[29] identification. Specific portions of bacterial cells have been probed with SERS[25] and it has been shown to be capable of differentiating between bacterial strains,[26] protozoa species,[32] and virus species.[31] To our knowledge, however, SERS has not been used to study virus viability.

SERS arises due to a combination of an electromagnetic enhancement and a chemical enhancement.[33-35] The electromagnetic effect, which produces the majority of the signal enhancement, stems from the small electromagnetic fields that form when surface plasmons oscillate at locations with nanometer-scale roughness on the noble metal surface. When this enhanced field combines with the electric field from the excitation source, the analyte gives off an enhanced Raman signal. Plasmon oscillations are dependent on the size, shape, and aggregation-state of the metal nanomaterials,[36, 37] and thus the electromagnetic SERS enhancement is dependent on these factors. Chemical enhancement, on the other hand, results from electronic coupling between the noble metal substrate and the analyte molecule and is thought to occur at spots with atomic-scale roughness.[38] For the electromagnetic effect to occur, the analyte biomolecule should be

within ~10 nm of the metal surface and for chemical enhancement,[39] the analyte should be in direct contact with the metal.[40]

Principal component analysis (PCA) is a multivariate statistical method that has been recently used to simplify and summarize biological spectral data collected with normal Raman and SERS.[26, 27, 41] In PCA, new variables are formed (principle components) that are linear combinations of the original variables and are orthogonal to one another. The principal components (PCs) summarize the sample variance with far fewer variables than were present in the original data. When used with Raman and SER spectra, PCA analysis can extract important spectral characteristics from the background features, can identify outlier spectra,[42] and allows for trends in the spectral data to be better visualized.[17, 43] PCA data scores can be subsequently combined with other statistical tools (e.g., discriminate analysis, cluster analysis) for sample classification and sample prediction.[26]

The simplicity of virus capsid structures makes SERS spectral analysis more straightforward than when it is used with more complex waterborne pathogens (e.g., bacteria, protozoa). In this work, we examine the SERS spectra of MS2 and PhiX174, two bacteriophage viruses that are often used as proxies for waterborne viral pathogens (Figure 5.1). MS2 is a small, icosahedral virus with a 26 nm diameter and an isoelectric point of 3.9.[44] The MS2 particle consists of single strand (ss) of RNA (3569 nucleotides) encapsulated by a protein coat. The protein coat consists of 180 copies of a coat protein and one copy of MS2 A protein. PhiX174, on the other hand, is a single strand DNA virus (5386 nucleotides) with a 27 nm diameter and an isoelectric point of 6.6.[44] The PhiX174 capsid contains 60 copies each of major capsid protein F, major spike protein G,

twelve copies of spike protein H, and a small DNA binding protein J. The twelve viral spikes on the viral capsid consist of pentamers of protein G.[45] The DNA binding protein J is bound to the inner side of the capsid.[46] The amino acid sequences of MS2 and PhiX174 major capsid proteins are presented in Table 5.1.

A goal of this research was to use SERS to provide insight into the mechanisms responsible for pathogen inactivation. The peptide sequences of the viral capsid proteins are readily available and so changes in the capsid proteins were connected to observed differences in the virus SERS spectra. The work presented here may ultimately lead to a rapid method for virus detection and appears to be capable of differentiating between active and inactive viruses.

5.2 MATERIALS AND METHODS

Ultrapure water (>18 $M\Omega cm^{-1}$) was used in all aqueous solutions. $AgNO_3$ (>=99.9999%), trisodium citrate dihydrate (+99%), $CuSO_4$, hydrogen peroxide, $CHCl_3$, polyethylene glycol (PEG), and streptomycin were purchased from Sigma (St. Louis, MO). NaCl, $CaCl_2$, yeast extract, and D-glucose were purchased from Fisher (Walthman, MA), Agar was purchased from Merck (Whitehouse Station, NJ), and Bacto Tryptone was purchased from BD (Franklin Lakes, NJ).

For ssRNA bacteriophage MS2 (ATCC 15597-B1) and ssDNA bacteriophage PhiX174 (ATCC 13706-B1), propagation was performed with *E. coli* (ATCC 700891 and ATCC WG49, respectively) using an established method[47] with slight modification. The growth and propagation of MS2 and PhiX174 were maintained in LB broth with streptomycin, $CaCl_2$, and D-glucose. The *E. coli* host suspensions were prepared by adding 5 mL of concentrated *E. coli* liquid culture into 1 L of warmed LB broth under

sterile conditions. The cells were grown at 37 ºC while shaking at 80 rpm until an O.D. of 0.04 at 600 nm was reached. At this point, 10 µL of 1×10^{11} PFU/mL virus stock in LB broth was added to the *E. coli* suspension and incubated at 37 °C for 4 to 5 hours without shaking. The bacterial cells were lysed by addition of 5 mL of $CHCl_3$ and after thoroughly mixing the suspension, the $CHCl_3$ was allowed to settle. The $CHCl_3$ phase was removed and discarded and the aqueous phase (containing both bacterial debris and virus particles) was centrifuged at 3385 × g for fifteen minutes. The supernatant was then combined with PEG (10% w/v) and NaCl (0.5 M) and left overnight at 4 °C. The following morning, the PEG-containing broth was centrifuged at 10,000 × g for 45 minutes and the liquid phase was carefully removed so as to not disrupt the pellet. At this point, 3-5 mL of dilution buffer was added to the pellet and was soaked for 2-12 hours. The resuspended pellet was transferred to a 50 mL tube, brought up to 40 mL, and the suspension was centrifuged at 10,000 × g for five minutes. The supernatant (containing the virus) was placed in a clean tube and to this 10 mL of $CHCl_3$ was added and the solution was mixed. Following centrifugation at 3000 × g for 10 minutes, the aqueous phase was placed in a new 50 mL tube. The $CHCl_3$ cleaning steps were repeated 4-5 times until no white emulsion remained between the aqueous and $CHCl_3$ phases. After the final $CHCl_3$ cleaning, the aqueous phase was transferred to a new tube and centrifuged for 10 minutes to remove residual $CHCl_3$. To concentrate the virus stock by approximately 100×, the aqueous phase was passed through a 100 kDa Ultracell Centricon tube (Millipore, Billerica, MA) via centrifugation at 3385 × g for 15-20 minutes. The suspension was washed three times with virus dilution buffer and collected

in a final volume of 500-1000 μL. Finally, the volume was filter sterilized using a Millex-W PVDF 0.1 μm filter (Millipore). MS2 and PhiX174 preparations were enumerated using the double-layer agar method.[47] The resulting MS2 stock solutions typically had virus concentrations of $\approx 1 \times 10^{13}$ Plaque Forming Units (PFU)/mL and the PhiX174 preparations were usually $\approx 1 \times 10^{11}$ PFU/mL. Both were stored at 4 ºC.

Silver nanoparticles were prepared by an established method.[48] Briefly, a 2 mL aliquot of 1% sodium citrate was added with rapid stirring to a boiling solution of $AgNO_3$ (100 mL of 1.06 mM). The reaction was allowed to proceed under reflux with stirring for 90 minutes at which point the heat was removed. Size analysis of the transmission electron micrographs (Figure 5.2) with NIH Image J software indicated that the nanoparticles had an average diameter of 53 nm.

As one aim of this research was to use SERS to differentiate between viable and non-viable virus, it was necessary to first establish if the SERS substrate would lead to virus inactivation. Silver nanoparticles, which were the substrate for SERS enhancement, have been shown to result in microorganism inhibition[49] and cell death.[50] Tests were therefore conducted in which silver nanoparticles were added to viable MS2 viruses and virus viability was tested after 6 hours of mixing via plaque assays. This period of time was much longer than the period of time virus samples were exposed to silver nanoparticles in the SERS experiments. After reacting for 6 hours with silver nanoparticles ($[Ag]_{total}$ = 0.1 mM), MS2 virus viability decreased slightly, although the decrease was not significant (-13.4±13.6%). It was therefore determined that the silver nanoparticle substrates did not result in extensive levels of virus inactivation over the timeframe of our experiments.

For SERS measurements to be successful, the analyte must be closely associated with the SERS enhancing metal surfaces. It was therefore important to optimize the solution pH to encourage virus-nanoparticle interactions. The isoelectric points of MS2 and phiX174 are 3.9 and 6.6, respectively, and thus at neutral pH both viruses are negatively charged. In addition, the silver nanoparticles are negatively charged at neutral pH due to surface associated citrate.[51] For this reason, the nanoparticle solution pH was adjusted to 4 with 0.1 M HCl. SERS solid substrates were then prepared by placing 30 μL of the pH 4 silver nanoparticle solution in a small spot on aluminum coated glass microscope slides. The spot was allowed to dry and another 30 μL was placed over the top of the first spot and allowed to dry. When inspected with an optical microscope, these spots consisted of large, fractal aggregates of the silver nanoparticles. Immediately prior to Raman measurement, virus samples were placed on the silver nanoparticle spots.

To obtain simple SERS spectra with few background peaks, virus stocks were rinsed of their dilution buffer with Microcon filters (Millipore) and resuspended in 15 mM NaCl. Control tests showed that 15 mM NaCl did not affect virus viability. For the virus heat inactivation experiments, small aliquots of virus stock at a concentration of 10^{13} PFU/mL (10-50 μL) in 15 mM NaCl were placed in centrifuge tubes and heated in a PTC-200 DNAEngine PCR thermocycler (MJ Research, Waltham, MA). The PhiX174 stock solution was 100× less concentrated than the MS2 stock solution and so PhiX174 was concentrated 100× with a Microcon centrifugal filter device prior to the heat treatment experiment. The temperature treatment consisted of elevating the virus solution temperature to 72 °C for 3 minutes. Prior tests in the Kohn lab showed that this

temperature leads to > 8 log inactivation of MS2 and > 4 log inactivation of PhiX174. Following heat treatment, 5 μL aliquots of the virus samples were placed on duplicate silver nanoparticle substrate spots and allowed to dry. Raman measurements were made immediately thereafter.

For metal-induced hydroxyl radical experiments, Cu^{2+} and H_2O_2 were combined with the MS2 virus. Specifically, 1 mL samples containing MS2 (1×10^{11} PFU/mL) were spiked with 10 μM Cu_2SO_4 and 50 μM H_2O_2. This concentration of Cu_2SO_4 and H_2O_2 was previously shown to cause > 6 logs of MS2 inactivation after 1 hour (unpublished results). Two control samples were prepared, one that contained only H_2O_2 and $CuSO_4$, and another that contained virus with Cu^{2+}. The samples were mixed for 3 hours at room temperature, then concentrated with a Microcon centrifugal filter and resuspended in 10 μL of 15 mM NaCl. The 10 μL samples were divided into two samples (5 μL each) that were then placed on the duplicate silver nanoparticle spots and dried prior to SERS measurements.

Raman spectra were collected with a Renishaw System RM1000 (Renishaw Plc, Wotton-under-Edge, UK) equipped with a Leica microscope. The Raman microspectrometer was operated nonconfocally and had a 50× objective (N.A.= 0.75). Excitation at 785 nm was used and analysis was performed with 25-100% laser power depending on the spectrum intensity and 2×10 s acquisitions were used for all measurements. A spectral range of 200-2000 cm^{-1} was collected for each sample. All data was collected with Grams instrument software (Thermo Scientific, Waltman, MA). Spectra were converted to ASCII data and subsequently exported to MATLAB 6.5 (The

Mathworks, Natick, MA). Spectral preprocessing and principal component analysis were conducted with PLS_Toolbox 4.2 (Eigenvector Research, Wenatchee, WA). Preprocessing was used to rid the spectra of large variances in baseline drift and to normalize the band intensities. Baseline correction was conducted using Savisky-Golay first derivatives (9-point window) and spectral normalization was performed by setting the largest peak in the spectra equal to one. This pretreatment has been previously used to treat biomolecule Raman spectra prior to Principal Component Analysis.[26, 52] PCA models were prepared for a number of sample combinations (live MS2 versus live phi, live MS2 versus heat treated MS2, etc…).

5.3 RESULTS AND DISCUSSION

Replicate SERS spectra were collected at ten different locations on the prepared duplicate samples and although the replicates appeared to have major peaks in the same locations (at the same wavelengths), their baseline drifts and peak intensities varied substantially (Figure 5.3). As a result, it was difficult to make conclusions about subtle sample differences by visually analyzing the spectra and comparing sample peak tables. Although baseline correction and spectral averaging helped illustrate major differences between samples (Figure 5.4), the statistical significance of the similarities and differences remained unclear. Figure 5.4 shows the average of 10 sample spectra collected for the NaCl blank, untreated MS2, and untreated PhiX174. Clearly, there are differences between these spectra, however, care should be taken with average spectra as spectral averages can be misleading. For instance, the average spectrum for MS2 shows a peak at 791.9 cm^{-1}; however, upon inspection of the individual samples, this peak was

only present in two of the ten MS2 spectra. PCA was therefore used to discriminate similarities and differences within the sample classes and amongst sample classes.

A large peak located at 1055 cm^{-1} was present in nearly every spectrum, including the control samples and the silver nanoparticle blanks. We have assigned this peak to a COO^- stretch of citrate molecules adsorbed to the silver nanoparticles.[53, 54] For spectral normalization, the largest peak in the spectrum was given a value of one after baseline correction, and in most of the spectra the largest peak was the 1055 cm^{-1} peak. PCA modeling focused on the spectral range between 500-1000 cm^{-1} as this window showed the most pronounced differences amongst the sample sets. The 1055 cm^{-1} was thus excluded from the models as this led to an improvement in sample class separation by the PCs.

For each of the PC models, 80% of the collected spectra for a given sample were used to build the model and 20% were excluded and later classified with the model. In the first experiment, the SERS spectra of live MS2 and PhiX174 were analyzed and compared. As illustrated in Figure 5.5, the majority of the variance between live MS2 and live PhiX174 within the 500-1000 cm^{-1} window is captured by the first two principal components. In Figure 5.6, the different sample classes are clearly separated by plotting the first principal component (44.6% of the total variance) against the second principal component (29.2% of the total variance). The model was then used to predict the classes of four samples, two MS2 and two PhiX174. As illustrated in Figure 5.6, the four samples were correctly classified using PC1 and PC2.

The loadings of the first two PCs are illustrated in Figure 5.7. These plots specify areas of variance in the SERS spectra that make up the individual PCs. The majority of

the loadings for PC1 and PC2 are due to variance in the 650-750 cm^{-1} range. Upon examination of the average spectra (Figure 5.4), these ranges contain peaks at 660.1 cm^{-1}, 725.5 cm^{-1}, and 740.3 cm^{-1} in the PhiX174 spectra and a peak at 731.2 cm^{-1} in the MS2 spectra. Variation in this region of SERS spectra for closely related viral species and strains have been previously reported[55, 56] and have been attributed to differences in capsid protein peptide sequences, secondary structure, and differences in their nucleic acid sequences. The thickness of the protein capsid of both MS2 and PhiX174 is only 2-3 nm[57, 58] and thus it is plausible that the electromagnetic SERS effect from the silver nanoparticles may cause an enhancement of the nucleic acids within the capsid. A previous Raman study with intact phage particles, however, reported that the intensities of Raman bands due to nucleic acids were relatively weak compared to those due to capsid proteins.[59]

Of the amino acids in the capsid proteins, those with aromatic side chains (tyrosine, tryptophan, phenylalanine, histidine) tend to dominate protein Raman spectra[60, 61] and strong bands also result from amide bands in the polypeptide backbones.[61] Based on previous virus and other biomolecule Raman/SERS reports, we predict that the PhiX174 660 cm^{-1} peak (present in 100% of the replicates) is due to the C-C twisting mode of tyrosine residues present in the PhiX174 capsid proteins or from the ring breathing modes of thymine and guanine bases.[55, 59, 62, 63] The 725.5 cm^{-1} peak (100% of replicates) and 740 cm^{-1} peak (90% of replicates) in the phiX174 spectra and the 731.2 cm^{-1} peak in the MS2 spectra (100% of replicates) are assigned to the symmetric benzene/pyrrole in-phase breathing mode of tryptophan residues or from the ring breathing modes of nucleic acid bases.[55, 62-64]

Loadings for PC 1 also incorporate variance near 950 cm^{-1} due to a peak at 959.8 cm^{-1} that has higher intensity and frequency in the PhiX174 replicates than the MS2 replicates (90% versus 40%). This peak has been assigned to C-C α-helix stretching.[62, 65] Additionally, PC2 loading at 510-570 cm^{-1} (Figure 5.7) is the result of the 516 cm^{-1} peak present in 50% of the PhiX174 samples that has not been assigned to a specific viral component.

It should be noted that characteristic Raman bands for amino acids have been shown to shift as their peptide sequence is changed[61] and thus shifts in the amino acid bands of MS2 and PhiX175 were expected. Although both viruses may have a particular residue in their protein capsid, it may or may not appear in the SERS spectra as a result of where the residue is located in the capsid relative to the silver enhancing particles.

5.3.1 Heat Treated Viruses

For the heat-treated virus experimental data, a PCA model was used to compare the SERS spectra of live MS2 and heat inactivated MS2 sample spectra. The average spectra showed significant differences between the untreated and treated virus between 500 cm^{-1} and 1000 cm^{-1} (Figure 5.8), however it was again difficult to make quantitative conclusions by visually studying the replicate spectra. As illustrated in Figure 5.9, a plot of the first PC (56.7% of total variance) and the second PC (10.7% of total variance) led to pseudo-classification of the untreated and treated samples, with the second PC carrying most of the variance in this class separation. Test samples were correctly classified when plotted on the ordination plots. The untreated samples made a tighter cluster than the treated samples in the PC1 versus PC2 plot. The blurring of the heat-treated MS2 response is likely due to alterations that occur in the virus capsid during heat treatment.

The temperature at which the MS2 capsid denatures is 68.8 °C[66] and thus it is likely that changes in the secondary structure of the MS2 capsid proteins occurred. Previous reports examining the effect of heating on protein Raman spectra suggest that denatured proteins exhibit an altered hydrophobic environment within the protein structure,[65, 67] show changes in disulfide bonding,[65, 67] and show changes in alpha helix secondary structure.[65] In general, the Raman spectra of proteins become less ordered and noisier after heat treatment[65] and thus less defined PCA clusters were expected.

The PC2 loading for live and heat-treated MS2 showed spectral variance in small spectral ranges centered around 675 cm^{-1}, 725 cm^{-1}, and 850 cm^{-1} (Figure 5.10). The sample spectra from live MS2 contain a peak at 680 cm^{-1} (80% of replicates) that is less intense and less common in the heat-treated sample spectra (40%). The 680 cm^{-1} peak is assigned to the C-C twisting mode of tyrosine although it is also possible that the peak is due to RNA bases.[55, 62 59, 63] A broad peak at 850 cm^{-1} is present in the heat treated MS2 (80% of spectra) and not present in the untreated samples and is assigned to the ring breathing mode of tyrosine or proline residues.[55, 62, 65, 68] It has previously been described that the hydrogen bonding nature of tyrosine is altered during protein heating and this may have caused intensity changes in the tyrosine Raman bands.[65] The variance around 725 cm^{-1} in the PC2 loading is most likely due to subtle shifts in the 731 cm^{-1} bands of both untreated and heat-treated MS2 and this peak was assigned to symmetric breathing of tryptophan and or adenine bases.[59, 62, 63, 65] Peak intensity changes and peak broadening of tryptophan bands due to changes in protein environment polarity have been previously observed.[65, 67] TEM images have shown that MS2 capsids expand during the heating conditions used here but do not rupture (data not shown) and so altered SERS RNA peaks

are due to changes in the RNA molecule within the capsid shell (i.e., interactions between the RNA and the capsid proteins).

Figure 5.11 illustrates average spectra for untreated and heat-treated PhiX174 samples. PCA was conducted on the replicate spectra and as shown in Figure 5.12, a PC ordination plot of the first two principal components (accounting for 76.7% of the total variance) shows distinguishable clusters and the test samples were correctly classified by these PCs. Most of the classification in Figure 5.12 occurs due to PC2 and variance in this PC primarily occurs in the 650-700 cm^{-1} and 725-750 cm^{-1} regions of the spectra (Figure 5.13). Both the treated and untreated PhiX174 spectra have peaks around 660 cm^{-1} and this peak is assigned to the C-C twisting mode of tyrosine residues in the capsid proteins and/or guanine and thymine ring breathing modes in the DNA.[55, 59, 62, 63] As mentioned above, heat-induced changes to tyrosine Raman peaks have previously been reported. Untreated PhiX174 has two peaks in the 725-750 cm^{-1} region, one at 725.5 cm^{-1} (90% of spectra replicates) and one at 740.3 cm^{-1} (80% of spectra replicates). The heat treated PhiX174, on the other hand, has only one peak in this region at 729 cm^{-1} (100% of the replicates). Peaks in this range have previously been assigned to symmetric breathing of tryptophan residues and to adenine bases.[59, 62, 63, 65, 68] A previous Raman study on heat-treated proteins reported that changes in tryptophan bands occurred as a result of changes in hydrophobic residue interactions.[67]

Like PC2, loading from PC1 was primarily focused on variance in the 650-700 cm^{-1} and 725-750 cm^{-1} spectral regions (Figure 5.13), but PC1 also carried variance in the 925-927 cm^{-1} spectral region. The PhiX174 spectra (Figure 5.11) include a 959 cm^{-1} peak in both the untreated (80% of replicates) and heat-treated (50% of replicates)

PhiX174 and this was assigned to C-C stretching within the α-helix secondary structures.[65] Decreases in this peak have previously been observed following protein heating and have been attributed to a decline in the α-helix structures[65] which are present in the PhiX174 major capsid protein F.[57]

5.3.2 Hydroxyl Radical Treated MS2

For the metal-catalyzed oxidation experiment, MS2 virus was treated with Cu^{2+} and H_2O_2. This combination produces hydroxyl radical through the following reaction pathway:[69]

$$Cu^{2+} + H_2O_2 \rightarrow Cu^{+} + H^{+} + HO_2^{\bullet}$$

$$Cu^{+} + H_2O_2 \rightarrow Cu^{2+} + OH^{-} + {}^{\bullet}OH$$

For proteins treated via metal-catalyzed oxidation, a metal ion bound to the protein undergoes the above reaction to create the hydroxyl radical,[70] which subsequently reacts with the protein in a site-specific manner.[71] Although it is established that treating with Cu^{2+}/H_2O_2 rapidly leads to virus inactivation,[72] the specific virus inactivation pathway is not currently understood.

Previously, the treatment of proteins with Cu^{2+}/H_2O_2 lead to oxidative deamination of a number of amino acids, and resulted in an increase in the number of protein carbonyl groups.[69] Specific amino acid groups that have been shown to be susceptible to oxidation by Cu^{2+}/H_2O_2 include histidine, arginine, proline, lysine, tyrosine, phenylalanine, and glycine.[73-77] Oxidation of histidine, arginine, and proline leads to the formation of carbonyl groups,[73-75] phenylalanine transforms to o-tyrosine,[77] and lysine is oxidized to form allysine (α-aminoadipic-δ-semialdehyde).[76]

Figure 5.14 shows average spectra from 500-1000 cm^{-1} of Cu^{2+}/H_2O_2 blank replicates, untreated MS2, MS2 treated with Cu^{2+}, and MS2 treated with Cu^{2+}/H_2O_2. PCA was performed on these four sample groups simultaneously and all sample groups were visually compared by plotting their PC scores. As demonstrated in Figures 5.15 and 5.16, the samples form clusters of their respective classes in PC ordination plots and "test" spectra are correctly classified when their scores are added to the plots. In Figure 5.15, PC1 scores are plotted against PC2 and PC3 scores leading to distinguishable clusters of untreated MS2, hydroxyl-treated MS2, and the Cu^{2+}/H_2O_2 blank. Cu^{2+}/H_2O_2-treatment therefore caused changes to MS2 that were detectable via SERS. Similarly, a plot of PC 1 versus PC 4 (Figure 5.16) effectively separates the metal-catalyzed virus from virus that was treated only with Cu^{2+} and this indicates that the changes observed in the MS2 SERS spectra after Cu^{2+}/H_2O_2 treatment were not caused by Cu^{2+} interacting with the MS2 particles.

Most of the separation in Figure 5.15 between untreated MS2 and Cu^{2+}/H_2O_2 -treated MS2 samples results from differences in the PC1 and PC2 scores (Figure 5.15), while PC3 and higher PCs did not contribute significantly to this classification. Plots of PC1 and PC2 loadings show that an area of high variance occurred around 680 cm^{-1} (Figure 5.17). This variance can be explained by peaks at 661 cm^{-1} and 680 cm^{-1} in the untreated MS2 spectra and a peak at ~680 cm^{-1} in the Cu^{2+}/H_2O_2 -treated MS2 spectra and the Cu^{2+} -treated MS2 spectra (Figure 5.14). Interestingly, a peak at ~680 cm^{-1} also caused variation in PCA scores in the MS2 heat treatment experiments and was assigned to the C-C twisting mode of tyrosine residues and/or the ring breathing modes of nucleic acid bases. As mentioned previously, changes in the hydrogen bonding nature of tyrosine

can alter the associated Raman bands and tyrosine residues are susceptible to hydroxyl oxidation. Therefore, we conclude that both Cu^{2+} and heat treatment affected the hydrogen bonding associated with tyrosine residues on MS2.

Loadings for PC2 also showed major areas of variance in the 700-750 cm^{-1}, 825-875 cm^{-1}, and 950-980 cm^{-1} spectral ranges (Figure 5.17). The variance around 700-750 cm^{-1} is due to a peak at ~730 cm^{-1} in both the untreated and treated MS2. This band shifted with MS2 heat treatment and was assigned to symmetric breathing of tryptophan residues and adenine bases. The variance at 825-875 cm^{-1} in PC2 is due to an increase in the intensity and frequency of the 853 cm^{-1} peak in the treated MS2 (70% of replicates) compared to untreated MS2 (30% of replicates). Proline and tyrosine bands in the 850 to 855 cm^{-1} range have been reported[62] and both of these residues are susceptible to hydroxyl radical oxidation.[77] Interestingly, the peak at ~853 cm^{-1} also increased after heat treatment in the heat-treated MS2 experiments. We therefore conclude that with both heat treatment and hydroxyl radical treatment, the environment or chemistry of the proline and/or tyrosine residues are modified, thus causing an increase in the 853 cm^{-1} peak.

It should be mentioned that peaks at ~630 cm^{-1}, 731 cm^{-1} and ~853 cm^{-1} have been assigned to nucleic acids in past studies,[55, 59, 62, 63] however past PCR experiments have shown that the treatment of MS2 with Cu^{2+}/H_2O_2 does not strongly affect the integrity of MS2 RNA (Kohn, unpublished results). If exposed, nucleic acids would be readily oxidized by hydroxyl radical and so it was concluded that the capsids were not ruptured by the Cu^{2+}/H_2O_2 treatment. If this is the case, amino acids in the protein capsid are in closer contact with the enhancing silver nanoparticles than the nucleic acids. We have thus concluded that the observed changes in MS2 SERS spectra resulting from

Cu^{2+}/H_2O_2 treatment are caused by changes in the capsid proteins and not by alterations to the nucleic acids.

5.4 CONCLUSIONS

In conclusion, SERS was successfully employed to differentiate between two virus species, MS2 and PhiX174, as well as between untreated virus samples and inactivated virus samples. Data was analyzed via PCA and this enabled sample classification and simplified interpretation of spectral features that would have been impossible to observe with the raw spectra. Test samples were correctly classified based on their PC scores. Based on the results, SERS spectral bands due to tyrosine and tryptophan were affected by heat inactivation and proline and tyrosine bands were affected by hydroxyl reactions. Currently, we are focusing on the application of discriminant analysis tools to conduct robust statistical classification and predictions with the virus data.

TABLES AND FIGURES

Table 5.1 Amino acid sequence of major MS2 and PhiX174 capsid proteins

Protein name and Swiss database code	Amino Acid Sequence
MS2 Capsid Protein P03612 (180 copies per capsid)[78]	ASNFTQFVLV DNGGTGDVTV APSNFANGVA EWISSNSRSQ AYKVTCSVRQ SSAQNRKYTI KVEVPKVATQ TVGGVELPVA AWRSYLNMEL TIPIFATNSD CELIVKAMQG LLKDGNPIPS AIAANSGIY
PhiX174 Capsid Protein F P03641 (60 copies per capsid)[57]	SNIQTGAER MPHDLSHLGF LAGQIGRLIT ISTTPVIAGD SFEMDAVGAL RLSPLRRGLA IDSTVDIFTF YVPHRHVYGE QWIKFMKDGV NATPLPTVNT TGYIDHAAFL GTINPDTNKI PKHLFQGYLN IYNNYFKAPW MPDRTEANPN ELNQDDARYG FRCCHLKNIW TAPLPPETEL SRQMTTSTTS IDIMGLQAAY ANLHTDQERD YFMQRYHDVI SSFGGKTSYD ADNRPLLVMR SNLWASGYDV DGTDQTSLGQ FSGRVQQTYK HSVPRFFVPE HGTMFTLALV RFPPTATKEI QYLNAKGALT YTDIAGDPVL YGNLPPREIS MKDVFRSGDS SKKFKIAEGQ WYRYAPSYVS PAYHLLEGFP FIQEPPSGDL QERVLIRHHD YDQCFQSVQL LQWNSQVKFN VTVYRNLPTT RDSIMTS

PhiX174 Spike Protein G P03643 (60 copies per capsid)[57]	MFQTFISRHN SNFFSDKLVL TSVTPASSAP VLQTPKATSS TLYFDSLTVN AGNGGFLHCI QMDTSVNAAN QVVSVGADIA FDADPKFFAC LVRFESSSVP TTLPTAYDVY PLNGRHDGGY YTVKDCVTID VLPRTPGNNV YVGFMVWSNF TATKCRGLVS LNQVIKEIIC LQPLK

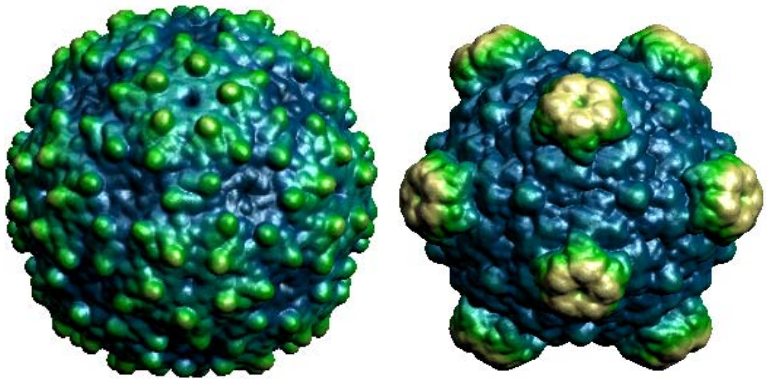

Figure 5.1 MS2 (left) and PhiX174 (right) bacteriophage viral capsid structures.[79] The MS2 capsid consists of 180 copies of a single capsid protein and the PhiX174 capsid consists of 60 copies of a capsid protein, 60 copies of a spike protein (5 on each of the 12 spikes), and 60 copies of a DNA binding protein on the inner side of the capsid.

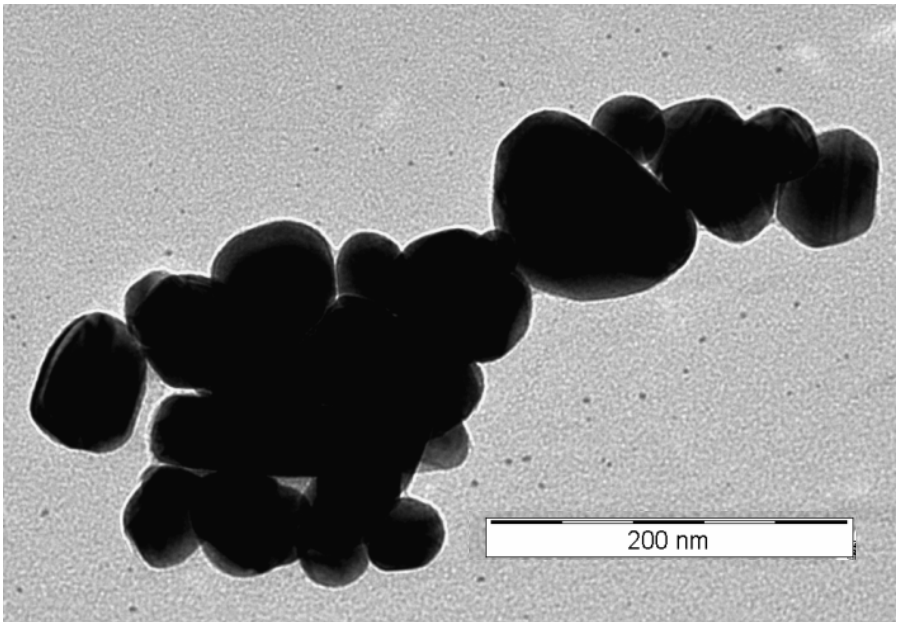

Figure 5.2 TEM image of silver nanoparticles prepared with citrate reduction. Average diameters: Major axis = 59.7 nm (S.D. = 19.7), minor axis = 45.9 nm (S.D. = 16.0) as determined by NIH ImageJ software.

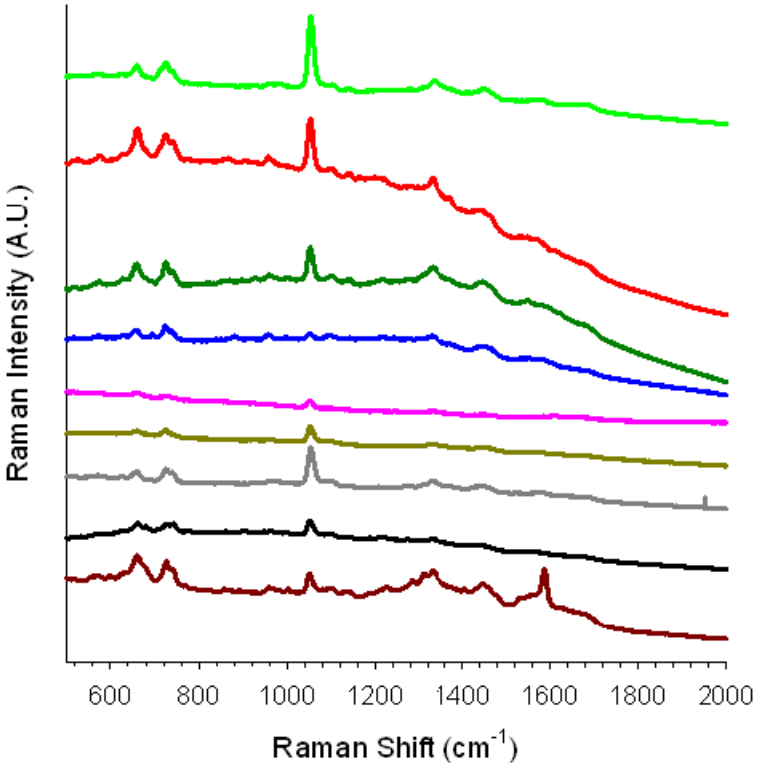

Figure 5.3 Replicate PhiX174 SERS spectra shown without baseline correction or intensity normalization. Acquisition conditions: 2 × 10 s acquisition times, 50× objective, 785 nm excitation.

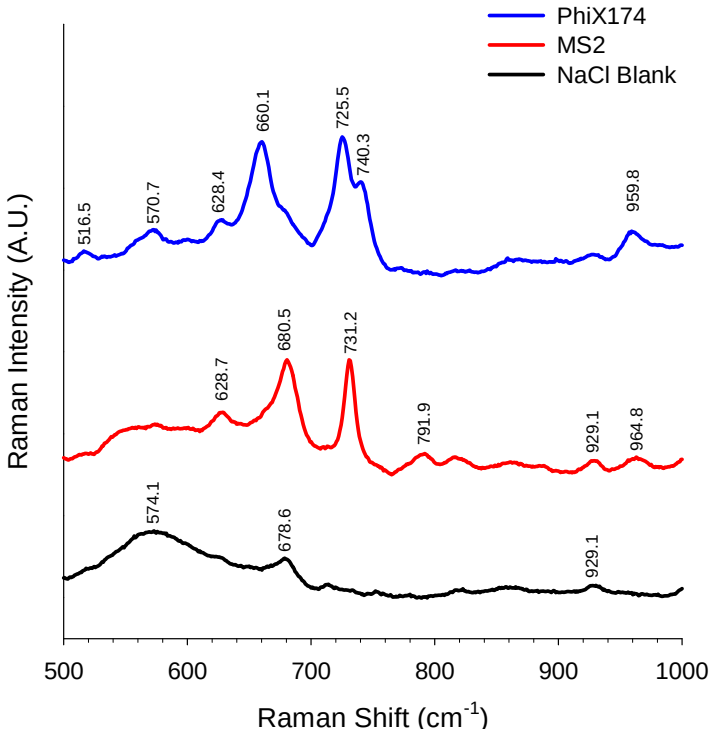

Figure 5.4 PhiX174, MS2, and NaCl-blank average SERS spectra. Each spectrum represents the average of 10 replicate sample spectra. Acquisition conditions: 2 × 10 s acquisition times, 50× objective, 785 nm excitation.

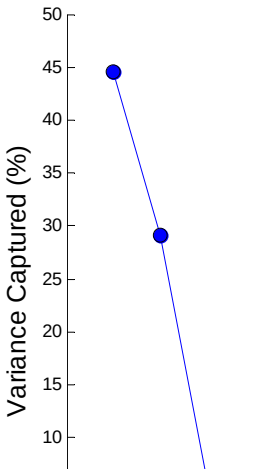

Figure 5.5 Captured variance as a function of the number of PCs for untreated MS2 and untreated PhiX174 PCA.

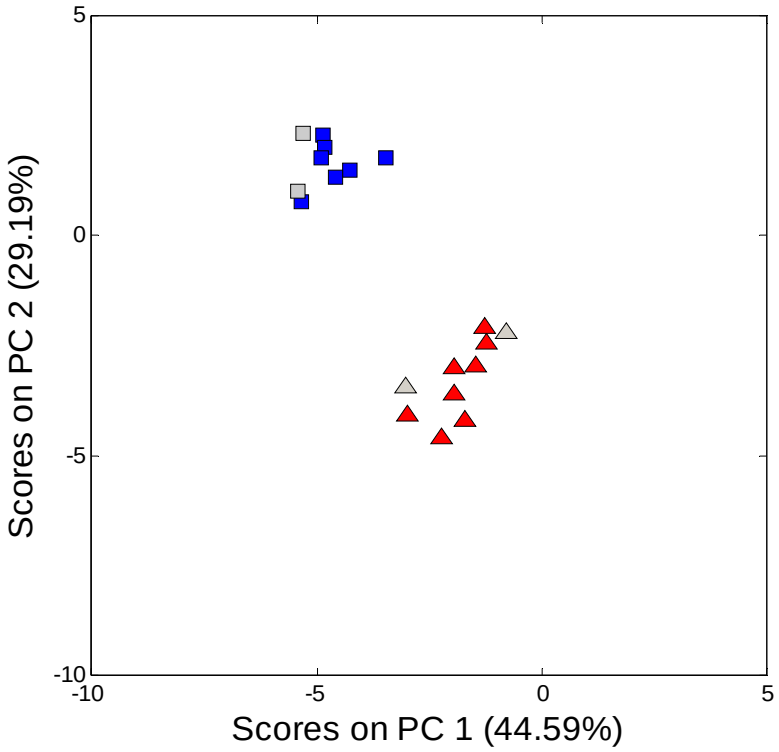

Figure 5.6 PC1 versus PC2 for untreated MS2 (red triangles) and PhiX174 (blue squares). Grey-filled shapes represent test samples predicted with PCA model.

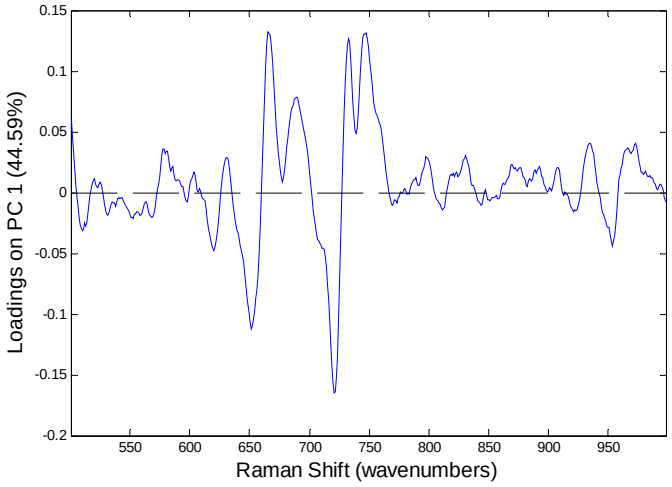
0.15
0.1
0.05
0
-0.05
-0.1
-0.15
-0.2
Loadings on PC 1 (44.59%)
550
600
650
700
750
800
850
900
950
Raman Shift (wavenumbers)

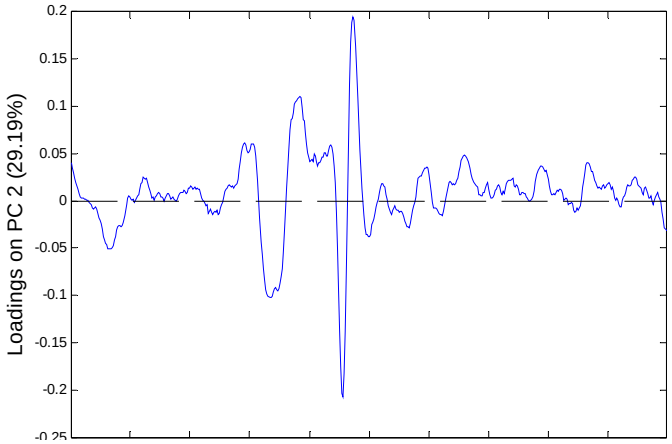
0.2
0.15
0.1
0.05
0
-0.05
-0.1
-0.15
-0.2
-0.25
Loadings on PC 2 (29.19%)

Figure 5.7 Loadings of PC1 (top) and PC2 (bottom) for untreated MS2 and untreated PhiX174 analysis.

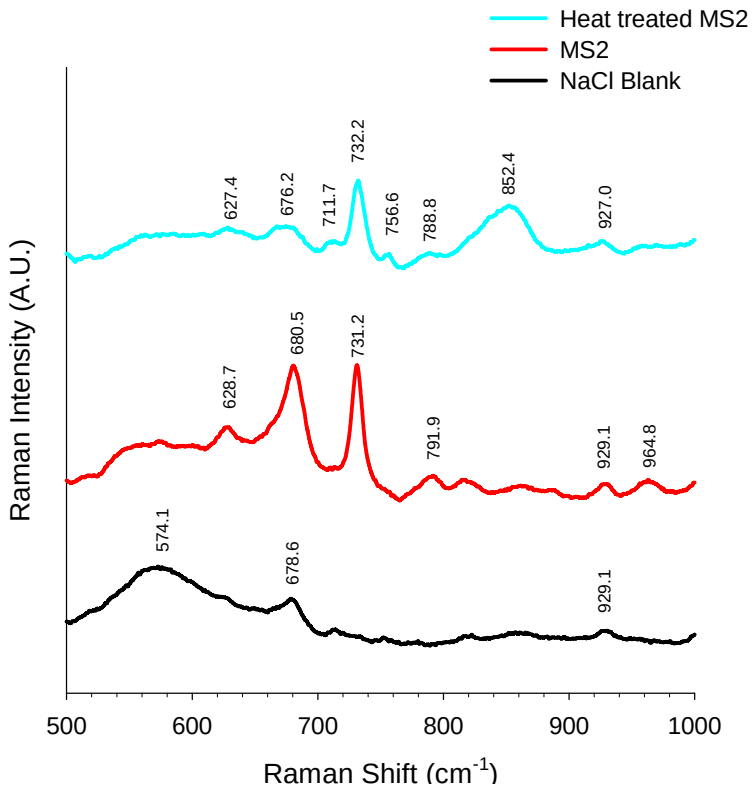

Figure 5.8 Untreated MS2, heat-treated MS2, and NaCl control average SERS spectra. Each spectrum represents the average of 10 replicate sample spectra. Acquisition conditions: 2 × 10 s acquisition times, 50× objective, 785 nm excitation.

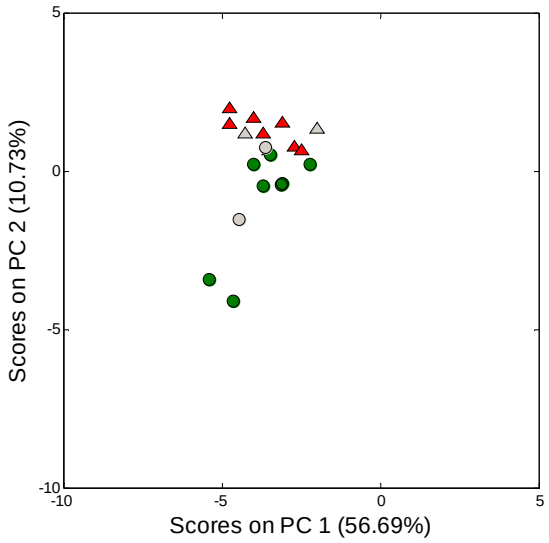

Figure 5.9 PC1 vs. PC2 from untreated MS2 (red squares) and heat-inactivated MS2 (green circles). Grey shapes represent test samples predicted by PCA model.

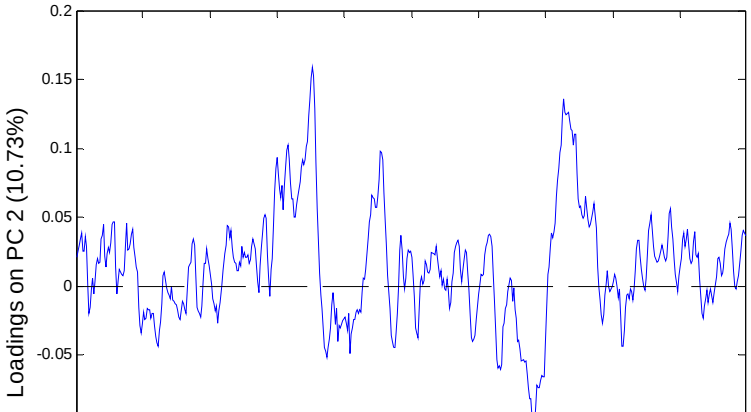

Figure 5.10 PC2 loading for untreated MS2 and heat-inactivated MS2 analysis.

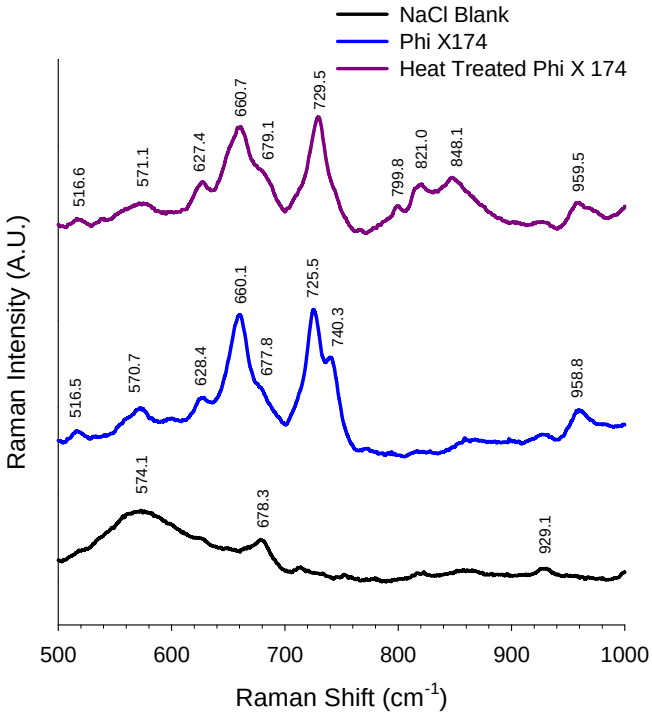

Figure 5.11 Untreated PhiX174, heat-treated PhiX174, and NaCl control average SERS spectra. Each spectrum represents the average of 10 replicate sample spectra. Acquisition conditions: 2 × 10 s acquisition times, 50× objective, 785 nm excitation.

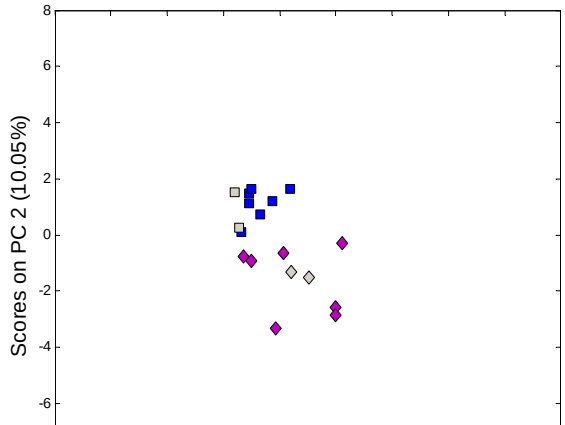

Figure 5.12 PC1 vs. PC2 for the untreated PhiX174 (blue squares) and heat-treated PhiX174 (pink diamonds) samples. Grey shapes represent test samples predicted with PCA model.

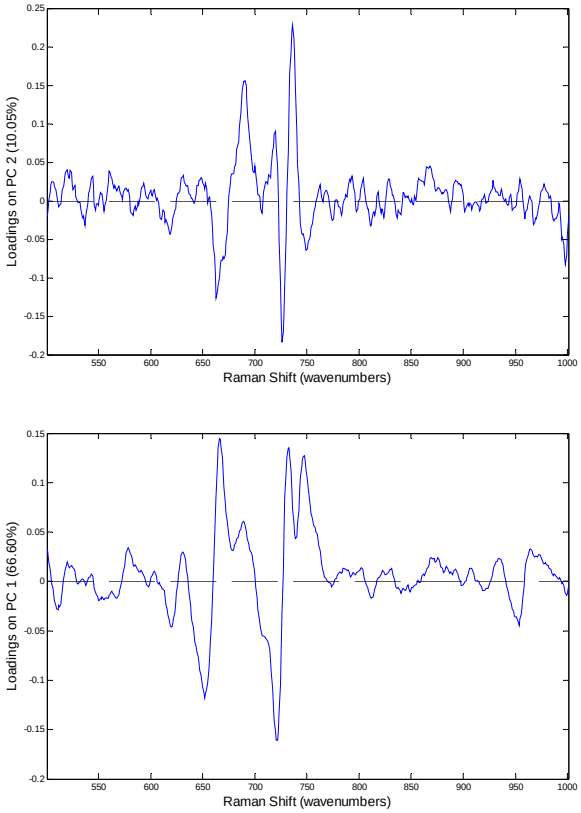

Figure 5.13 PC1 and PC2 loadings for untreated and heat-treated PhiX174 samples. The first PC (top) accounts for 66.6% of the total variance and the second PC (bottom) accounts for 10.05% of the data variance.

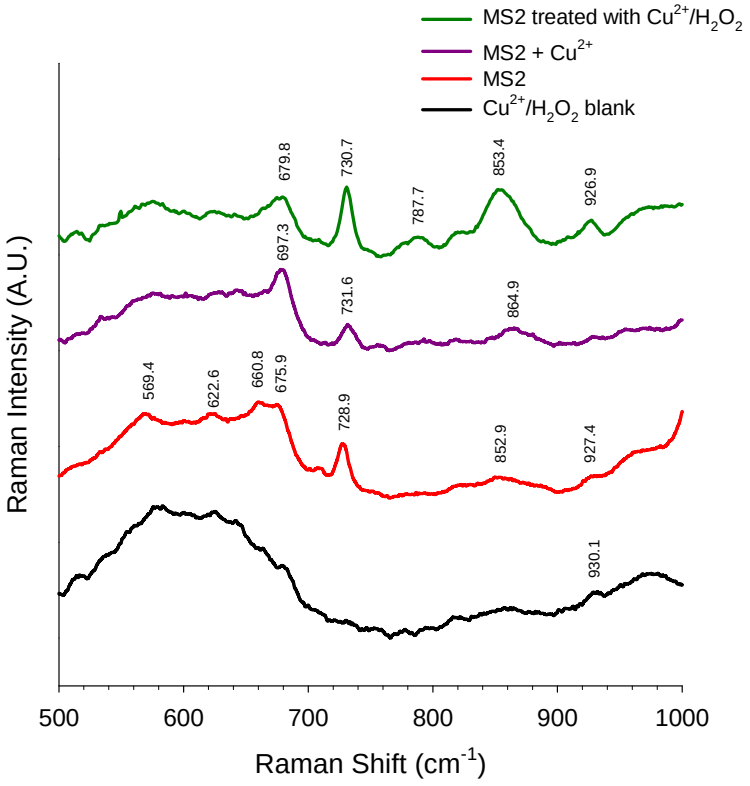

Figure 5.14 SERS spectra of Cu^{2+}/H_2O_2-treated MS2, Cu^{2+}-treated MS2 control, untreated MS2, and NaCl control. Each spectrum represents the average of 10 replicate sample spectra. Acquisition conditions: 50× objective, 785 nm excitation.

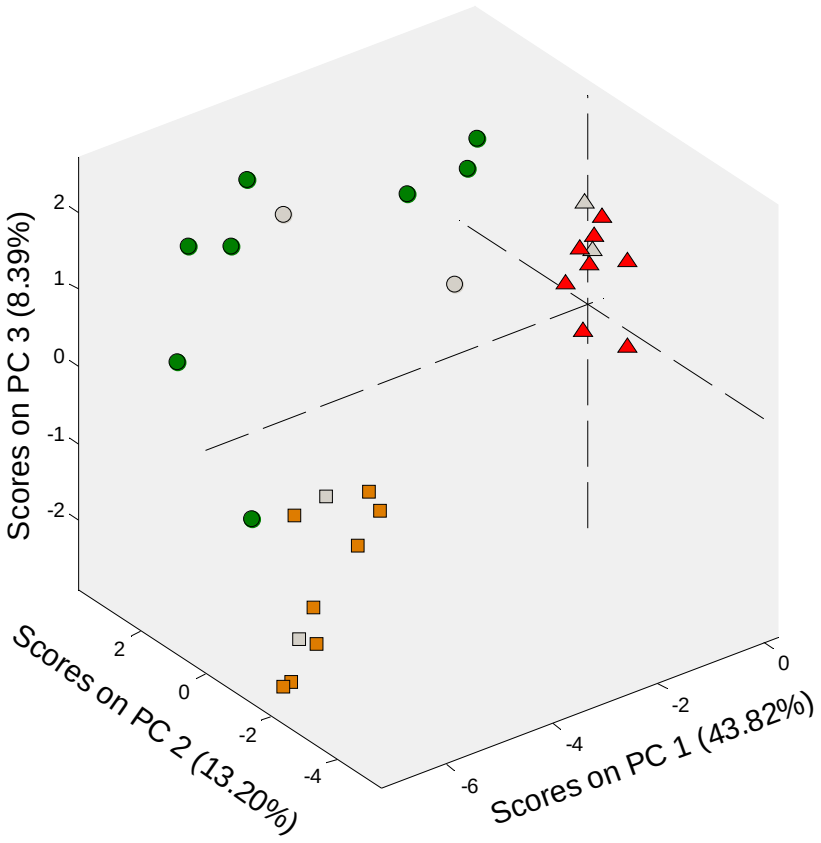

Figure 5.15 PC1 vs. PC2 and PC3 from metal-catalyzed hydroxyl radical experiment with untreated MS2 samples (red triangles), hydroxyl radical-treated

MS2 samples (green circles), and Cu^{2+}/H_2O_2 blanks (orange squares). Grey shapes represent test samples predicted with PCA model.

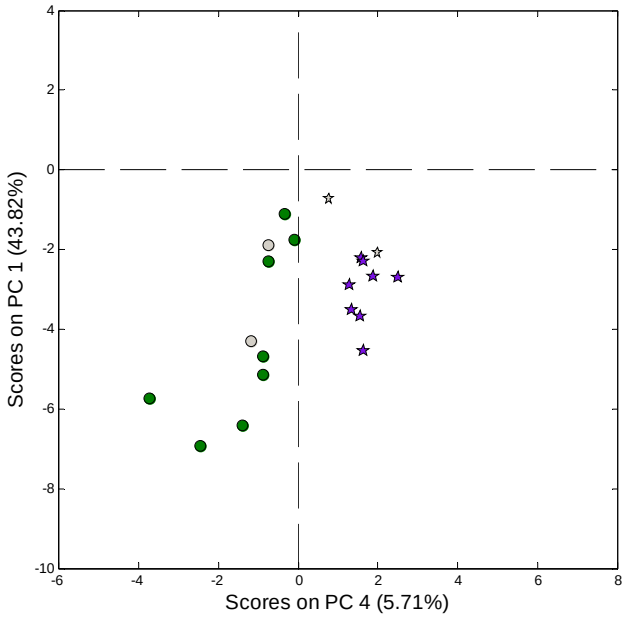

Figure 5.16 PC1 vs. PC4 from metal-catalyzed hydroxyl radical experiment with hydroxyl radical-treated MS2 (green circles) and Cu^{2+}-treated MS2 controls (purple stars). Grey shapes represent test samples predicted with PCA model.

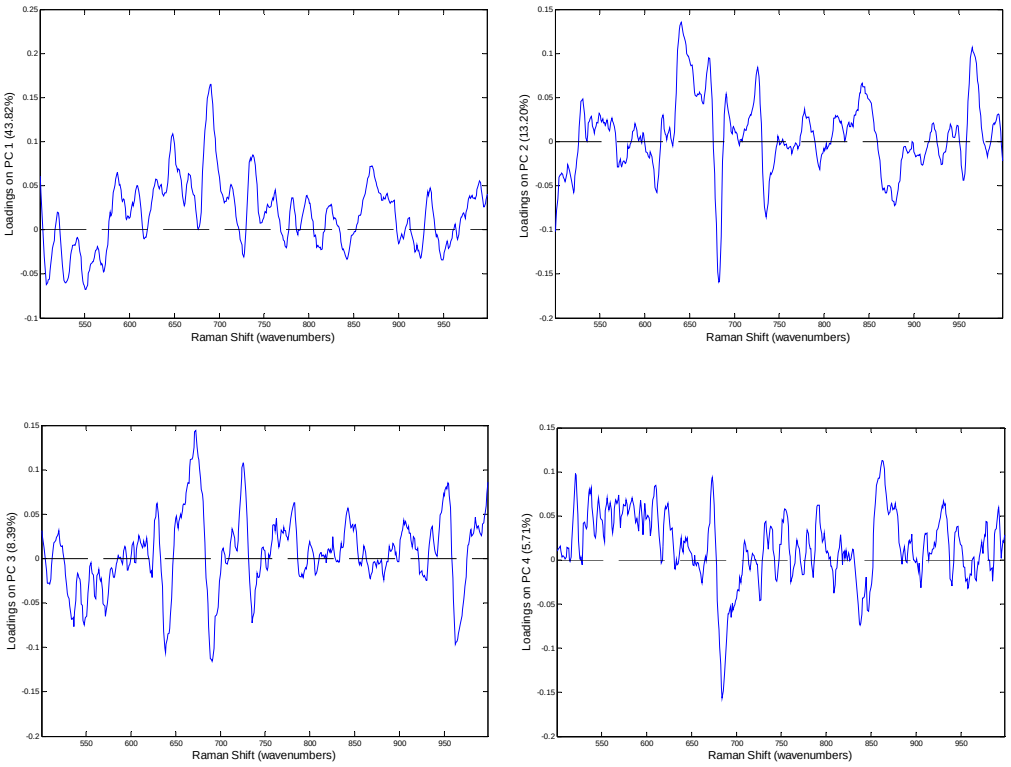

Figure 5.17 PC1 (top left), PC2 (top right), PC3 (bottom left) and PC4 (bottom right) loading for hydroxyl radical treatment PCA.

WORKS CITED

1. WHO *Guidelines for Drinking Water Quality: Volume 2 – Health Criteria and Other Supporting Information*; Geneva, 1996.
2. Caballero, S., Guix, S., El-Senousy, W. M., Calico, I., Pinto, R. M., Bosch, A., Persistent gastroenteritis in children infected with astrovirus: Association with serotype-3 strains. *Journal of Medical Virology* **2003,** 71, (2), 245-250.
3. Percival, S. L. A., *Microbiology of waterborne diseases*. Elsevier Academic Press: Amsterdam, 2004.
4. Tyrrell, S. A., Rippey, S. R., Watkins, W. D., Inactivation of bacterial and viral indicators in secondary sewage effluents, using chlorine and ozone *Water Research* **1995,** 29, (11), 2483-2490.
5. USEPA, Virus monitoring protocol for the Information Collection Requirements Rule. Government Printing Office: Cincinnati, Ohio, 1995.
6. Chapron, C. D., Ballester, N. A., Fontaine, J. H., Frades, C. N., Margolin, A. B., Detection of astroviruses, enteroviruses, and adenovirus types 40 and 41 in surface waters collected and evaluated by the information collection rule and an integrated cell culture-nested PCR procedure. *Applied and Environmental Microbiology* **2000,** 66, (6), 2520-2525.
7. USEPA Information Collection Rule (ICR). http://www.epa.gov/enviro/html/icr/ (September 12, 2008),
8. Grabow, W. O. K., Taylor, M. B., de Villiers, J. C., New methods for the detection of viruses: call for review of drinking water quality guidelines. *Water Science and Technology* **2001,** 43, (12), 1-8.
9. Harwood, V. J., Levine, A. D., Scott, T. M., Chivukula, V., Lukasik, J., Farrah, S. R., Rose, J. B., Validity of the indicator organism paradigm for pathogen reduction in reclaimed water and public health protection. *Applied and Environmental Microbiology* **2005,** 71, (6), 3163-3170.
10. Kneipp, K., Wang, Y., Kneipp, H., Perelman, L. T., Itzkan, I., Dasari, R., Feld, M. S., Single molecule detection using surface-enhanced Raman scattering (SERS). *Physical Review Letters* **1997,** 78, (9), 1667-1670.
11. Nie, S. M., Emery, S. R., Probing single molecules and single nanoparticles by surface-enhanced Raman scattering. *Science* **1997,** 275, (5303), 1102-1106.
12. Ni, J., Lipert, R. J., Dawson, G. B., Porter, M. D., Immunoassay readout method using extrinsic Raman labels adsorbed on immunogold colloids. *Analytical Chemistry* **1999,** 71, (21), 4903-4908.
13. Xu, S. P., Ji, X. H., Xu, W. Q., Li, X. L., Wang, L. Y., Bai, Y. B., Zhao, B., Ozaki, Y., Immunoassay using probe-labelling immunogold nanoparticles with silver staining enhancement via surface-enhanced Raman scattering. *Analyst* **2004,** 129, (1), 63-68.
14. Driskell, J. D., Kwarta, K. M., Lipert, R. J., Porter, M. D., Neill, J. D., Ridpath, J. F., Low-level detection of viral pathogens by a surface-enhanced Raman scattering based immunoassay. *Analytical Chemistry* **2005,** 77, (19), 6147-6154.

15. Ghiamati, E., Manoharan, R., Nelson, W. H., Sperry, J. F., UV resonance Raman spectra of Bacillus spores *Applied Spectroscopy* **1992,** 46, (2), 357-364.
16. Wu, Q., Hamilton, T., Nelson, W. H., Elliott, S., Sperry, J. F., Wu, M., UV Raman spectral intensities of E. coli and other bacteria excited at 228.9, 244.0, and 248.2 nm. *Analytical Chemistry* **2001,** 73, (14), 3432-3440.
17. Escoriza, M. F., VanBriesen, J. M., Stewart, S., Maier, J., Raman spectroscopic discrimination of cell response to chemical and physical inactivation. *Applied Spectroscopy* **2007,** 61, (8), 812-823.
18. Escoriza, M. F., VanBriesen, J. M., Stewart, S., Maier, J., Treado, P. J., Raman spectroscopy and chemical imaging for quantification of filtered waterborne bacteria. *Journal of Microbiological Methods* **2006,** 66, (1), 63-72.
19. Escoriza, M. F., Vanbriesen, J. M., Stewart, S., Maier, J., Studying bacterial metabolic states using Raman spectroscopy. *Applied Spectroscopy* **2006,** 60, (9), 971-976.
20. Maquelin, K., Choo-Smith, L.-P. i., Vreeswijk, T. v., Endtz, H. P., Smith, B., Bennett, R., Bruining, H. A., Puppels, G. J., Raman Spectroscopic Method for Identification of Clinically Relevant Microorganisms Growing on Solid Culture Medium. *Analytical Chemistry* **2000,** 72, 12-19.
21. Rosch, P., Schmitt, M., Kiefer, W., Popp, J., The identification of microorganisms by micro-Raman spectroscopy. *Journal of Molecular Structure* **2003,** 661, 363-369.
22. Kneipp, K., Haka, A. S., Kneipp, H., Badizadegan, K., Yoshizawa, N., Boone, C., Shafer-Peltier, K. E., Motz, J. T., Dasari, R. R., Feld, M. S., Surface-enhanced Raman Spectroscopy in single living cells using gold nanoparticles. *Applied Spectroscopy* **2002,** 56, (2), 150-154.
23. Efrima, S., Bronk, B. V., Silver colloids impregnating or coating bacteria. *Journal of Physical Chemistry B* **1998,** 102, (31), 5947-5950.
24. Zeiri, L., Bronk, B. V., Shabtai, Y., Czege, J., Efrima, S., Silver metal induced surface enhanced Raman of bacteria. *Colloids and Surfaces a-Physicochemical and Engineering Aspects* **2002,** 208, (1-3), 357-362.
25. Zeiri, L., Bronk, B. V., Shabtai, Y., Eichler, J., Efrima, S., Surface-enhanced Raman spectroscopy as a tool for probing specific biochemical components in bacteria. *Applied Spectroscopy* **2004,** 58, (1), 33-40.
26. Jarvis, R. M., Goodacre, R., Discrimination of bacteria using surface-enhanced Raman spectroscopy. *Analytical Chemistry* **2004,** 76, (1), 40-47.
27. Jarvis, R. M., Brooker, A., Goodacre, R., Surface-enhanced Raman scattering for the rapid discrimination of bacteria. *Faraday Discussions* **2006,** 132, 281-292.
28. Jarvis, R. M., Brooker, A., Goodacre, R., Surface-enhanced Raman spectroscopy for bacterial discrimination utilizing a scanning electron microscope with a Raman spectroscopy interface. *Analytical Chemistry* **2004,** 76, (17), 5198-5202.
29. Sengupta, A., Laucks, M. L., Davis, E. J., Surface-enhanced Raman spectroscopy of bacteria and pollen. *Applied Spectroscopy* **2005,** 59, (8), 1016-1023.
30. Sengupta, A., Mujacic, M., Davis, E. J., Detection of bacteria by surface-enhanced Raman spectroscopy. *Analytical and Bioanalytical Chemistry* **2006,** 386, (5), 1379-1386.

31. Bao, P. D., Huang, T. Q., Liu, X. M., Wu, T. Q., Surface-enhanced Raman spectroscopy of insect nuclear polyhedrosis virus. *Journal of Raman Spectroscopy* **2001,** 32, (4), 227-230.
32. Grow, A. E., Wood, L. L., Claycomb, J. L., Thompson, P. A., New biochip technology for label-free detection of pathogens and their toxins. *Journal of Microbiological Methods* **2003,** 53, (2), 221-233.
33. Campion, A., Kambhampati, P., Surface-enhanced Raman scattering. *Chemical Society Reviews* **1998,** 27, (4), 241-250.
34. Moskovits, M., Surface-enhanced Raman spectroscopy: a brief retrospective. *Journal of Raman Spectroscopy* **2005,** 36, (6-7), 485-496.
35. Haynes, C. L., McFarland, A. D., Van Duyne, R. P., Surface-enhanced Raman spectroscopy. *Analytical Chemistry* **2005,** 77, (17), 338A-346A.
36. Link, S., El-Sayed, M. A., Spectral properties and relaxation dynamics of surface plasmon electronic oscillations in gold and silver nanodots and nanorods. *Journal of Physical Chemistry B* **1999,** 103, (40), 8410-8426.
37. Link, S., El-Sayed, M. A., Size and temperature dependence of the plasmon absorption of colloidal gold nanoparticles. *Journal of Physical Chemistry B* **1999,** 103, (21), 4212-4217.
38. Otto, A., Mrozek, I., Grabhorn, H., Akemann, W., Surface-Enhanced Raman Scattering. *Journal of Physics-Condensed Matter* **1992,** 4, (5), 1143-1212.
39. Naja, G., Bouvrette, P., Hrapovic, S., Luong, J. H. T., Raman-based detection of bacteria using silver nanoparticles conjugated with antibodies. *Analyst* **2007,** 132, (7), 679-686.
40. Kneipp, K., Kneipp, H., Itzkan, I., Dasari, R. R., Feld, M. S., Surface-enhanced Raman scattering and biophysics. *Journal of Physics-Condensed Matter* **2002,** 14, (18), R597-R624.
41. Guicheteau, J., Argue, L., Emge, D., Hyre, A., Jacobson, M., Christesen, S., Bacillus spore classification via surface-enhanced Raman spectroscopy and principal component analysis. *Applied Spectroscopy* **2008,** 62, (3), 267-272.
42. Eliasson, C., Engelbrektsson, J., Loren, A., Abrahamsson, J., Abrahamsson, K., Josefson, M., Multivariate methodology for surface enhanced Raman chemical imaging of lymphocytes. *Chemometrics and Intelligent Laboratory Systems* **2006,** 81, (1), 13-20.
43. Shetty, G., Kendall, C., Shepherd, N., Stone, N., Barr, H., Raman spectroscopy: elucidation of biochemical changes in carcinogenesis of oesophagus. *British Journal of Cancer* **2006,** 94, (10), 1460-1464.
44. Dowd, S. E., Pillai, S. D., Wang, S. Y., Corapcioglu, M. Y., Delineating the specific influence of virus isoelectric point and size on virus adsorption and transport through sandy soils. *Applied and Environmental Microbiology* **1998,** 64, (2), 405-410.
45. Fujisawa, H., Hayashi, M., Assembly of bacteriophage-PhiX174- Identification of a virion capsid precursor and proposal of a model for functions of bacteriophage gene products during morphogenesis. *Journal of Virology* **1977,** 24, (1), 303-313.
46. Bernal, R. A., Hafenstein, S., Esmeralda, R., Fane, B. A., Rossmann, M. G., The phi X174 protein J mediates DNA packaging and viral attachment to host cells. *Journal of Molecular Biology* **2004,** 337, (5), 1109-1122.

47. APHA, AWWA, WEF, *Standard Methods for the Examination of Water & Wastewater*. 21 ed.; American Public Health Association, American Water Works Association and Water Environment Federation: Washington, D.C., 2005.
48. Lee, P. C., Meisel, D., Adsorption and surface-enhanced Raman of dyes on silver and gold sols. *Journal of Physical Chemistry* **1982,** 86, (17), 3391-3395.
49. Choi, O., Deng, K. K., Kim, N. J., Ross, L., Surampalli, R. Y., Hu, Z. Q., The inhibitory effects of silver nanoparticles, silver ions, and silver chloride colloids on microbial growth. *Water Research* **2008,** 42, (12), 3066-3074.
50. Sondi, I., Salopek-Sondi, B., Silver nanoparticles as antimicrobial agent: a case study on E-coli as a model for Gram-negative bacteria. *Journal of Colloid and Interface Science* **2004,** 275, (1), 177-182.
51. Tan, S., Erol, M., Sukhishvili, S., Du, H., Substrates with discretely immobilized silver nanoparticles for ultrasensitive detection of anions in water using surface-enhanced Raman scattering. *Langmuir* **2008,** 24, (9), 4765-4771.
52. Maquelin, K., Dijkshoorn, L., van der Reijden, T. J. K., Puppels, G. J., Rapid epidemiological analysis of Acinetobacter strains by Raman spectroscopy. *Journal of Microbiological Methods* **2006,** 64, (1), 126-131.
53. Siiman, O., Bumm, L. A., Callaghan, R., Blatchford, C. G., Kerker, M., Surface-enhanced Raman-Scattering by citrate on colloidal silver. *Journal of Physical Chemistry* **1983,** 87, (6), 1014-1023.
54. Siiman, O., Ledis, S., Surface-enhanced Raman scattering (SERS) of random silver or gold particle arrays on aminodextran-coated polystyrene beads. *Journal of Raman Spectroscopy* **2005,** 36, (12), 1125-1133.
55. Shanmukh, S., Jones, L., Driskell, J., Zhao, Y. P., Dluhy, R., Tripp, R. A., Rapid and sensitive detection of respiratory virus molecular signatures using a silver nanorod array SERS substrate. *Nano Letters* **2006,** 6, (11), 2630-2636.
56. Shanmukh, S., Jones, L., Zhao, Y. P., Driskell, J. D., Tripp, R. A., Dluhy, R. A., Identification and classification of respiratory syncytial virus (RSV) strains by surface-enhanced Raman spectroscopy and multivariate statistical techniques. *Analytical and Bioanalytical Chemistry* **2008,** 390, (6), 1551-1555.
57. McKenna, R., Xia, D., Willingmann, P., Ilag, L. L., Krishnaswamy, S., Rossmann, M. G., Olson, N. H., Baker, T. S., Incardona, N. L., Atomic-structure of single-stranded-DNA bacteriophage-Phi-X174 and its functional implications *Nature* **1992,** 355, (6356), 137-143.
58. Kuzmanovic, D. A., Elashvili, I., Wick, C., O'Connell, C., Krueger, S., The MS2 coat protein shell is likely assembled under tension: A novel role for the MS2 bacteriophage A protein as revealed by small-angle neutron scattering. *Journal of Molecular Biology* **2006,** 355, (5), 1095-1111.
59. Aubrey, K. L., Thomas, G. J., Studies of virus structure by laser Raman spectroscopy 34. Raman spectroscopy of filamentous bacteriophage-FF (FD, M13, F1) incorporating specifically deuterated alanine and tryptophan sidechains - assignments and structural interpretation *Biophysical Journal* **1991,** 60, (6), 1337-1349.
60. Wei, F., Zhang, D., Halas, N. J., Hartgerink, J. D., Aromatic Amino Acids Providing Characteristic Motifs in the Raman and SERS Spectroscopy of Peptides. *J. Phys. Chem. B* **2008,** 112, (30), 9158-9164.

61. Stewart, S., Fredericks, P. M., Surface-enhanced Raman spectroscopy of peptides and proteins adsorbed on an electrochemically prepared silver surface. *Spectrochimica Acta Part a-Molecular and Biomolecular Spectroscopy* **1999,** 55, (7-8), 1615-1640.
62. Movasaghi, Z., Rehman, S., Rehman, I. U., Raman spectroscopy of biological tissues. *Applied Spectroscopy Reviews* **2007,** 42, (5), 493-541.
63. Krafft, C., Knetschke, T., Siegner, A., Funk, R. H. W., Salzer, R., Mapping of single cells by near infrared Raman microspectroscopy. *Vibrational Spectroscopy* **2003,** 32, (1), 75-83.
64. Stone, N., Kendall, C., Smith, J., Crow, P., Barr, H., Raman spectroscopy for identification of epithelial cancers. *Faraday Discussions* **2004,** 126, 141-157.
65. Ikeda, S., Li-Chan, E. C. Y., Raman spectroscopy of heat-induced fine-stranded and particulate beta-lactoglobulin gels. *Food Hydrocolloids* **2004,** 18, (3), 489-498.
66. Stonehouse, N. J., Valegard, K., Golmohammadi, R., vandenWorm, S., Walton, C., Stockley, P. G., Liljas, L., Crystal structures of MS2 capsids with mutations in the subunit FG loop. *Journal of Molecular Biology* **1996,** 256, (2), 330-339.
67. Ngarize, S., Adams, A., Howell, N. K., Studies on egg albumen and whey protein interactions by FT-Raman spectroscopy and rheology. *Food Hydrocolloids* **2004,** 18, (1), 49-59.
68. Prescott, B., Sitaraman, K., Argos, P., Thomas, G. J., Protein-RNA interactions in belladonna mottle virus investigated by laser Raman-spectroscopy. *Biochemistry* **1985,** 24, (5), 1226-1231.
69. Akagawa, M., Suyama, K., Oxidative deamination by hydrogen peroxide in the presence of metals. *Free Radical Research* **2002,** 36, (1), 13-21.
70. Chevion, M., A site-specific mechanism for free-radical induced biological damage- the essential role of redox-active transition metals *Free Radical Biology and Medicine* **1988,** 5, (1), 27-37.
71. Stadtman, E. R., Metal ion-catalyzed oxidation of proteins - biochemical-mechanisms and biological consequences. *Free Radical Biology and Medicine* **1990,** 9, (4), 315-325.
72. Yamamoto, N., Damage, repair, and recombination : II. Effect of hydrogen peroxide on the bacteriophage genome. *Virology* **1969,** 38, (3), 457-463.
73. Uchida, K., Kawakishi, S., Selective oxidation of imidazole ring in histidine-residues by the ascorbic-acid copper-ion system. *Biochemical and Biophysical Research Communications* **1986,** 138, (2), 659-665.
74. Climent, I., Levine, R. L., Oxidation of the active-site of glutamine-synethetase - Conversion of Arginine-344 to Gamma-glutamyl semialdehyde. *Archives of Biochemistry and Biophysics* **1991,** 289, (2), 371-375.
75. Ayala, A., Cutler, R. G., The utilization of 5-hydroxyl-2-amino valeric acid as a specific marker of oxidized arginine and proline residues in proteins. *Free Radical Biology and Medicine* **1996,** 21, (1), 65-80.
76. Daneshvar, B., Frandsen, H., Autrup, H., Dragsted, L. O., Gamma-glutamyl semialdehyde and 2-amino-adipic semialdehyde: Biomarkers of oxidative damage to proteins. *Biomarkers* **1997,** 2, (2), 117-123.
77. Leeuwenburgh, C., Hansen, P., Shaish, A., Holloszy, J. O., Heinecke, J. W., Markers of protein oxidation by hydroxyl radical and reactive nitrogen species in tissues

of aging rats. *American Journal of Physiology-Regulatory Integrative and Comparative Physiology* **1998,** 274, (2), R453-R461.
78. Golmohammadi, R., Valegard, K., Fridborg, K., Liljas, L., The refined structure of bacteriophage-MS2 at the 2.8-angstrom resolution *Journal of Molecular Biology* **1993,** 234, (3), 620-639.
79. Shepherd, C. M., Borelli, I. A., Lander, G., Natarajan, P., Siddavanahalli, V., Bajaj, C., Johnson, J. E., C. L. Brooks, I., Reddy, V. S., VIPERdb: a relational database for structural virology. *Nucleic Acids Research* **2006,** 34, D386-D389.

6) Engineering Significance

Drinking water specialists agree that there is an urgent need for improved pathogen detection methods. When discussing *Cryptosporidium* and *Giardia* monitoring, Martin J. Allen, director of technology transfer at the American Water Works Association Research Foundation (AwwaRF), stated:[1]

> *"Unlike standardized chemical, radiological, and some bacterial methods, currently available pathogen methods do not produce credible data for making public health decisions. The three parameters necessary to ensure statistically valid microbial data are sensitivity, specificity, and reproducibility…Although it has been well-established that all current protozoan detection methods lack acceptable specificity, sensitivity, and reproducibility, many utilities nevertheless cling to the belief that protozoan monitoring…will enable them to make better public health decisions."*

We believe that the SERS based strategies presented in the previous chapters would provide a number of advantages over the methods currently used for pathogen monitoring. Unlike the fluorescence-based *C. parvum* and *G. lamblia* EPA 1622/1623 methods, a SERS method could be expanded to measure numerous pathogens simultaneously. Detection would be rapid (the acquisition times presented in the previous chapters ranged from 1 to 10 seconds) unlike many of the current methods that can take up to weeks to obtain results. Raman instruments are straightforward to use and spectral recognition can be fully automated. A SERS method would therefore not require large amounts of work by highly trained personnel and would thus cost less than current pathogen methods. Additionally, a SERS method has the potential to be incorporated into an in-line, real-time monitoring strategy.

A rapid and reliable method for the detection of protozoan, viral, and bacterial

pathogens alike would be of enormous help to drinking water utilities. An in-line, automated SERS method would allow utilities to monitor microorganisms at more frequent intervals and would result in a more complete pathogen monitoring program. Improved concentration histories would assist in making it possible to link pathogen concentration fluxes with alterations in water quality caused by natural (or unnatural) events. A method allowing for the quick and reliable attainment of pathogen data would allow utilities to quickly respond to heightened pathogen concentrations and to adjust their water treatment practices accordingly. Post-treatment in-line monitoring would help alleviate outbreaks, would indicate when water treatment deficiencies have occurred, and would help improve our understanding of which types of treatment techniques are best for oocyst removal. Finally, as bioterrorism has become a common threat to water utilities, a method that could continuously monitor high-risk treated waters for bioterrorism organisms such as small pox or anthrax would be invaluable to national security.

WORKS CITED

1. Allen, M. J., Clancy, J. L., Rice, E. W., The plain, hard truth about pathogen monitoring. *Journal of the American Water Works Association* **2000,** 92, (9), 64-76.

Appendix A: Experimental Protocols

SYNTHESIS OF GOLD NANOPARTICLE SEEDS (13 NM) AND SEEDED PARTICLES (> 13 NM)

Glasssware cleaning and reagent preparation

1. Aqua Regia preparation
    a. One part concentrated nitric acid to three part concentrated HCl solution prepared in hood
    b. Between 40 mL to 80 mL of solution prepared for cleaning glassware in plastic 100 mL graduated cylinder
    c. Proper personal protective equipment (goggles, gloves and lab coat) always used when preparing aqua regia

2. Sparkleen wash (this step important)
    a. Dishes soaked and scrubbed with Sparkleen and tap water solution
    b. Dishes washed and rinsed with tap water
    c. Dishes placed in plastic dish pan

3. Aqua Regia wash
    a. Aqua Regia was allowed to fully develop before use
        i. Darker orange color
        ii. Bubbles along side of graduated cylinder
    b. Dish pan placed in hood
    c. Excess water drained from dish pan
    d. Aqua regia poured into pieces of glassware, one at a time.
    e. Aqua regia swished around in glassware to clean all surfaces
    f. Care was taken to avoid pressure build-up in glass from aqua regia
    g. All glassware rinsed with Nanopure water (filtered through 0.22 μm using Steri-cup apparatus). Rinsing was repeated until glassware not longer smelled like chlorine.
    h. Clean glassware capped or sealed until use

4. $HAuCl_4 \bullet 3H_2O$ solution

a. 150 - 200 mg gold citrate ($HAuCl_4 \cdot H_2O$) weighed in clean weigh glass. Mass of gold chloride was recorded once stable (when waited too long, water absorbed to gold chloride).
b. 2-5 mL nanopure water added to gold in weigh glass with disposable plastic repipette.
c. Solution transferred to 25 mL volumetric with disposable plastic repipette.
d. Weigh glass rinsed twice with nanopure and rinse transferred to volumetric.
e. Solution brought to 25 mL with nanopure.
f. Solution concentration calculated with following formula (solution is 20.3 mM if exactly 200 mg dissolved)

$$\left(\frac{A\ mg}{0.025\ L}\right)\left(\frac{mmol}{393.8\ mg}\right) = B\ mM$$

g. Filter this solution through a 200 μm Millipore membrane into a clean storage vial with the molarity and date of solution prepared.
h. Store at 4 °C

5. Citrate Solution
a. Prepare a 38.8 mM sodium citrate solution by dissolving 570 mg in 50 mL nanopure water.
b. Use a weigh glass and add citrate. Dissolve in 5-10 mL of nanopure. Transfer to volumetric. Rinse weigh glass with nanopure and transfer rinsate to 50 mL volumetric.
c. Filter this solution through a 200 μm Millipore membrane into a clean poly storage vial with the molarity and date of the solution prepared.
d. Store at 4 °C

Seed preparation: 13 nm particle synthesis

Notes: Use nanopure water filtered through 0.22 micron filter (SteriCup filters)

Certain stir bars cause problems during nanoparticle synthesis and result in heterogeous nanoparticle sizes

a. Determine the amount of the gold solution (C) needed to make 100 mL of 1 mM gold.

$$C = \frac{(100\ mL)(1\ mM)}{B\ mM}$$

b. Spike C mL into a 100 mL volumetric flask and bring almost to line with nanopure water. Pour into round bottom flask with stir bar. Rinse volumetric with 1 mL nanopure. Bring to boil.

c. Rinse 5 mL Eppendorf tip with Millipore water. Quickly spike boiling solution with 10 mL citrate solution. Place reflux apparatus on top of the boiling solution and allow to reflux for 10 minutes. Remove reflux apparatus and allow to boil for additional five minutes.

d. Remove from heat and allow solution to continue stirring for 15 minutes (on a cool secondary stir plate).

e. Pour solution into 100 mL volumetric and bring to exactly 100 mL.

f. Filter solution through 0.2 μm polycarbonate Millipore filter into a storage vial.

g. Measure with UV-Vis between 400 and 800 nm. Peak should be at 517-518 nm. Determine peak width at half height.

h. Compare with previous 13 nm particle UV-Vis peaks. PWHH should be less than 90 nm

i. Store at 4°C

j. For TEM samples, 25 μL of nanoparticles was placed on the top of a TEM grid suspended by tweezers with a syringe. After sitting for 5 minutes, the drop was wicked away with a piece of filter paper. The TEM sample was inverted onto a drop of clean water and left in contact with the water for approximately 5 seconds. The grid was then dried face-up.

Seeded Particle Preparation (for larger gold nanoparticles)

a. Determine the amount of the prepared HAuCl4•3H2O solution needed to make 0.254 mM Au.

$$D = \frac{(0.254\ mM)(100\ mL)}{B\ mM}$$

b. Prepare 100 mL 0.254 mM Au solution in 100 mL volumetric flask. Pour into round bottom flask, taking care to transfer all of the mass of the gold to the round bottom flask.
c. Bring solution to reflux.
d. Pre-rinse pipette tips with nanopure prior to spiking solutions. Spike with x mL (depending on size wanted) 13 nm seeds and 0.44 mL 38.8 mM citrate solution. Spike seeds then citrate. If possible, spike one solution immediately after the first.

1. A spike of approximately 1.4 mL seeds in step 4 will produce seeded particles around 30-40 nm in diameter. Smaller volumes will produce larger particles.

e. Reflux 10 minutes and then boil without reflux for 5 minutes.
f. Remove from heat and stir for 15 more minutes with a cool stir plate.
g. Bring to 100 mL and transfer to amber storage vial.
h. Measure with UV-Vis and TEM.
i. For TEM sample preparation
    a. 25 μL of the seeded nanoparticles placed on the top of a TEM grid suspended by tweezers with a syringe.
    b. After sitting for 5 minutes, the drop wicked away with a piece of filter paper.
    c. The TEM sample inverted onto a drop of clean water and left in contact with water drop for approximately 5 seconds.
    d. Grid dried face-up.
    e. Repeated 3 times for each sample on the same grid to create a grid surface sufficiently concentrated with nanoparticles.
    f. Transmission electron micrographs were collected with a JEOL 100 CX-II transmission electron microscope (TEM). Average nanoparticle diameters were determined with Image J software. For each batch of nanoparticles, the length of major and minor axis of 50 nanoparticles were measured and recorded.

IMMUNOGOLD SYNTHESIS

Notes: For immunogold synthesis, only nanoparticle solutions with average diameters between 35 and 45 nm were employed.

Solutions and buffers

1. Rhodamine B isothiocyanate (RBITC) (536.08 mg/mmol) and Malachite green isothiocycante (MGITC) (485.98 mg/mmol) stocks were prepared in methanol.

    a. Prepared primary standards by dissolving 7 mg in 25 mL methanol. [RBITC] ≈ 522 μM RBITC and [MGITC] ≈ 576 μM.

    b. Placed aliquots in 2 mL crimp-sealed vials and labeled vials.

    c. Prepared secondary standards at 5000 nM (5 μM) in MeOH from the primary stocks. 14.4 μL RBITC in 1.5 mL MeOH to make 5 μM. 13 uL MGITC in 1.5 mL MeOH to make 5 uM.

2. 10 mM PBS at pH 7.4

    1. Prepare two solutions, each in a 1 L volumetric flask. The first solution consists of a, c, and d. The second solution consists of b, c, and d. Stir the two solutions in beaker until pH 7.4 is reached. Store at 4 °C until use. Make certain the pH meter was recently calibrated.

        a. 10 mM KH_2PO_4 (136.09 mg/mmol if anhydrous) – 1.361 g in 1 L

        b. 10 mM Na_2HPO_4 (141.96 mg/mmol if anhydrous)- 1.42 g in 1 L

        c. 150 mM NaCl (58.4 mg/mmol) – 8.76 g in 1 L

        d. 3 mM KCl (74.5 mg/mmol) – 0.22 g in 1 L

3. PBS with 0.1% Tween

    1. Dissolve 0.1 g Tween80 in 100 mL PBS solution. Store at 4 °C until use.

4. 5% BSA- Dissolve 500 mg BSA in 10 mL borate buffer or PBS buffer.

5. 2 mM Borate buffer

1. Prepare the two following solutions

    a. 30.9 mg boric acid (61.83 g/mol) in 250 mL with stir bar, let dissolve

    b. 190.7 mg sodium tetraborate (381.42 g/mol) in 250 mL with stir bar, let dissolve

2. Add solution 1 to 2 with stirring until pH 9 is obtained.

6. Antibody solutions

    1. When received, antibodies were aliquoted into working volumes in 300 µL centrifuge tubes and marked. For the 2-4 mg/mL stocks (pAbs and anti-C. parvum IgM ascites liquid), 5 or 10 µL aliquots were stored separately and for the 0.1 mg/mL samples (IgG mAbs), volumes of 50 or 100 µL were stored separately. The aliquots were frozen in a non-frost free freezer (not stored in frost free), or stored in the 4 °C refrigerator if used within few months. Care was taken to avoid freeze-thaw cycles. Prior to use in the immunogold, the 2-4 mg/mL antibody aliquots were diluted 10× with distilled water.

        a. Mouse monoclonal IgG1 antibodies against *G. lamblia* (catalogue # C65361M, 100ug/ml, purified, liquid>90% pure, protein A chromatography)

        b. Mouse polyclonal IgG fraction antibodies against *G. lamblia* were obtained from Meridian Life Sciences (Cincinnati, OH).

        c. Mouse monoclonal IgM antibodies against *C. parvum* were obtained from Millipore Antibodies (Temecula, CA, catalogue # MAB8935, ascites fluid),

        d. Mouse monoclonal IgG1 antibodies against *C. parvum* were obtained from Abcam Inc. (Cambridge, MA, catalogue # ab20510, 0.1 mg/mL = 685 nM, protein A purified),

        e. Mouse polyclonal IgG fraction antibodies against *C. parvum* were purchased from Abcam Inc., (Cambridge, MA, catalogue # ab20787, goat polyclonal, 4 mg/mL, IgG fraction, protein G purified).

        f. Fluorescent-tagged antibodies specific to *G. lamblia* and *C. parvum* were obtained from Waterborne, Inc. and stored at 4°C prior to use.

Immunogold synthesis

1) For anti-*Giardia* and anti-*Cryptosporidium* immunogold preparation, 0.3 mL aliquots of the 40 nm gold nanoparticles in 0.3 mL centrifuge tubes were spiked with 1.2 μL of 5000 nM MGITC and 1.2 μL of 5000 nM RBITC, respectively. Each were prepared in triplicate.
    a. This resulted in 20 nM MGITC and RBITC which was approximately 25% of the concentration that lead to aggregation of the nanoparticles in dye-stabilization experiments.

2) Samples were shaken briefly and then reacted overnight at room temperature.

3) The following morning, conjugates were collected by centrifuging sample at 2000 rpm for 10 minutes.

4) Clear centrate containing unbound dye molecules was discarded and the loose sediment was resuspended in 2 mM borate buffer. The wash was repeated and again the loose sediment was resuspended in 2 mM borate buffer.

5) Prior to antibody spiking, one MGITC and one RBITC triplicate sample is measured by Raman spectroscopy (first placed in a microtiter plate) to confirm that the dye is conjugated with the nanoparticles. The signal of the highest MGITC and RBITC peak after baseline correction is recorded.

6) To the RBITC nanoparticle conjugates, 30 μL of *C. parvum* IgM antibody (10 × dilution from purchased liquid which was 2.1 – 5.26 μM) concentrate was added resulting in 21-52.6 nM (20.0-50.0 μg/mL).

7) To the MGITC nanoparticle conjugates, 40 μL of *G. lamblia* IgG1 antibody concentrate was added leading to a concentration of 90 nM or 13.1 μg/mL.

8) After reacting for 20 minutes, 30 μL of 10% BSA in borate buffer was added to each of the immunogold solutions to prevent immunogold loss during the following centrifugation steps.

9) After reacting for another 90 minutes, the immunogold conjugates were centrifuged for 10 minutes at 2000 RPM. The centrate was discarded and the loose sediment was resuspended in borate buffer.

10) After a final centrifugation, the immunogold conjugates were resuspended in PBS buffer containing 0.1% Tween 80. The immunogold conjugates were then filtered through a 25 mm silver membrane filter with 0.45 μm pores into a clean 50 mL Erlenmeyer filter flask with a vacuum filtration unit.

11) An additional 100-200 μL PBS 0.1 % Tween was used to rinse out immunogold captured in the filter and the immunogold was then transferred to a clean, marked centrifuge tube. This solution should be a light pink color.

12) The Raman signal of these were measured immediately to confirm that the RBITC and MGITC signals are strong. Finished immunogold is stored at 4 °C and should be used within 24 hours of synthesis.

CRYPOSPORIDIUM PARVUM AND GIARDIA LAMBLIA LABELLING

Notes

- *C. parvum oocysts and G. lamblia cysts were purchased from Waterborne, Inc. (New Orleans, LA).*
- *(Oo)cysts were washed twice by centrifugation (5000 rpm × 5 min) and stored in a reagent water/0.1% Tween 80 solution at 4 °C.*
- *Oocyst solutions were used within three months of purchase and cysts were used within one month of purchase.*

Oocyst and cyst prep for experimental use

1. Prior to use, (oo)cyst stocks are centrifuged at 5000 rpm for 2 minutes and then shaken and lightly vortexed. This centrifugation step was found to prevent clumps of (oo)cysts.

2. For enumeration, 10 μL of 250,000 (oo)cysts/mL stock solution was pipetted into a hemecytometer chamber with the glass coverslip in place.

a. The hemecytometer was placed into a clean Petri dish directly outside of the hood. Gloves and labcoat were removed, hands were washed, and the Petri dish was covered. The dish was carried to the microscope room.

b. Hemecytometer was removed from Petri dish and placed on microscope stage.

c. With 20× objective, (oo)cysts in four outer corners of grid were counted and added together.

d. This number of oocysts was then divided by 0.4 and multiplied by 1000 which results in the (oo)cysts/mL concentration. This counting procedure was repeated 2 more times and the averages and standard deviations were recorded.

e. Cyst and oocyst stocks were enumerated every 2-3 weeks to assure that concentrations were not decreasing.

3. For secondary oocyst solutions, concentrated (oo)cysts were spiked into a centrifuge tube with the appropriate volume of 10 mM PBS. For example, to prepare a 10,000 (oo)cyst/mL stock, 40 μL of the stock was pipetted into a

centrifuge tube containing 960 μL PBS. Diluted stock should also be enumerated with a hemcytometer prior to use.

Labelling cysts and oocysts fixed on slides

1. Waterborne SuperStick™ slides with two wells were used for fixing C. parvum and G. lamblia.

2. 10 μL of the C. parvum or G. lamblia stock of the appropriate concentration were placed in the slide wells, smeared around with the pipette tip, and allowed to dry.

3. 50 μL 5% BSA was placed over (oo)cyst spot area and allowed to incubate in a humidity chamber for 30 minutes. The drop of BSA was removed by tipping the slide onto a paper towel and allowing the BSA solution to drip onto the paper towel.

4. The slides were submerged in a PBS/Tween wash 10 mM PBS and then dried by setting on papertowel with the slides resting at an incline.

5. Once dry, 50 μL of the immunogold solution was placed on top of the sample well and incubated in a humidity chamber for one hour. After one hour, the immunogold was removed by gently tipping the slide onto a paper towel.

6. The slides were rinsed by submerging in a PBS/Tween wash for 1 minute and then dried at an incline on a paper towel.

7. To the dried well, one drop of 60% glycerol/40% PBS mounting media was droped. A coverslip was added to the tope of the mounting media drop, and the coverslip was sealed into place with clear fingernail polish.

8. Once dried, the sample were stored in biohazard sample containers in the refrigerator.

9. For mapping experiments on glass slides, Raman spectra from 1000 to 1800 cm^{-1} were collected at each map position with 1 s acquisition. This spectral range was large enough to include several characteristic reporter molecule peaks and was small enough to prevent the 600 lines/mm grating from moving during collection.

RAMAN MAPPING

Instrument prep

1) Turn on the key switch located on the 633 nm (red) laser box to the left of the microscope. A second red light will appear when the key switch is "on," otherwise, only one red light is lit.

2) Remove the cover from the microscope eyepieces.

3) Make sure the x-y mapping stage is on the instrument. An Allen wrench is required to lock the x-y mapping stage in place. No tools are needed to remove and replace the manual stage.

4) Open the biohazard sample box with gloves, remove a slide with one hand, place the slide on the microscope stage, clamp in place, remove gloves and discard. The stage is moved in the x-y direction with the joystick.

5) Turn the microscope light box on, located to the left of the microscope instrument with the knob and continue to turn counterclockwise until the light is sufficiently bright.

6) Pull out the knob directly to the right of the eyepiece is pulled out.

7) Use the 40× objective. Do not grab the objective directly; instead, turn the base objective wheel.

8) Move the stage with the joystick until the light traveling through the 40x objective is directly over the sample area on the slide.

9) Look through the eyepiece and focus with the rough (big knob) and fine (small knob) focus knobs. Focus on the green edge of the well. This is approximately the same depth as the oocysts.

10) Use the joystick to move the sample in the x and y direction while looking through the eyepiece. Scan the surface for oocysts. When an oocyst is located, place it in the upper left corner of the area seen through the eyepiece.

Raman mapping settings

1) Adjust the following software settings
    a. Make sure the 633 laser is selected in the bottom left field of the screen. If the 513 laser was used last, the filter will need to be switched within the Raman instrument.
    b. Typically the "slit" and "filter" fields are left alone.
    c. For most mapping experiments, 1 second acquisitions are collected at each pixel. In the acquisition window, enter 1 for the number of averaged spectra, and 1 for the acquisition time.
    d. Choose the 40× objective in the software objective window.
    e. The 600 grating should be selected. If not, select 600 and wait while the grating within the Raman instrument automatically moves to the 600 position and clicks.
    f. Click on the "Spectral Windows" icon at the top of the screen, (the icon with a spectrum divided into three different colors).
        i. Choose "multiwindow" in the Acquisition Mode field.
        ii. Enter 1000 under the "from" column and 1800 under the "to" column
        iii. Make certain the following boxes are checked: "Combination after acquisition," "Remove combined objects" and "Adjust objects intensity," then close the window.

2) On the Raman instrument, place the main knob in the back of the instrument to the "down" position. Push the knob to the right of the eyepiece to the "in" position. The surface can no longer be seen through the eyepiece and instead the image is sent to the computer screen.

3) Select the camera button located in the second row of icons along the top of the screen. The sample surface image should appear on the computer screen in a video window. The image on the screen moves with the joystick. Focus on the selected oocyst on the screen with the microscope focus knobs.

4) Click the mouse arrow on the camera image window to capture a picture. This creates a freeze frame of the image. Care should be taken to not bump the stage or joystick from this point on. If this happens the mapping results will not match the captured image. This image can be saved as a picture file.

5) Select the "square" selection icon in the lower, right corner of the picture window.

6) Click on the icon with picture of the XY map in the second row of icons at the top of the screen. If you hover over it you see "Acquisition data parameters".

7) Prepare the mapping square area by moving the square around the captured picture. The mapping data parameters will change as the square is moved and increased or decreased. For practice, select for a 10 × 10 map with 1 μm steps.

Once the square is in the desired position with the desired size map, close the "Acquisition data parameters" window.

8) Turn the light box off. Pull the knob in the back of the instrument to the up position and lock it in position (turn the knob slightly to lock).

9) Turn the laser switch to "on" (switch to the right of the key on the red laser box).

10) On the computer screen, press the icon in the second row of icons at the top of the screen with a picture of 9 small spectra. "Acquisition" appears when hovering above this button. The instrument should begin to collect the map data.

11) An approximate remaining acquisition time is given in the bottom left corner of the screen.

12) Under the "Window" tab at the top of the software screen, click on "rearrange windows". Four windows should be displayed.

13) Once the map has finished turn off the laser switch.

14) Save the data before closing any. Select the "Spectral_Image" window to save the mapping data. Save the file in a folder with the days date. Save the file twice with the same name, once as a spectral file (spc) and once as a text file (txt).

15) Close all of the windows.

16) Unlock the knob in the back of the instrument by turning it slightly and then lower the knob (do not let it drop freely).

17) Pull the knob to the right of the eyepieces to the out position.

18) With the microscope oculars, search slide surface for additional oocysts and/or cysts.

19) Change step size and mapping area size to obtain the desired maps.

FABRICATION OF GOLD-COATED PC MEMBRANES

Materials Needed

- Anhydrous $SnCl_2$
- $AgNO_3$
- Trifluoroacetic acid
- Na_2SO_3
- Formaldehyde
- Anhydrous Methanol
- Concentrated HNO_3
- Milli Q 18-MΩ Water
- "Track- etch" polycarbonate membrane filters
- Commercial Gold Electroless Plating Solution, $Na_3Au(SO_3)$
- Ice

Solution preparations

1. 0.026 M Cl_2Sn and 0.07 M Trifluoroacetic acid solution
    a. Prepare solution of 30 ml water and 30 ml methanol in beaker
    b. In 50 mL volumetric flask, dissolve 247 mg Cl_2Sn in ~40 mL of H_2O/MeOH
    c. Add 0.27 mL of Trifluoroacetic acid.
    d. Bring volume to 50 mL with H_2O/MeOH

2. 0.029 M $AgNO_3$ solution
    a. Dissolved 246 mg $AgNO_3$ in 50mL of water in volumetric flask.

3. $Na_3Au(SO_3)_2$, Na_2SO_3, and Formaldehyde Solution
    a. Dilute 1.25 mL $Na_3Au(SO_3)_2$ in ~30 ml water.
    b. Measure 800 mg of Na_2SO_3 and add to solution.
    c. Add 2.54 ml of formaldehyde into solution.
    d. Bring to 50 mL with water.
    e. Put onto ice-salt solution.

4. 25% Nitric Acid Solution
    a. Place 18 ml nitric acid into 50 ml water

Procedure

1. Rinse membrane in 50:50 MeOH:H_2O
2. Immerse membrane in Cl_2Sn, trifluoroacetic acid solution for 3 minutes.
3. Rinse membrane with three 50 mL portions of methanol.
4. Immerse membrane in $AgNO_3$ solution for 2 minutes.
5. Rinse membrane in two 100 mL portions of methanol and one 100 mL portion of distilled water
6. Immerse membrane in $Na_3Au(SO_3)_2$, Na_2SO_3, and Formaldehyde solution for 6-10 hours.
7. Remove membrane and rinse with two portions of water.
8. Immerse membrane into Nitric Acid solution for 12 hours.
9. Rinse membrane thoroughly in water and allow to air dry.
10. Prior to use in immunoassay experiment, soak filter in 10% BSA overnight to discourage nonspecific binding of immunogold labels.